# Optical levitation of stuck micro particles with a pulsed laser tweezers

# ABSTRACT

Amol A. Ambardekar, **OPTICAL LEVITATION OF STUCK MICROPARTICLES WITH A PULSED LASER TWEEZERS** (Under the direction of Dr Yong-qing Li) Department of Physics, June 2005.

We developed a pulsed laser tweezers and used it successfully for levitation and manipulation of microscopic particles stuck on a glass surface. A pulsed laser tweezers contains all the characteristics of a CW laser tweezers with addition of a pulsed laser for levitation of stuck microparticles. An infrared pulse laser at 1.06 μm was used to generate a large gradient force (up to $10^{-9}$ N) within a short duration (~45 μs) that overcomes the adhesive interaction between the stuck particles and the surface; and then a low-power continuous-wave diode laser at 785 nm was used to capture and manipulate the levitated particle. We demonstrated that both the stuck dielectric and biological micron-sized particles can be levitated and manipulated with this technique, including polystyrene beads, yeast cells, and bacillus cereus bacteria. We also measured the single pulse levitation efficiency for polystyrene beads as the functions of the pulse energy, the axial displacement from the stuck particle to the pulsed laser focus, and the percentage NaCl present in the sample. The results showed that the levitation efficiency was as high as 88% for 2.0 μm polystyrene spheres.

# OPTICAL LEVITATION

# OF STUCK MICROPARTICLES

# WITH A PULSED LASER TWEEZERS

A Thesis

Presented to

the Faculty of the Department of Physics

East Carolina University

In Partial Fulfillment

of the Requirements for the Degree

Master of Science in Applied Physics

by

Amol A. Ambardekar

June 2005

# OPTICAL LEVITATION OF STUCK MICROPARTICLES WITH A PULSED LASER TWEEZERS

**by**
**Amol A. Ambardekar**

**APPROVED BY:**
**ADVISOR OF THESIS**

YONG-QING LI, PH.D
DEPARTMENT OF PHYSICS, ECU

**COMMITTEE MEMBER**

JAMES JOYCE, PH.D
DEPARTMENT OF PHYSICS, ECU

**COMMITTEE MEMBER**

MARTIN BIER, PH.D
DEPARTMENT OF PHYSICS, ECU

**COMMITTEE MEMBER**

THOMAS McCONNELL, PH.D
DEPARTMENT OF BIOLOGY, ECU

**DEAN OF THE GRADUATE SCHOOL**

PAUL TSCHETTER, PH.D

# ACKNOWLEDGEMENTS

I would like to thank all the faculty members of the Physics Department of ECU for the contributions they have made towards my education. Many people deserve credit for helping me complete this thesis. Most of all, I am greatly indebted to Dr. Yong-qing Li, who has been generous with his dual talent for questioning the details and developing the large vision. His ability and originality made this project and writing of this manuscript possible.

I would like to thank Dr. Larry Toburen, our graduate director for his encouragement and the guidance throughout the years. Thanks and appreciations are also due to Dr. James Joyce, Dr. Martin Bier, and Dr. Thomas McConnell for serving on my thesis committee, reviewing this manuscript, and for making sure that I meet all the graduation requirements set by the department and the university. I must also thank my friend Dr. Changan Xie for helping me to understand new techniques and concepts.

My appreciation is also due to my friends Sandeep and Amit, who gave me great help for the writing of this thesis. Mr. James Saupe also gave me enormous help in the instrumentation development. I must also thank Ms. Sonia Chinn, our department

secretary for taking care of all the administrative obligations. I would also like to thank Mr. Charles Goodman for his support and encouragement. My heartiest thanks also go to the staff in the department of physics for their friendship and immaculate cooperation.

I owe much gratitude to my uncle, Raj, who encouraged me to come to United States for my masters. Finally, I would like to thank my family members and friends for their support and encouragement throughout the years.

# TABLE OF CONTENTS

# LIST OF TABLES

# LIST OF FIGURES

# 1. INTRODUCTION

The development of modern laser technology made it possible to realize the techniques which can manipulate and analyze microparticles in liquid medium. Microparticles include biological particles (cells, bacteria, viruses, organelles and even chromosomes), and non-biological particles. Microparticles in the liquid medium are always in Brownian motion. To trap and manipulate a single microparticle, an external force is required to overcome Brownian motion. In the 1970's, Arthur Ashkin at the Bell Telephone Laboratories, started experiments with optical beams to manipulate objects.[1,2] His pioneer work led to the development of the single-beam gradient force optical trap,[3] or "optical tweezers" as it has come to be known.[4] Optical tweezers use a highly-focused continuous-wave (CW) laser to trap and manipulate microparticles suspended in aqueous medium. The CW-lasers used are generally below hundreds of milliwatts and exert forces on the order of piconewtons on the trapped particle.[5] This weak force is efficient to confine micro-particles suspended in liquids, but not sufficient to levitate the particles that are stuck on the glass surface, where it has to overcome the binding force. Therefore, the stuck particles cannot be manipulated with the optical tweezers that only employ CW lasers. To overcome this limitation, "pulsed laser tweezers" were developed. This thesis addresses the development and characteristic of the pulsed laser tweezers, with its application in levitation of stuck microparticles. A pulsed laser tweezers is the combination of a CW laser tweezers and a pulsed laser for levitation. In this chapter, we

will discuss the history and applications of a CW laser tweezers, conventionally known as optical tweezers, and applications of a pulsed laser in optical manipulation.

## 1.1. History of optical tweezers

In the seventeenth century, the German astronomer Johannes Kepler proposed that the reason comet tails point away from the sun is because they are pushed in that direction by the sun's radiation. In 1873, James Clerk Maxwell showed in his theory of electromagnetism that light itself can exert optical force, or *radiation pressure*, but this was not demonstrated experimentally until the turn of the century. One reason for the lapse of nearly three centuries between hypothesis and verification is that radiation pressure is extraordinarily feeble. Milliwatts of power (corresponding to very bright light) impinging on an object produce piconewtons of force. After the invention of laser in the 1960s, researchers were able to study radiation pressure through the use of intense, collimated source of light. Early work on such studies was started by Arthur Ashkin at AT&T (Bell) Laboratories. By focusing laser light into narrow beams, Ashkin and others demonstrated that tiny particles, such as polystyrene spheres, having diameter of only few micrometers, could be displaced and even levitated against gravity using the force of radiation pressure.[1,2,6-9] Ashkin's work on the effects of radiation pressure laid much of the groundwork for the development of laser-based atom trapping and cooling methods employed by today's physicists.[2,10]

One particular optical trapping scheme, proposed in 1978 and demonstrated in 1986,[3,6] simply consisted of bringing a beam of laser light to a diffraction limited focus using a good lens, such as microscope objective. The intense light gradient near the focal region can achieve a stable three dimensional trap under the right conditions. Optical traps employing this design do not trap atoms at room temperature, but they can be used to capture and remotely manipulate a wide range of large particles, varying in size from several nanometers up to tens of micrometers. The term *optical tweezers* was coined to describe this single-beam scheme. The first of such scheme was implemented by Ashkin and Chu in 1986.[3] Ashkin *et al.* in 1987, showed that optical tweezers could be used to trap and manipulate living as well as inanimate, material particles in solution and through proper choice of wavelength, optical damage to biological specimen could be minimized. In his scheme, he employed a continuous-wave (CW) near-infrared laser (Nd:YAG, $\lambda$ = 1064 nm) to capture bacteria and small numbers of tobacco mosaic virus,[11] then to manipulate single cells[12] and cell organelles[13] and finally to measure the force of cell organelle movement inside living cells.[14]

Laser based optical traps have already had significant impact, because they can afford an unprecedented means to manipulate on the microscopic scale. Even though optical forces are very small on the scale of larger organisms, they can be significant on the scale of macromolecules, organelles, and even a whole cell. A force of the order of ten piconewtons can tow the bacterium faster than it can swim, halt a swimming sperm cell in its track, or arrest the transport of the intracellular vesicle.[15] A force of this magnitude can also be used to stretch, bend, or otherwise distort single macromolecules,

such as DNA or RNA.[16] Optical traps are therefore well suited for studying the mechanics or dynamics of cellular or subcellular levels.

## 1.2. Review of applications

Biologists were quick to take advantage of optical tweezers as a tool for purposes such as measuring the compliance of bacterial tails,[17] the forces exerted by single motor proteins[18] and the stretching of single deoxyribonucleic acid (DNA) molecules.[16] Optical tweezers have also been used with the combination of optical scissors[19] or used as part of fluorescence,[20] confocal,[21] or scanning force probes.[22] The first biological studies were made on material that was large enough to manipulate directly using optical tweezers. After initial work from Ashkin *et al.* to trap *E. coli* and yeast cells with optical tweezers, the laboratories of K. Greulich and M. Berns combined a CW infrared optical tweezers with either pulsed ultraviolet or pulsed Nd: YAG laser microbeams, which function as optical scalpels, to cut and paste within the cell.[23,24] With this arrangement, they performed various kinds of microsurgery, such as laser-assisted cell fusion. Optical tweezers has also been used to manipulate chromosomes or chromosome fragments in order to study cell division.[25--32]

In 1989, Block *et al.*[17] made the first calibrated measurement of the compliance of bacterial flagellae, using the tweezers to grab and forcibly rotate bacteria that had become tethered to a microscope coverglass by their flagellum. They calibrated the force applied by the optical tweezers from the time constant of elastic recoil of the bacterium in the viscous medium. This study paved the path for making calibrated measurements using

optical tweezers as a force transducer. In most of the applications, rather than manipulating the biological material directly it is usual to attach a latex (polystyrene) microsphere. Biological molecules such as DNA and proteins are less than 25 nm in diameter and are therefore difficult to manipulate directly. Also, the reproducibility of synthetic microspheres allows easy calibration of the system. When a microsphere is used in this way to manipulate material indirectly, it is often referred to as a "handle". One such interesting application of this technique was demonstrated in 1994, in which twin optical tweezers were used to hold a single actin filament suspended between two polystyrene beads as shown in Figure 1. [18] The filament was then placed in the vicinity of a third, fixed microsphere sparsely coated with myosin. Movements produced by the intermittent acto-myosin interactions were measured from movements of the image of one of the trapped beads cast onto the quadrant photodiode detector.[18] In 1995, a further study of the trapped beads (200 nm) held in the compliant optical tweezers (of stiffness 0.02 pN/nm) randomized the starting point of each protein interaction. By monitoring the variance of the position signal to measure stiffness, binding interactions could be identified from the increase in the stiffness (by reduction in signal variance). This enabled the movement produced by the motor proteins to be determined with greater accuracy.[33] This technique can be applied to follow the folding and unfolding of amino acid sequences and so to deduce the energy profile of the folding process. Such study is crucial in understanding of the new genomic data.[34] There exists another type of motor proteins which rotate and are found in the cell membrane, and are driven by the flow of ions across transmembrane electrochemical gradients. One such rotary motor is the

bacterial flagellar motor. It was first studied by Steven Block and others.[17] Since then Berry and Berg have made a more detailed study of the forward and reverse rotation of the bacterial flagella rotary motor protein.[35,36]

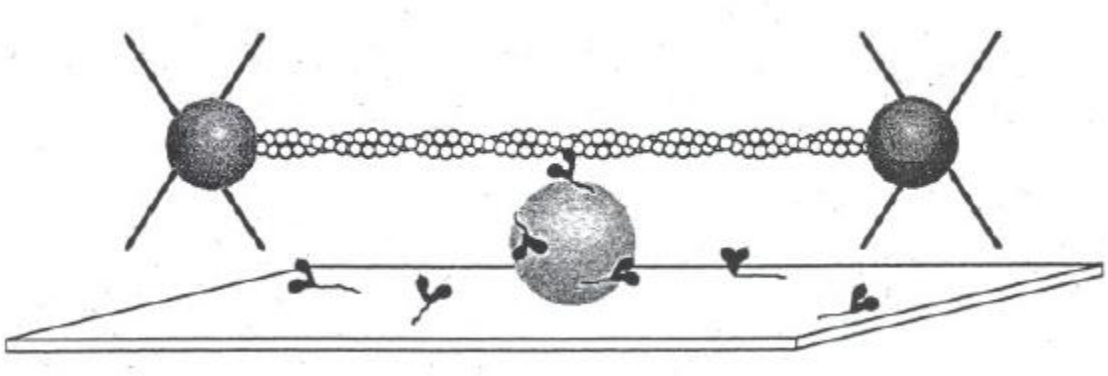

Figure 1. Application of optical tweezers as a "handle". Schematic diagram (not drawn to scale) illustrating use of two optical traps that are focused on beads attached to a single actin filament, which is held near a single HMM (heavy meromyosin) molecule. The filament is pulled taut and lowered to a silica bead that is firmly fixed to a microscope coverslip and sparsely coated with skeletal muscle HMM. (Reproduced from Spudich *et al.*[18])

Optical tweezers have also been used for measuring forces of the DNA. And it is supposed that this kind of study will reveal more details about motion of enzymes along DNA. After the initial study by Chu *et al.*,[37] Bustamante *et al.* investigated elastic responses of single and double stranded DNA molecules after overstretching and they found that conformational changes follow overstretching.[38] It may play a significant role in DNA recombination.

Experiments in different laboratories in last 15 years have begun to explore the rich possibilities offered by optical tweezers in the field of biology.[39-41] In other biological applications of optical tweezers, some researchers have reported the use of

optical force to stretch cell membranes into slender filaments to study their viscoelastic properties.[42-46] Zahn *et al.* have developed cell sorting to make cell patterns for drug screening.[47] Raucher *et al.* have studied membrane tension[48] and mobility of membrane proteins.[49] Sako *et al.* have measured the rigidity of microtubules.[50] Different groups of researchers reported of studying the elasticity of the cytoplasm[51] and cell membrane[13] and bringing together immune cells and their target cells under the microscope.[52] Li *et al.* combined near-infrared Raman spectroscopy technique with optical tweezers to characterize optically trapped living cells and dielectric particles.[53-55]

Other than biological applications of optical tweezers, it has been used extensively in the field of colloids and mesoscopic systems.[56-61] In 1994, Grier *et al.* used optical tweezers to measure the interaction potential between isolated pairs of charged colloidal spheres.[61] In 2000, Lin *et al.* reported the results of direct measurements, using video microscopy in combination with optical tweezers, of constrained diffusion of an isolated uncharged PMMA sphere in a density-matched fluid confined between two parallel flat walls.[59] In 2002, Grier *et al.* reported measurements of colloidal transport through arrays of micrometer-scale potential wells created with holographic optical tweezers.[57]

Optical rotation of trapped microparticle, holographic optical traps, and combination of optical trapping with single-molecule fluorescence are some of the most promising recent applications of optical trapping technology.[5]

## 1.3. Pulsed lasers for optical manipulation

Today, there exist two principles of micromanipulation that depend on nature of the applied laser source: optical trapping and laser ablation. Optical trapping is realized using a CW near infrared laser; whereas, laser ablation is based on a pulsed UVA laser that is focused through the microscope for laser cutting or laser microsurgery.[62] Thus, a pulsed laser has its own niche in the field of optical manipulation. They are generally used in the laser scissors to cut individual cells and organelles. Researchers have been using the pulsed laser for laser scissors for a quite some time now. The first laser microscope system employed a pulsed ruby laser at 694.3 nm with pulse duration of 500 μs was developed by Besis *et al.*[63,64] The pulsed (50 μs) argon ion laser at 514 and 488 nm in combination with vital stain, acridine orange, to selectively alter chromosomes was described.[65] The next major advance in the field of laser inactivation of cells and organelles was the advent of the solid-state Q-switched neodymium:yttrium aluminum garnet (Nd:YAG) laser. This laser produces wavelengths at its fundamental wavelength of 1.06 μm, or at harmonically generated wavelengths of 532 nm, 355 nm, and 266 nm. Apart from this, it can be used to pump a dye laser, which provides tunable wavelengths throughout the UV and visible spectrum.[66] Compared to previous laser systems, these lasers produce beams with pulses in the nanosecond and picosecond ranges, with hundreds of millijoules per pulse.[67] By the mid 1980s, laser microscope systems were available that could be used to alter cells and sub cellular regions. Many of the subcellular laser scissors effects are likely due to nonlinear multiphoton-induced UV-like

photochemistry or optical breakdown due to the generation of microplasma with a high electric field and consequent acousto-mechanical effects.[67]

The combination of laser microdissection with laser trapping enables even more interesting experiments not only in cell and developmental biology but also in the entire field of molecular medicines.[68-70] Laser cutting is frequently used to dissect biological material. Using highly restricted laser focal spot, drilling holes not only into living mammalian cells, embryos, or plant cells but also microsurgery within living specimens is possible without destroying their viability. The pioneers in using pulsed UV lasers for microsurgery were Michael Berns in Irvine, California and Bereiter-Hahn in Frankfurt, Germany.[62] In developmental biology, laser microsurgery is used to study single cells or organelles to follow the subsequent behavior of the treated cells or small organisms.[69]

After initial work of laser assisted microdissection in the late 70's, first in 1996, UVA laser assisted capture of small samples from routinely formalin fixed, archival tissue for subsequent genetic analysis was reported.[71] In this early work, laser microdissection was used to ablate the surrounding of the selected specimen in order to avoid contamination during the capture with routine syringe needles, which clearly speeded up specimen capture. But, mechanical tools were still required. The major advance in laser based microdissection came with the invention of laser pressure catapulting (LPC). It is an interesting technology that allows precise capture of pure cell populations from morphologically preserved cells and tissue sections without any mechanical contact, solely by the force of the focused laser light.[72] With a single laser pulse, the selected sample can be ejected out of the object plane and transported over

centimeter-wide distances into an appropriate collection vial. This process was named LPC. The basics of LPC are believed to be a gas pressure force developing under the specimen caused by laser ablation due to the extremely high photon density within the focal laser spot.[62] Depending on specimen, it is sometimes advisable to do microdissection before catapulting to avoid contamination with neighboring tissue. Since the invention of LPC, much research work has been done using either direct catapulting or a combination of laser capture microdissection and catapulting: LCMC.[62] Figure 2 shows an example of LCMC using a PALM microbeam system developed by Zeiss, Germany for LCMC. Using this system hepatic cell area from mouse tissue section was captured.[62]

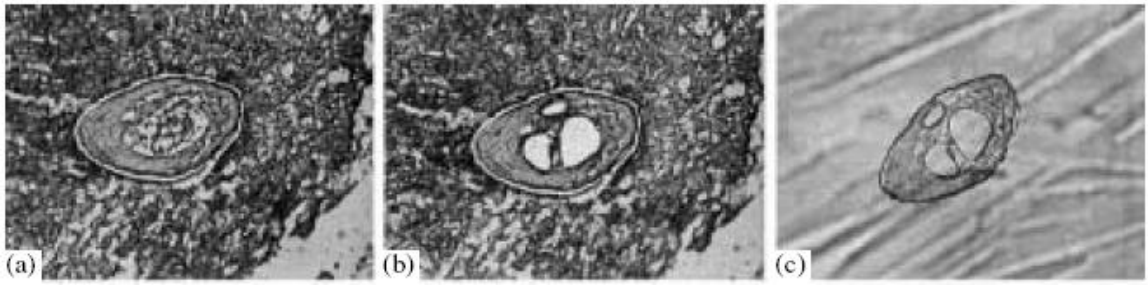


Figure 2. Laser microdissection of hepatic cell areas from mouse tissue section. (a) Circumcision of the cell area of interest; (b) ablation of unwanted cell areas; (c) with a single laser shot, the specimens are ejected from the slide and catapulted into the cap of a microfuge tube and are visualized in the microfuge cap. (Reproduced from Thalhammer *et al.*[62])

In one of such interesting applications of LCMC, R. Hobza *et al.* used 337 nm nitrogen laser for chromosome dissection and collection. Energy of 1.5-11.7 μJ/pulse was used for dissection and 2 μJ/pulse was used for catapulting.[73]

# 2. PRINCIPLES OF OPTICAL TRAPPING

## 2.1. Forces involved in optical trapping

Optical traps use radiation pressure, a term that refers to forces imparted to matter by the absorption, scattering, emission, or reradiation of light (i.e. by photons). The most familiar form of the force is the scattering force, which is defined as the force due to light scattering that is proportional to the light intensity, and acts in the direction of the propagation of light. This force may also be viewed as the force exerted as a consequence of the momentum delivered by the scattered photons. Optical tweezers, however, owe their trapping to the gradient force, which instead is proportional to the spatial gradient in light intensity and acts in the direction of that gradient. This force arises from fluctuating electric dipoles that are induced when light passes through the transparent objects, which consequently experience a time-averaged force in the direction of the field gradient. It can be further elucidated by taking two limiting cases, one based on ray optics for particles in the Mie regime (where the diameter of a particle is much larger compared to wavelength $\lambda$ of the light, $d >> \lambda$) and the other based on the electric field associated with the light for Rayleigh particles (where the diameter of a particle is much smaller compared to wavelength $\lambda$ of the light, $d << \lambda$). Particles in the Rayleigh and Mie regimes compared to $\lambda$ can be seen in Figure 3.

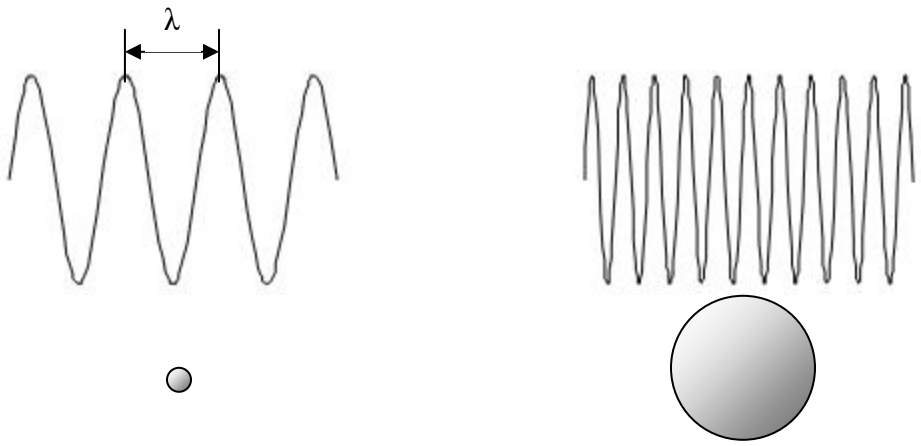


Rayleigh Regime Mie Regime

Figure 3. Rayleigh and Mie regimes. In the Rayleigh regime the particle is much smaller than the wavelength of light and in the Mie regime the particle is larger than the wavelength of light.

Even though these theoretical models are useful to suggest improvements in experimental geometry and choice of trapping material, they will probably never replace direct measurements because of sensitivity of optical forces to small perturbation in geometry. To date, force calculations have dealt only with spherical dielectrics, primarily because electromagnetic models for other geometries are harder to compute.[15]

Optical forces are customarily defined by the relationship,

$$F = \frac{Q n_m P}{c}, \qquad (2.1)$$

where, $Q$ is a dimensionless efficiency and represents the fraction of power utilized to exert force, $n_m$ is the index of refraction of the suspending medium, $c$ is the speed of light and $P$ is the incident laser power.

### 2.1.1. Mie regime

When the trapped sphere is much larger than the wavelength of the trapping laser, i.e. the diameter d >> λ, the conditions for Mie scattering are satisfied. For this case, optical forces can be calculated using simple ray optics.[74] Building on the work of Roosen,[75] Ashkin computed the resultant optical force for the Mie regime.[3] The effect of a laser beam on a transparent sphere can be modeled using a bundle of rays. A photon of wavelength λ has a momentum $p = h/\lambda$ (or $\hbar k$) where $h$ is Planck constant, $\hbar$ is $h/2\pi$, and $k$ is the wave number. If an object causes light to change direction for instance on reflection or refraction which corresponds to change in the momentum carried by light, by Newton's third law, an equal and opposite momentum change will be imparted to the object. This force is proportional to light intensity. When the index of refraction of the object is greater than that of surrounding medium, the optical force arising is in the direction of the intensity gradient. This force is not large enough to move macroscopic objects. However, the forces involved in the transfer of momentum from focused laser light to microscopic objects are of the order of piconewtons and can move micron sized particles.

Within the Mie regime, if a transparent microscopic particle is situated within a gradient of light, the refraction of rays of differing intensity (due to the gradient) through the particle results in a change in total momentum of the exiting light beam, and hence a corresponding reaction force on the particle, which draws the particle into the region of the highest light intensity of the beam (Figure 4). An equilibrium position is reached and

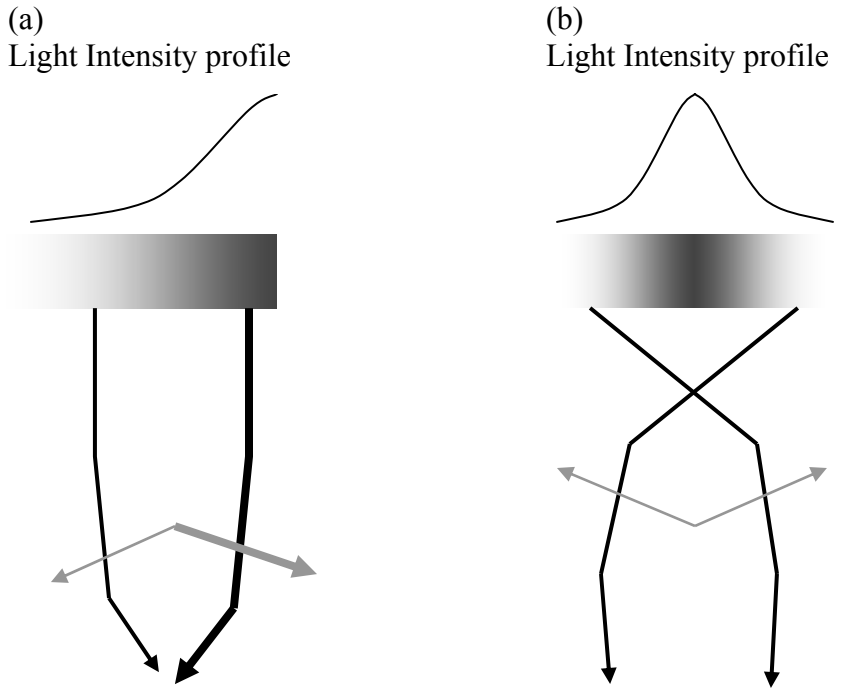


Figure 4. Ray optics description of the gradient force. (a) A transparent sphere is illuminated by a parallel beam of light with an intensity gradient increasing from left to right. Two representative rays of light of different intensities (represented by black lines of different thickness) from the beam are shown. The refraction of the rays by the sphere changes the momentum of the photons, equal to the change in the direction of the input and output rays. Conservation of momentum dictates that the momentum of the bead changes by an equal but opposite amount, which results in the forces depicted by gray arrows. The net force on the sphere is to the right, in the direction of the intensity gradient, and slightly down. (b) To form a stable trap, the light must be focused, producing a three-dimensional intensity gradient. In this case, the sphere is illuminated by a focused beam of light with a radial intensity gradient. Two representative rays are again refracted by the sphere but the change in momentum in this instance leads to a net force towards the focus. Gray arrows represent the forces. The lateral forces balance each other out and the axial force is balanced by the scattering force (not shown), which decreases away from the focus. If the sphere moves in the focused beam, the imbalance of optical forces will draw it back to the equilibrium position. (Reproduced from Neumann *et al.*[5])

the particle is held in the centre of the beam as the rays of light passing through and existing the particle are balanced with no overall change in momentum of the beam. This trapping force is due to the transverse gradient force which is a result of the Gaussian

intensity distribution of the laser mode, however, an axial gradient force is also required in order to lift the particle and manipulate it in three dimensions.

A three dimensional trap or so-called optical tweezers is a result of axial trapping in the z (vertical) direction. It is created by the tight focusing of the laser beam which results in the axial gradient force. Off-axis rays come in at an angle towards the particle and gain momentum in the direction of beam propagation. This change in momentum leads to a force which pushes the sphere upwards against the direction of beam propagation towards the focal region of the beam resulting in a trapping force in the z-direction, and thus, a three dimensional optical trap (Figure 4(b)). The equilibrium position is reached when the scattering force and gravity (which both act to push the sphere downwards) is balanced by the axial gradient force (which pushes the sphere upwards). On axis rays are unfavorable to the axial trapping ability of the tweezers. When the laser beam is directed into the sample from above, the reflected (or backscattered) component of the on-axis rays gives rise to radiation pressure and exerts a force on the particle in the direction of beam propagation. This results in the particle being pushed downwards, away from the beam focus. Thus, axial rays contribute destructively to the axial gradient force. Therefore, expanding a Gaussian laser beam to slightly overfill the objective entrance pupil can increase the ratio of trapping to scattering force, resulting in improved trapping efficiency.[5,76]

### 2.1.2. Rayleigh regime

In the Rayleigh regime, where d << λ, the ray optics approach is not sufficient to calculate forces, as only a fraction of the wave has an effect on the particle.(Figure 3) It is advisable to consider the force in terms of the electric field in the region of the trapped particle. When a polarizable particle is placed in an electric field it will develop an electric dipole moment in response to the light's electric field and therefore can be treated as induced point dipole.[15] However, a focus can not be represented as a point, but as a diffraction-limited region whose overall dimensions are close to λ.[15] Particle's trapping forces decompose naturally into two components. For this limit the electromagnetic field is uniform across the dielectric particle. The scattering force $F_{scat}$ and gradient force $F_{grad}$ are given by equation 2.2 and 2.4, respectively,[11,15,77]

$$F_{scat} = \frac{I_0 \sigma n_m}{c}, \tag{2.2}$$

where, $$\sigma = \frac{128\pi^5 r^6}{3\lambda^4}\left(\frac{m^2-1}{m^2+2}\right)^2, \tag{2.3}$$

and $$F_{grad} = -\frac{2\pi\alpha}{c n_m{}^2}\nabla I_0, \tag{2.4}$$

where, $$\alpha = n_m{}^2 r^3\left(\frac{m^2-1}{m^2+2}\right), \tag{2.5}$$

where, $I_0$ is the intensity of incident light, λ is the wavelength of light in the medium, $\sigma$ is the scattering cross section of the sphere, $n_m$ is the refractive index of medium, $m$ is the relative index of refraction (the ratio of the index of refraction of the particle to the index of refraction of the medium $n_p / n_m$).[5,1]

### 2.1.3. Intermediate region

When the dimensions of the trapped particle are comparable to the wavelength of the trapping laser (d ~ λ), neither the ray optics nor the point dipole approach is valid. Unfortunately, most biological particles fall into this intermediate size range (0.1-10 λ). As a matter of fact, it can be practically difficult to work with objects smaller than that can be readily observed by video microscopy (0.1 μm), although particles as small as ~35 nm in diameter have been successfully trapped.[5] Dielectric microspheres used as handles to manipulate other objects are typically in the range of ~0.2-5 μm, which is the same size range as biological specimens that can be trapped directly, e.g. bacteria, yeast, and organelles of larger cells. Some theoretical progress in calculating the optical force in this intermediate region has been made,[78] but unfortunately more general description does not provide insight into the physics of optical trapping.

Not long ago, Chaumet and Nieto-Visperinas obtained an expression for the total time averaged force on a sphere in the Rayleigh regime[79]

$$< F^i >= (\frac{1}{2}) \mathrm{Re}[\alpha E_0 \partial^i (E_0^j)^*], \qquad (2.6)$$

where, $\alpha = \alpha_0 (1 - \frac{2}{3} ik^3 \alpha_0)^{-1}$ is a generalized polarizability that includes a damping term, $E_0$ is the complex magnitude of the electric field, $\alpha_0$ is the polarizability of a sphere given by equation (2.5), and $k$ is the wave number of the trapping laser. This expression contains the separate expressions for the scattering and gradient components of the optical force (Equation (2.2) and (2.4)) and can be applied to the description of the use of the coupled dipole moment.[80] The Rayleigh theory predicts the forces comparable to those calculated with the more complete generalized Lorenz-Mie theory (GLMT) for spheres of diameter up to $\sim \omega_0$ (the laser beam waist) in the lateral dimension, but only up to ~0.4λ axial dimension.[81] More general electrodynamic theories have been implemented to solve for the case of the spheres of diameter ~λ trapped with tightly focused beams.

One approach to calculate forces in intermediate region has been to generalize the Lorenz-Mie theory describing the scattering of a plane wave by a sphere to the case of Gaussian beams. Fifth-order corrections to the fundamental Gaussian beam were used to derive the incident and scattered fields of sphere, which enabled the force to be calculated by means of stress tensor.[82,83] The time-averaged force due to an arbitrary electromagnetic field, acting on an arbitrary particle, is given by the following integral over the surface enclosing the particle,[15]

$$\vec{F}_i = \left\langle \oint_s \vec{T}_{i,j} \vec{n}_j \, da \right\rangle, \qquad (2.7)$$

where $\vec{T}_{i,j}$ is the Maxwell stress tensor, $\vec{n}_j$ is the outward unit normal vector, and the brackets denote a temporal average.

Another approach implemented by Gouesbet *et al.*, expands the incident beam in an infinite series beam shape parameters from which radiation pressure cross-sections can be computed.[84] More recently, Rohbrach *et al.* extended the Rayleigh theory to larger particles through the inclusion of second-order scattering terms, valid for spheres that introduce a phase shift, $k_0(\Delta n)D$, less than $\pi/3$, where $k_0 = 2\pi/\lambda_0$ is the vacuum wave number, $\Delta n = (n_p - n_m)$ is the difference in refractive index between the particle and the medium, and $D$ is the diameter of the sphere.[78] For polystyrene beads ($n_p$ = 1.57) in water ($n_m$ = 1.33), this amounts to a maximum particle size of, ~0.7λ. In this approach, the incident field is expanded in plane waves, which permits the inclusion of apodization and aberration transformations, and the forces are calculated directly from the scattering of the field by the dipole without resorting to the stress tensor approach.[5] Computed forces and trapping efficiencies compare well with those predicted by GLMT, and the effects of spherical aberration have been explored.[78] Since the second-order Rayleigh theory calculates the scattered and unscattered waves, the far field interference pattern, which is the basis of the three-dimensional position detection, can be readily calculated.[85,86]

## 2.2. Trap efficiency

The force on a spherical particle of radius $r$ in viscous medium of viscosity $\eta$, when the particle is more than a few diameters away from the sample cell walls (Stokes' law) is given by[87]

$$F_i = 6\pi\eta v_i r \,, \tag{2.8}$$

where, $\eta$ is the viscosity of the medium, $v_i$ is the fluid velocity, with $i = (z, r)$. The maximum force that the optical trap can exert at the specified laser power is given by $F_i$. This force can be derived by moving the particle at the critical velocity $v_c$ at which the trapping was no longer active i.e. particle escaped from the trap.[88] The critical velocity of the trapped particle scales linearly with the laser power in the optical trap (as shown in eq. 2.9). The trapping efficiency of any optical tweezers configuration is usually described in terms of a dimensionless parameter $Q$, the fraction of momentum transferred to the trapping force from the trapping laser beam, which is related to the force on the sphere, $F_{stokes}$, the power of the laser, $P$, and the refractive index of the surrounding medium, $n_m$, through the equation,

$$F_{stokes} = \frac{Q n_m P}{c} \,. \tag{2.9}$$

Possible values of $Q$ range between 0 and 1. A $Q$ value of 1 corresponds to all of the light beam's momentum being transferred to the particle. Optical tweezers configurations can be examined experimentally to determine the $Q$ values for trap efficiency in the lateral and axial directions. For optical forces acting on small dielectric

particles $Q$ values tend to be in the range 0.03 to 0.1.[89] Within conventional optical tweezers, the lateral trapping force ($Q_{lateral}$) is typically one order of magnitude greater than the axial trapping force ($Q_{axial}$).[87]

## 2.3. Trap stiffness

Most force measurements have been made using variations of the escape-force method as described in the last section (finding critical escape velocity). Convenience, sensitivity, and versatility, however, can be greatly enhanced if the force is instead determined as a function of the displacement from the trap. The displacement of the trapped object from the centre of the trap, under an applied viscous fluid force can be monitored using a position sensitive detector.[88,90] This determines the spring (elastic) constant, in other words the stiffness of the optical trap. The stiffness of the optical tweezers can also be calculated from analysis of the thermal motion of the trapped object. Trap stiffness tends to be in the range 0.001 to 1 pN/nm depending on the application.[90] Optical tweezers can also be placed under feedback control so that any particle movement out of equilibrium position can be immediately corrected by repositioning of the trap itself, so that the particle remains stationary within the trap. It is necessary to measure optical trap stiffness before investigating very low forces such as those in biological processes. Biologists are mainly concerned with measuring trap stiffness so that molecular forces can be measured, whereas physicists are more interested in the $Q$ value of an optical trap (efficiency).

## 2.4. Additional forces in optical tweezers

The gradient force is the central force in the operation of all optical tweezers and provides a restoring force which, over distances up to several hundred nanometers, is linear function of displacement $x$. The equation of motion which governs the behavior of a trapped object of mass $m$, in medium that gives a viscous damping $\beta$ is a balance between inertial, viscous, and elastic forces[89]

$$m\frac{\partial^2 x}{\partial t^2} + \beta\frac{\partial x}{\partial t} + \kappa x = 0, \qquad (2.10)$$

where $\kappa$ is the elastic constant or the stiffness of the optical trap. In the absence of any damping (i.e. in air or in vacuum) the result would be oscillatory with resonant frequency

$$f_{res} = \frac{1}{2\pi}\left(\frac{\kappa}{m}\right)^{1/2}. \qquad (2.11)$$

In typical biological applications, the stiffness is around 0.05 pN/nm and the trapped object are around 1 μm diameter (corresponding to a mass of $5 \times 10^{-16}$ kg).[82] Hence, $f_{res}$ is approximately 50 kHz. Biological experiments are generally made in aqueous medium which results in significant damping force. Strokes drag constant $\beta$ is given by equation (2.8). The combination of viscous damping and the spring like stiffness gives rise to a single pole low pass filter with -3 dB frequency $f_0$ given by,

$$f_0 = \frac{\kappa}{2\pi\beta}. \qquad (2.12)$$

For typical biological application Molloy *et. al* found the roll-off frequency well below 1kHz. As this is much lower than the resonant frequency, the motion is

overdamped. This means that inertial and gravitational forces can be neglected altogether.[89] In addition to providing damping, the surrounding fluid also works as a coolant minimizing the heating effect of the laser light.

# 3. A STANDARD TWEEZERS CONFIGURATION

Although optical tweezers can be commercially obtained, they are also surprisingly simple to assemble by anyone with an expertise in building optical systems. For many cell biology laboratories, a basic laser tweezers system capable of picking up cells, beads, or other microscopic objects and planning them at appropriate places is sufficient. This basic system would include a low-power infrared (IR) lasers, mirrors, and focusing lenses, which can be added to a good research microscope for $10,000-$20,000.[91] Given that an optical tweezers has many of the components used in common microscopes, a research grade microscope represents a good starting point for a custom built instrument.

## 3.1. Microscope basics[91]

Any high quality microscope with an equi-illumination port can have laser tweezers added to it, but fluorescence microscopy is compromised. For simultaneous fluorescence and tweezers microscopy, an inverted microscope with a bottom port is commonly used (Figure 5). There are three critical considerations for the microscope: (a) a dichroic mirror to reflect the IR laser beam and pass the video light, (b) a high numerical aperture (NA) objective (1.0 or higher NA), and (c) the stability of the stage and the coupling between the video camera and the microscope.

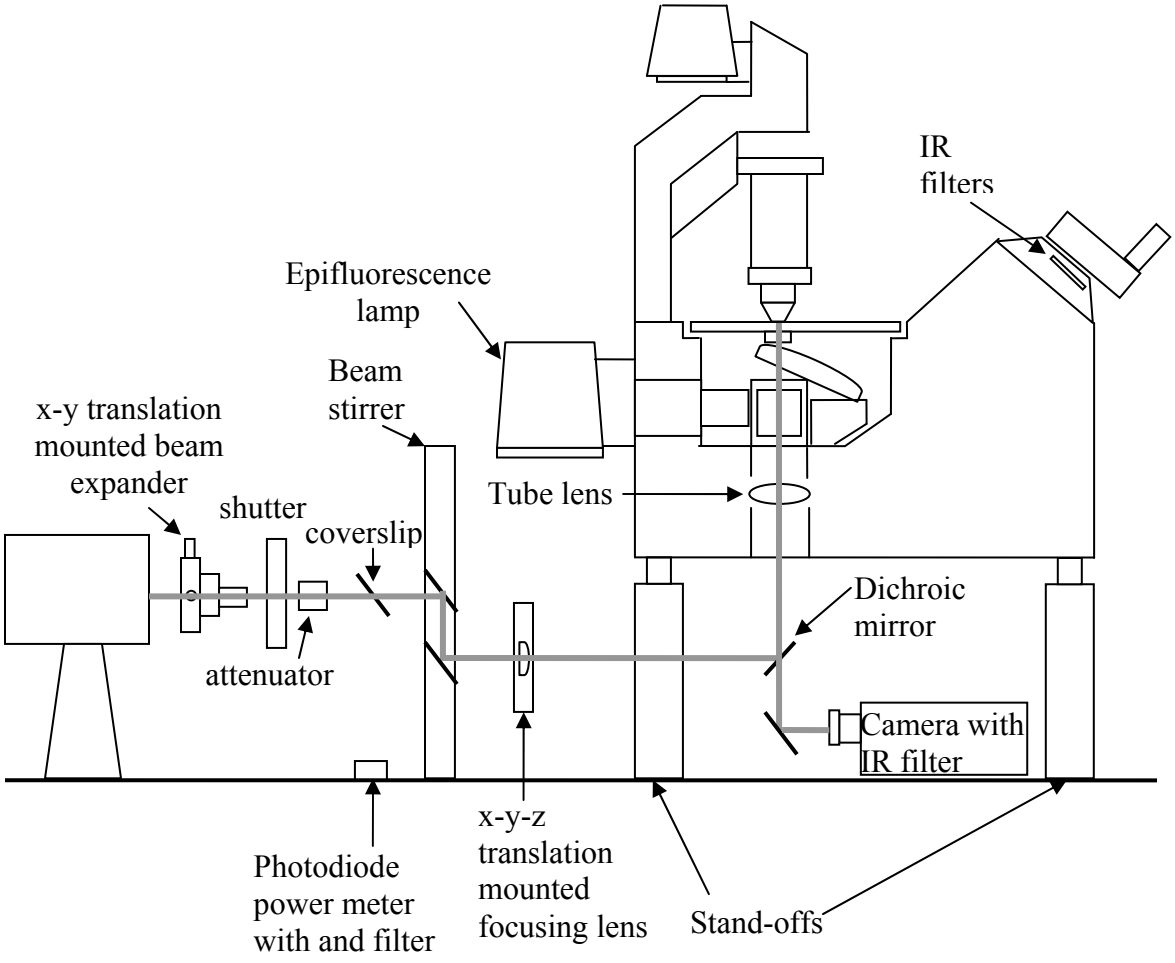


Figure 5. Trapping system using bottom port for laser access allowing use of epifluorescence lamp. (Adapted from Berns *et al.*[91])

### 3.1.1. Dichroic mirror

The dichroic mirror is very important as it should reflect the laser light while letting the transillumination light pass through to the camera. Several dichroic mirrors are available from different optics firms for the IR region. While choosing the dichroic mirror, one should choose the dichroic mirror having the wavelength of maximum reflectance that matches the wavelength of laser light. The wavelength dependence of the

transmission of light by the dichroic mirror should be known to avoid loss of transmitted light. For simultaneous fluorescence and tweezers microscopy, a dichroic holder should be machined for the bottom part of the microscope. This dichroic holder should reflect all visible light to the camera and pass the laser light into the bottom port.

### 3.1.2. Objective lens[92]

The objective lens used in the microscope is another important component of the tweezers system. The basic function is to gather the light passing through the specimen and then to project an accurate, real, inverted image of the specimen on the camera plane. In case of optical tweezers it also focuses the laser light at a sufficient gradient angle to form an effective trap. The objective with high transmittance and NA $\geq$ 1 is typically used.[15] The choice of objective determines overall efficiency of the optical trapping system. Due to the importance of objective, related terminology is discussed here in more detail.

Modern objectives are made up of many glass elements. Modern technology has reached a high state of quality and performance. The extent of corrections and flatness of the image field determines the usefulness and cost of the objective. The least expensive objectives are generally achromats and they are corrected to bring red and blue light to a common focus. The next higher level objectives are fluorites and are corrected chromatically for two colors red and blue with green not so separate. They are better suited for color photomicrography.[92] The highest level of objectives is apochromatic objective. These objectives are corrected chromatically for four colors deep blue, blue,

red and green; they are spherically corrected for two or three colors: deep blue, blue, green. They are the best objectives for color recording and viewing. These objectives have generally higher NA than do achromats and fluorites and therefore, are the best choice for the optical tweezers system.[92]

There are two types of aberrations for which the objective should be corrected. a) Chromatic aberration: The various color frequencies (or wavelengths) of white light pass through an uncorrected convex lens and, instead of being brought to a common focus, come to different foci (Figure 6). The lens designer makes every effort by combining various kinds of glass and lens elements of different shapes, to bring the main colors of red, green, and blue to a common focus.

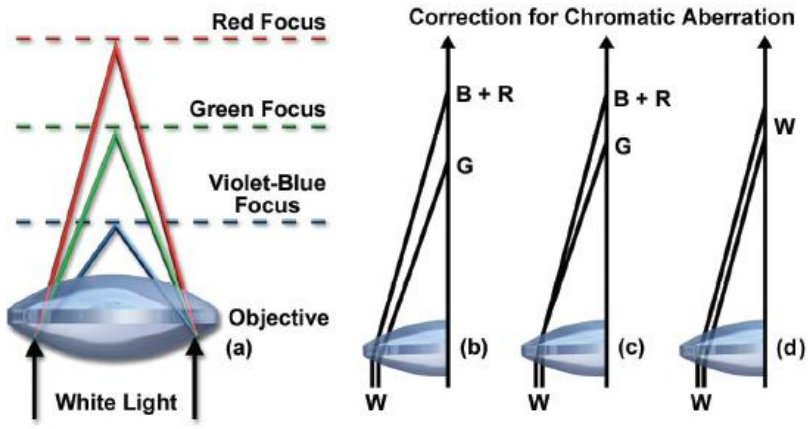


Figure 6. Chromatic aberrations. (a) Chromatic aberration of white light. A simple lens fails to bring light of different wavelengths to a common focus. (b) Achromatic lens. Green is brought to the shortest focus. The color error is much reduced. (c) Fluorite lens. The color error is similar to (b) but still further reduced. (d) Apochromatic lens. For all practical purposes chromatic aberration may be considered eliminated. (Reproduced from Abramowitz.[92])

b) Spherical aberration: Light passing through an uncorrected convex lens will be brought to different foci depending upon whether the light passes through nearer the center of the

lens or closer to the periphery. Lens designers rectify this kind of zonal aberration by using lens elements of different shapes to bring the more central and more peripheral rays to common focus.

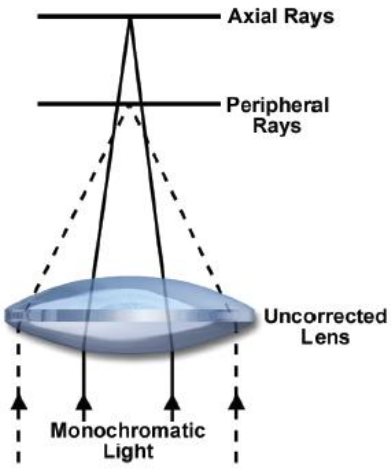


Figure 7. Spherical aberration. Failure of the lens system to image central and peripheral rays at the same focal point arises with spherical lenses. Optical correction is possible, but care must be taken not to introduce additional spherical aberration when setting up the microscope. (Reproduced from Abramowitz.[92])

Spherical aberrations, which degrade trap performance, are related to the refractive index mismatch between the immersion oil and the aqueous trapping medium. The degrading effect of these aberrations increases with focal depth. Working distance and the immersion medium of objective (oil water or glycerol) will set practical limits on the depth to which object can be trapped. The working distance of most high NA oil immersion objective is quite short (0.1 mm), and the large refractive index mismatch between the immersion oil ($n$~1.512) and the aqueous medium leads to significant spherical aberrations. Often particles escape the trap when the focal point is over 20 μm from the glass surface.[91]

Numerical aperture of an objective plays a significant role in determining the amount of useful magnification. The ability to distinguish clearly minute details lying close together in the specimen is known as resolving power. It deteriorates by diffraction and scattering of light as it passes through minute parts and spaces in the specimen and the circular back of the objective, resulting in the Airy disks. Airy disks consist of small concentric light and dark circles at the plane of image.

The ability of an objective to include or "grasp" the various rays of light coming from each illuminated part of the specimen is directly related to the angular aperture of the objective. Objectives with lower angular aperture can include only a narrower cone of light as compared to objectives with higher angular aperture. The equation for numerical aperture (N.A.) is

$$N.A. = n\sin(\mu), \qquad (3.1)$$

where, $N.A.$ is the numerical aperture, $n$ is the index of refraction of the material in the object space, i.e. the space between the specimen and the front (lowest) lens of the objective. The $\mu$ is 1/2 the angular aperture of the objective.[85] There are two ways by which one can increase N.A., by increasing angular aperture and by using immersion oil. Since $\mu$ cannot exceed 90°, $\sin(\mu)$ must be 1 or less. Since a "dry" objective is used with air in the object space (n for air is 1.00+), the maximum theoretical N.A. of a "dry" objective is 1; in practice, not more than 0.95. Increasing the angular aperture of an objective increases μ and thus increases $\sin(\mu)$ and thus increases numerical aperture. Since immersion oil has a refractive index of 1.515, it is theoretically possible to utilize

oil immersion objectives which can yield a numerical aperture of 1.5; in practice, not more than 1.4. Figure 8 shows how immersion oil helps grasp rays from the specimen. Optical tweezers for this very purpose implement oil immersion objectives to obtain higher N.A.[92]

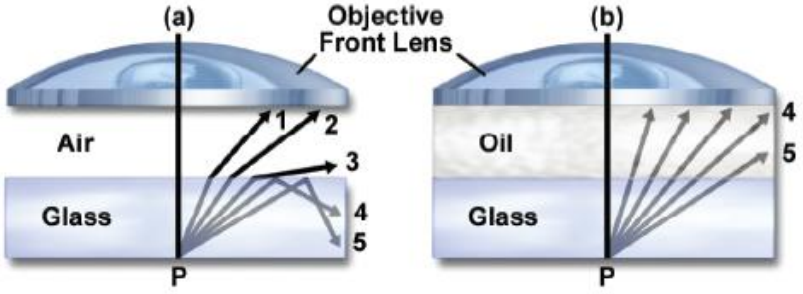


Figure 8. The principle of oil immersion. (a) Five rays are shown passing from the point P in the object through the coverslip into the air space between the latter and the lens. Only rays 1 and 2 can enter the objectives. Rays 4 and 5 are totally reflected. (b) The air space is replaced by oil of the same refractive index as glass. The rays now pass straight through without deviation so that rays 1, 2, 3, and 4 can enter the objective. The N.A. is thus increased by the factor n, the refractive index of oil. (Reproduced from Abramowitz.[92])

A high NA objective (typically, 1.2-1.4 NA) is required to produce an intensity gradient sufficient to overcome the scattering force and to produce a stable optical trap.[5] The vast majority of high NA objectives are complex optical assemblies specifically designed for imaging visible light, and not for focusing infrared light. Therefore, the optical properties of different objectives can vary widely over the near infra red region.[93]

### 3.1.3. Stability

For optical tweezers applications, the microscope must have a stable stage and very good coupling between the video camera system and the microscope. Any vibration

of the stage, particularly vertical instability will cause particles to be lost from the tweezers. Furthermore, thermal stage drift, mechanical backlash and hysteresis from piezo-electric positioners are some other considerations one should remember while choosing the microscope and related system. Motorized mechanical stages can be used, but have limitation of large step size commonly as large as 150 nm. For more precise movement piezo-electric stage can be used. For the measurement of small displacements using a video camera, the video camera system should be attached firmly without any relative movement between the video camera system and the microscope.

## 3.2. Laser and opticution

Since the first demonstration of optical trapping by Ashkin, applications of it have arisen in biology, both *in vivo* and *in vitro*. Optical trapping comes with one inherent drawback. Intense trapping laser light used for trapping produces photodamage in the trapped microparticle. In practice, such damage limits the exposure time for trapped specimens and has proved to be a significant problem for some optical trapping studies, particularly those *in vivo*. Indeed, Ashkin first encountered this problem and coined the colorful term "opticution" to describe the laser-induced death of specimens.[94] The potential for damage is readily appreciated by computing the light level at the diffraction-limited focus of a typical trapping laser: for a power of just 100 mW, the intensity is 107 $W/cm^2$, with an associated flux of 1026 photons/s.$cm^2$ (traps used in cell biology are generally based on lasers producing from 25 mW to 2 W in the specimen plane).[93] Proposed mechanisms for photodamage include transient local heating,[95] two-photon

absorption,[95-97] and photochemical processes leading to the creation of reactive chemical species.[15,95,98]

The selection of laser system should take into consideration requirements of wavelength, laser power, beam pointing stability, beam mode quality, low power fluctuations, and noise. Pointing instability leads to unwanted displacements of the optical trap positions in the specimen plane, whereas, power fluctuations lead to temporal variations in the optical trap stiffness. As discussed above, this system should inflict minimum or no opticution. Wavelength is an important consideration when biological material is trapped, particularly *in vivo* trapping of cells and organisms. There exists a window of transparency for biological material which arises from two opposing trends (Figure 9). First, natural biological chromosphores, such as hemoglobin or the ubiquitous cytochromes, absorb increasingly less light towards the near infrared, dropping out beyond wavelengths of ~800 nm. Second, water absorption rises dramatically as one farther into infrared, peaking around 3 μm.[15] Therefore, there is a window of relative transparency in the near infrared portion of the spectrum (~750-1200 nm).[5] Substantial variation in optical damage to biological specimens is observed even with a small variation in wavelength within near infrared region.[93]

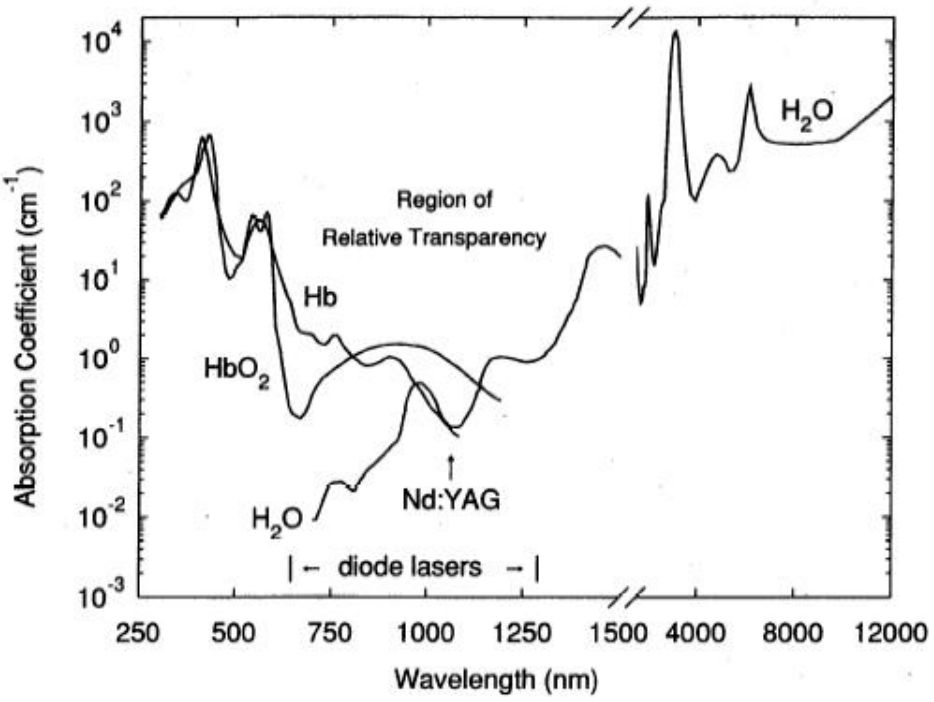


Figure 9. A graph illustrating the relative transparency of biological material in the near infrared region, showing the absorption of water and some common chromosomes as a function of wavelength. Hb and $HbO_2$ stand for deoxyhemoglobin and oxyhemoglobin, respectively (at concentration of $2 \times 10^{-3}$). Note the break in scale. (Reproduced from Svoboda *et al.*[15])

To form a stable trap, the laser light should be continuous output low noise beam that can be focused to as small a focal point as possible. The diameter of smallest focal point will be on the order of the wavelength of the light and is described as a diffraction limited spot.[91] The laser beam must be a single Gaussian peak with minimal side bands to form a diffraction limited spot in the sample plane. This single peak is known as single mode or $TEM_{00}$. A laser with a continuous output is known as a continuous wave or CW laser. Laser systems which are not of continuous-wave type are described as Q-switched or mode-locked lasers and have a high frequency pulsing output.

A variety of lasers has been employed for trapping in practice. The factors discussed above, along with the cost will determine the final selection of a trapping laser. Currently, laser systems are available commercially in four different types (Table 1).

Table 1. Continuous-wave near-infrared trapping lasers (Reproduced from Berns *et al.*[91])

| Laser type | $TEM_{00}$ power | Wavelength | Price range |
|---|---|---|---|
| Solid state<br>ND:YAG<br>ND:YLF | 100 mW - 10 W | 1064 nm<br>1047, 1057 nm | $5000-$40,000 |
| Ti:sapphire | 2 W | 650-1100 nm<br>Continuous<br>Tunable | $20,000-$30,000,<br>not including argon or Nd:YAG laser |
| Semiconductor laser diode | 5-250 mW | 780-1020 nm | $5--$1000, not including power supply |
| Semiconductor<br>MOPA laser<br>(SDL Inc.) | 1 W | 985 nm | $10,000, not including power supply |

The most preferred choice of laser for biological application is neodumium:yttrium-aluminium-garnet (Nd:YAG) laser and its counterparts, neodymium:yttrium-lithium-fluoride (Nd:YLF), and neodymium:yttrium-orthovanadate ($Nd:YVO_4$). These lasers are available in relatively high powers (1-3 W). These lasers operate in the near infrared region of the spectrum at 1.047, 1.053, or 1.064 μm, which helps to limit photodamage. Diode pumped versions of these lasers offer high power up to 10 W with superior amplitude and pointing stability. An additional benefit of diode-pumped solid state (DPSS) lasers is that the noise and heat of the laser power supply can be physically isolated from the laser itself and the immediate region of the optical trap.

The output of the pump diodes can be delivered to the laser head via an optical fiber bundle, in some cases up to 10 m in length.[5] The main drawback of such DPSS lasers is their cost, currently on the order of *$*5–10 K per W of output power.[5]

The second laser system type is a CW tunable Ti: sapphire laser system. It has the advantage of being tunable over a range in the near infrared (NIR) laser from 650 nm to 1100 nm. This large tuning range is useful for parametric studies of optical trapping, to optimize the trapping wavelength, or to investigate the wavelength-dependence of optical damage.[93] This system has been employed for optical trapping *in vivo*,[99] since it is the only system available that can deliver over ~250 mW at the most benign wavelengths (830 and 970 nm).[100] The only disadvantage of this system is cost which is $100 K or more for the entire system.[5]

The third laser system type is the low power but inexpensive CW single-mode diode laser system. A forward-biased p-n junction will emit photon that lases in a reflective cavity. The lasing photons are directed by a wave guide constructed of layers of material with different refractive indices and are emitted from one end of wave guide. The emission divergence of diode laser is elliptical due to manufacturing limitations. But, it can be collimated and circularized using an aspheric lens.[91] Diode laser also suffers significantly from mode instabilities. Therefore it needs precise temperature control instrumentation.

The fourth laser system type is a special type semiconductor laser system described as monolithically integrated master oscillator/power amplifier (MOPA). It is a single-mode collimated laser system integrated with thermoelectric cooling system and

emitting at a single frequency of 985 nm at a power of 1 W. It has advantages of being relatively small, stable, and easy to maintain.

The pulsed laser tweezers, we built for our laboratory employs a diode laser for trapping. The following section discusses the operating principles of laser diodes.

### 3.2.1. Laser diode

Each electron in an atom or molecule has a specific discrete energy level, as shown in Figure 10. The translation of electrons between energy levels is sometimes accompanied by light absorption or emission with the wavelength, $\lambda$, expressed as

$$\lambda = \frac{c}{\upsilon} = \frac{hc}{|E_2 - E_1|}, \qquad (3.2)$$

where, $h$ is Planck constant, $c$ is speed of light, $\upsilon$ is the frequency of absorbed or transmitted light, $E_1$ is energy level before transition, and $E_2$ is energy level after transition.[100]

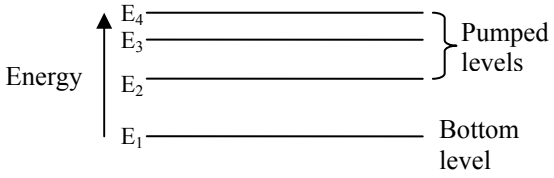


Figure 10. Energy levels.

There are three processes of transition as shown in Figure 11. The first process of transition, shown in fig. 11 (a), is known as resonant absorption. An electron transits from stable low energy level, $E_1$, to the higher energy level, $E_2$, by absorbing light. Figure 11 (b) shows spontaneous emission. An electron transits from high energy level, $E_2$, to a

more stable low energy level, $E_1$. At the same time, energy balance of $|E_2-E_1|$ is released in terms of light. Since each electron at level, $E_1$, transits independently, light is emitted at random and out of phase. Such light is referred to as incoherent light and is one of the typical characteristic of spontaneous emission.

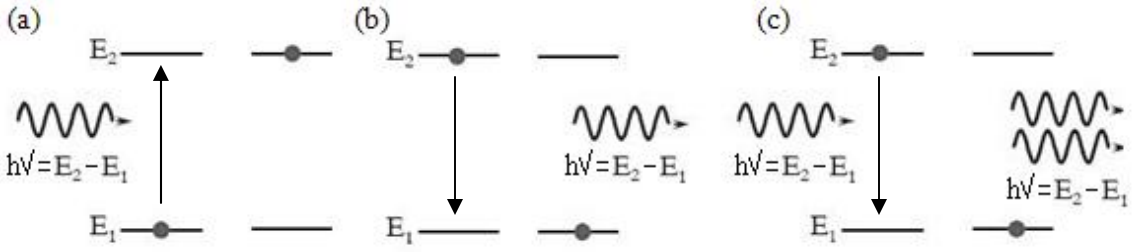


Figure 11. Electronic transition (a) Absorption (b) spontaneous emission (c) stimulated emission.

Under thermal equilibrium, the probability of an electron being in the lower energy level is more than being in higher energy level. Therefore, light absorption is more probable compared to light emission. To emit light, electrons must exist in higher level $E_2$ with high probability, which is referred to as population inversion. The third type of transition, shown in Figure 11 (c), is stimulated emission. The electrons in the higher energy level, $E_2$ are sent to the lower energy level, $E_1$, by incident light. The light generated this time is referred to as stimulated emission light. It has same phase as that of incident light, as stimulated emission light is emitted in resonance with the incident light. Such stimulated emission light is highly coherent.[100]

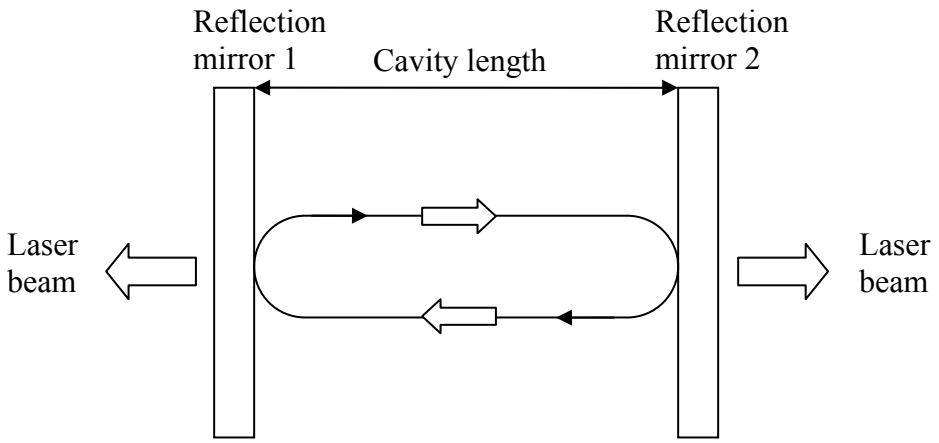


Figure 12. Fabry-Pérot resonator. (Adapted from Hitachi.[100])

The structure of an LD (Laser Diode), in principle, is the same as shown in Figure 12. It uses a Fabry-Pérot resonator for positive feedback to amplify the signal. In this structure, the incident spontaneous emission light heading to the reflection mirror is amplified by stimulated emission process and comes back to initial position after reflection.[100] This process is subject to losses due to diffraction at the reflection mirrors and scattering or absorption within the cavity. When the loss is higher than the amplification gain, signal attenuates. Injected current helps amplification gain in an LD and when the gain and losses are balanced, initial light intensity equals returned light intensity. This condition is referred to as threshold. A laser oscillates above the threshold when the gain is high enough. This principle earned a name as "Light Amplification by Stimulated Emission of Radiation" or LASER.

Injection pumping mainly takes place at the p-n junction in a semiconductor laser diode. A semiconductor crystal can achieve higher gain compared to a gas laser due to

the higher density of atoms available within the cavity. Figure 13 (a) shows the typical GaAlAs laser diode external structure (can type) and Figure 13 (b) shows its element structure.

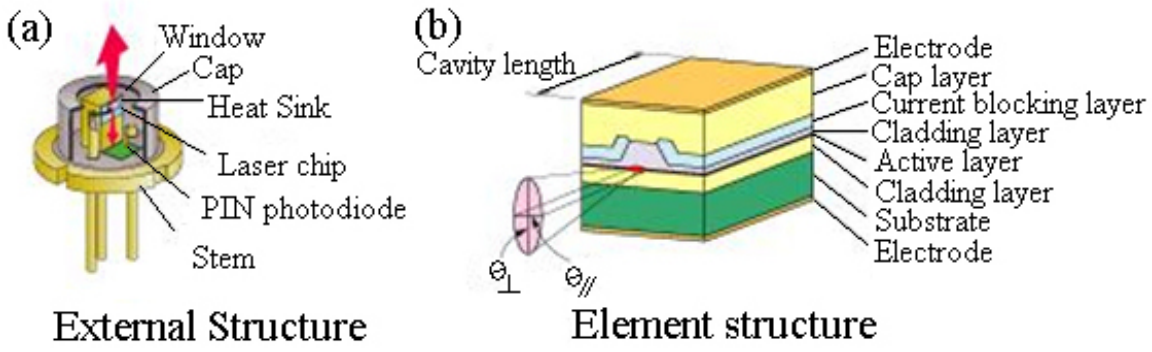


Figure 13. Laser diode (a) External structure (can type). (b) Element structure. (Adapted from http://www.sanyo.com/semiconductors/laser_diode/)

## 3.3 Optics and layout

Mechanical stability is very important for optical tweezers system. For that reason, the optical trapping system must be set up on a vibration isolated optical table. It is easier to work with inverted microscope, because most of the access ports to the objective side of optical path are relatively low and close to the table surface. A dichroic mirror is generally mounted in the 45$^{o}$ mirror position to reflect laser light and pass the imaging illumination.

When working with infrared invisible light it is important to wear laser safety goggles that block the specific laser wavelength. IR wavelengths greater than 800 nm are invisible to eye, an infrared sensor card is used to visualize the beam. These infrared sensor cards fluoresce at visible wavelengths when excited with infrared laser light.

To fine adjust laser light into the microscope a two-mirror beam stirrer is generally used. The mirrors used should be able to reflect at least 95% of light at specific wavelength or the range of wavelengths. A laser beam expander should be used to expand the laser's exit beam diameter to the objective lens back aperture diameter. One can use commercially available beam expanders that come with fixed entrance and exit aperture diameters. Many of them also come with focus control, if not; a corrective lens system can be used to focus. Focus changes the beam divergence and is a convenient way to adjust the trap focus in the sample plane. It is important that both the beam expander and additional lenses be antireflection coated for the laser wavelength to ensure efficient laser transmission and to minimize stray laser light, which is an eye hazard and may also contaminate video camera image.[91]

## 3.4. A CW laser tweezers limitation:

Optical tweezers employing the CW lasers deliver maximum trapping force of the order of 1 pN per 10 mW.[5] The output power of the CW laser is generally less than hundreds of milliwatts.[5] Therefore, typical trapping force range is few piconewtons to maximally few tens of piconewtons. Such a trap is efficient to trap and manipulate particles suspended in medium (Figure 14 (a) and (b)). But, the suspended particles have tendency to get stuck to the coverslip. The stuck particles can not be trapped using the CW laser tweezers (Figure 14 (c)), because the interaction force between such stuck particle and the coverslip is generally few order of magnitude greater than piconewton forces that can be generated using the CW laser trap. Increasing the power of the CW

laser can be a solution that can be applied successfully to some of the particles which are loosely bound (stuck), but the increase in laser power poses greater threat of optical damage to the particle under consideration. To trap the stuck particle efficiently and non-invasively, the pulsed laser tweezers was developed.

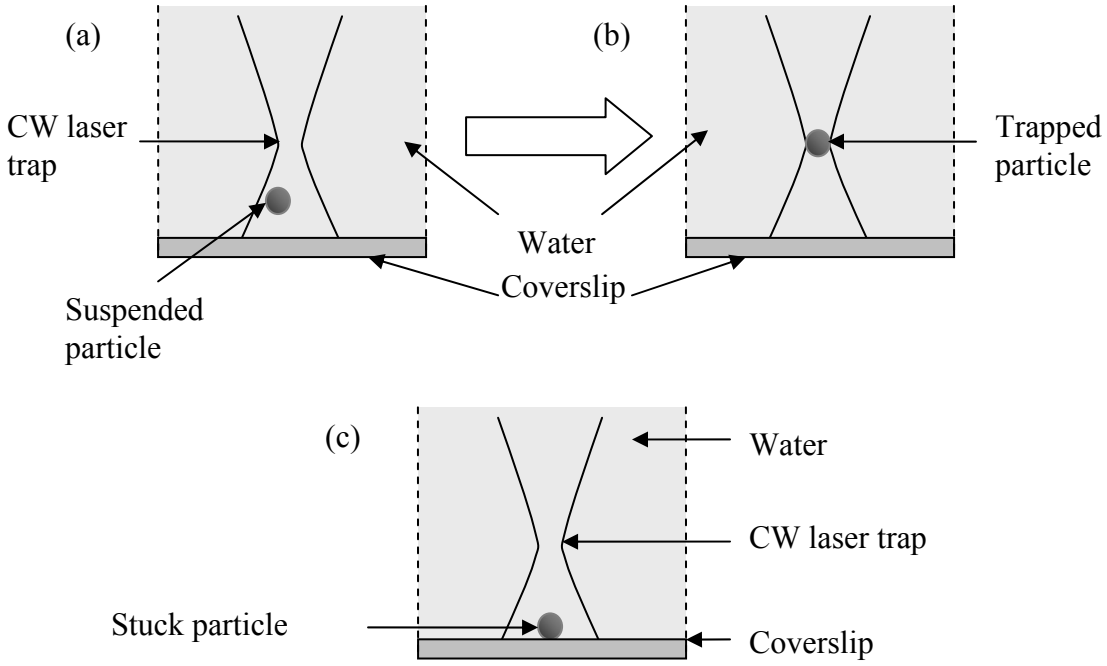


Figure 14. A CW laser tweezers limitation. Figures (a) and (b) show that, when a particle suspended in water is brought near the CW laser trap, it experiences force towards the focus of the CW laser and finally gets trapped. Figure (c) shows a particle stuck to the coverslip can not be trapped using the CW laser tweezers. (Figures not to the scale)

# 4. BUILDING A PULSED LASER TWEEZERS

As explained in the last chapter, a CW laser tweezers fails to trap and manipulate the stuck microparticles. We developed a pulsed laser tweezers which can trap and manipulate the stuck microparticles. A pulsed laser tweezers has all the benefits of the CW laser tweezers with a bonus of ability to manipulate stuck microparticles. Before going into details of the design of the pulsed laser tweezers, it is important to know how pulsed laser tweezers manipulates the stuck microparticles.

## 4.1. Main Idea

A pulsed laser tweezers overcomes the limitations of the CW laser tweezers by implementing the pulsed laser along with conventional tweezers. It is apparent that the force required to levitate the stuck particle can not be realized using a CW laser. To solve this problem, a pulsed laser beam is inserted in the microscope to aid the levitation of the stuck particles. A minimum number of high peak energy pulses is used to deliver the required force to levitate the stuck particles. In most cases, a single pulse does the work. As shown in Figure 15, a pulsed laser tweezers is a combination of the CW laser tweezers with insertion of the pulsed laser beam. Both the laser beams are focused at the same position in the sample plane. When a pulse is applied, high peak power of the pulse generates the required force to detach the particle from the coverslip, and as it is detached, it can be trapped by the CW laser. The fascinating thing about this technique is

that instead of applying high continuous pulses, a minimum number of pulses is used which minimizes the possibility of optical damage to the particle.

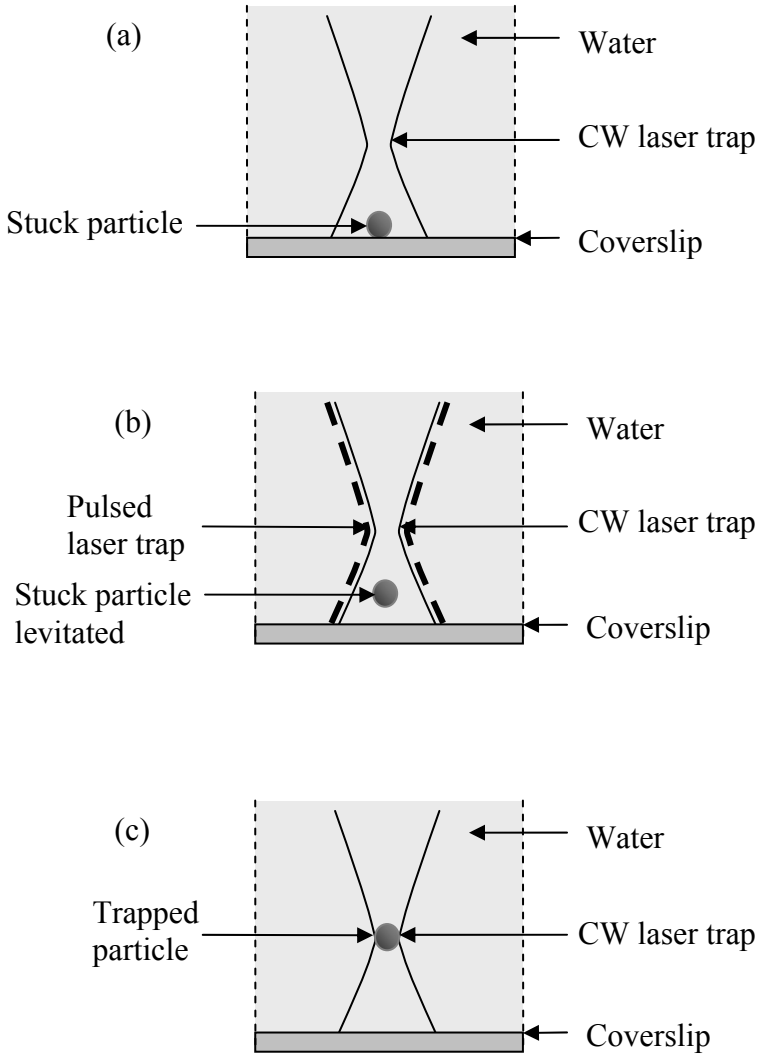


Figure 15. A pulsed laser tweezers. (a) A CW laser trap fails to levitate the stuck particle. (b) A single shot of the pulsed laser levitates the stuck particle. The pulsed laser trap which exists momentarily for the duration of the pulse is shown by dashed line. (c) Such levitated particle gets trapped by the CW laser and can be further manipulated. (Figures not to the scale)

Figure 15 (a) shows the inability of the CW laser tweezers to trap stuck particle. Figure 15 (b) shows that a pulse from the pulsed laser was applied and the stuck particle was detached or levitated from the coverslip. Figure 15 (c) shows that such a levitated particle can get trapped in the CW laser trap. Now this particle could be manipulated easily.

Thus, the pulsed laser tweezers can be used to levitate and manipulate stuck microparticles and of course including suspended particles. This gives a tool to researchers to select any particle in the sample to trap and manipulate. To levitate the particle, the same gradient force comes into play, instead of laser ablation used for microdissection or laser gas pressure used for laser pressure catapulting. During the duration of a pulse, a trap with much higher stiffness compared to the CW laser trap is formed. It forces the stuck particle to levitate. As typical duration of the pulse used in our system was ~45 μs, it posed no threat of optical damage. Pulse energy of typically of the order of 400 μJ was delivered per pulse at the sample plane which corresponds to about ~10 W of peak power. This is hundreds of magnitude greater than the CW laser power which was typically 18 mW at the sample plane, so that the gradient force is increased by hundreds of magnitude in the duration of the pulse.

## 4.2. Design and implementation

This part of thesis covers the design and implementation of the pulsed laser tweezers. The pulsed laser tweezers is a combination of the CW laser tweezers and the

pulsed laser for levitation. Therefore, building the pulsed laser tweezers requires the CW laser tweezers to be built first.

## 4.2.1. A CW laser tweezers

### 4.2.1.1. Modifying a microscope

To build a CW laser tweezers, we modified the inverted microscope with customized parts which housed a dichroic mirror, an optical mirror, a video camera, and an objective. The schematic of the microscope is shown in Figure 16. To decrease the complications, piezo-electric kinematic mount is not included in the schematic. Instead of that a simple sample clamper is shown. Figure 17 is an actual picture of the system which shows the microscope. Figure 16 is a side view and figure 17 is the front view. Custom part 3 which had dichroic mirror attached to it was fixed in custom part 2. The dichroic mirror was positioned at $45^{o}$ angle and reflected laser light into the objective. Custom part 2 was fixed into custom part 1 and in turn custom part 1 was fixed in the microscope. A metallic mirror was fixed at the bottom of the custom part 2 to reflect the sample image from the objective to the video camera. The objective was fixed onto custom part 1 at top. Schematics of all these parts are in appendix A. In Figure 16, the laser beam direction is into the paper towards dichroic mirror where it gets reflected in the objective. An optical image of the sample was captured by the video camera that was attached to the other end of custom part 2. It is the property of a dichroic mirror to reflect laser light and allow visible light to pass. An IR camera filter was used to block laser light entering into camera, giving better visibility of the sample. The video camera was connected to a

monitor (Television) to observe the sample. Custom part 4, shown in Figure 17, was used to hold a piezo-electric kinematic mount (PZKM) for sample holder. Explanation for PZKM can be found in the later part of the thesis.

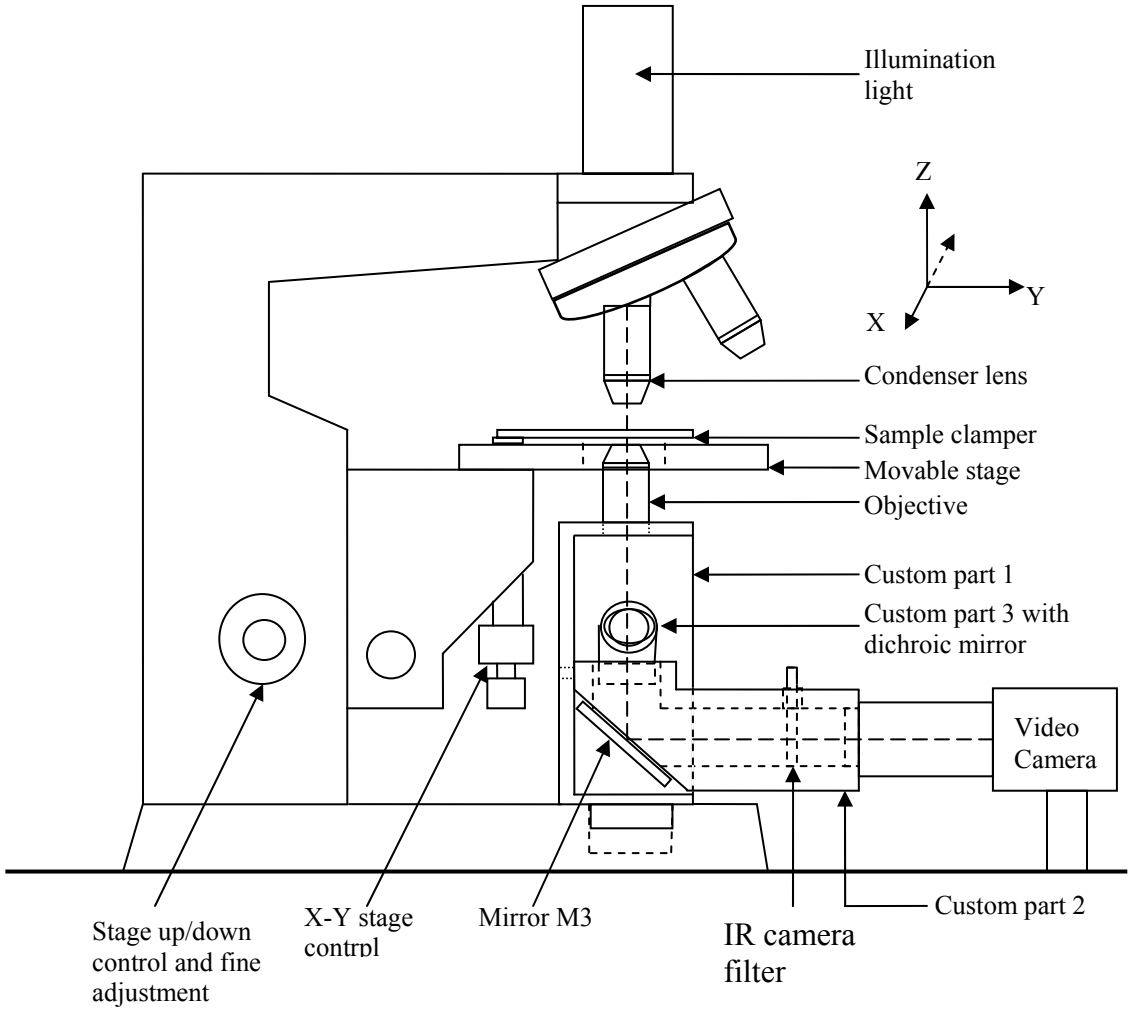


Figure 16. Modified microscope for the pulsed laser tweezers. (Figure not to scale)

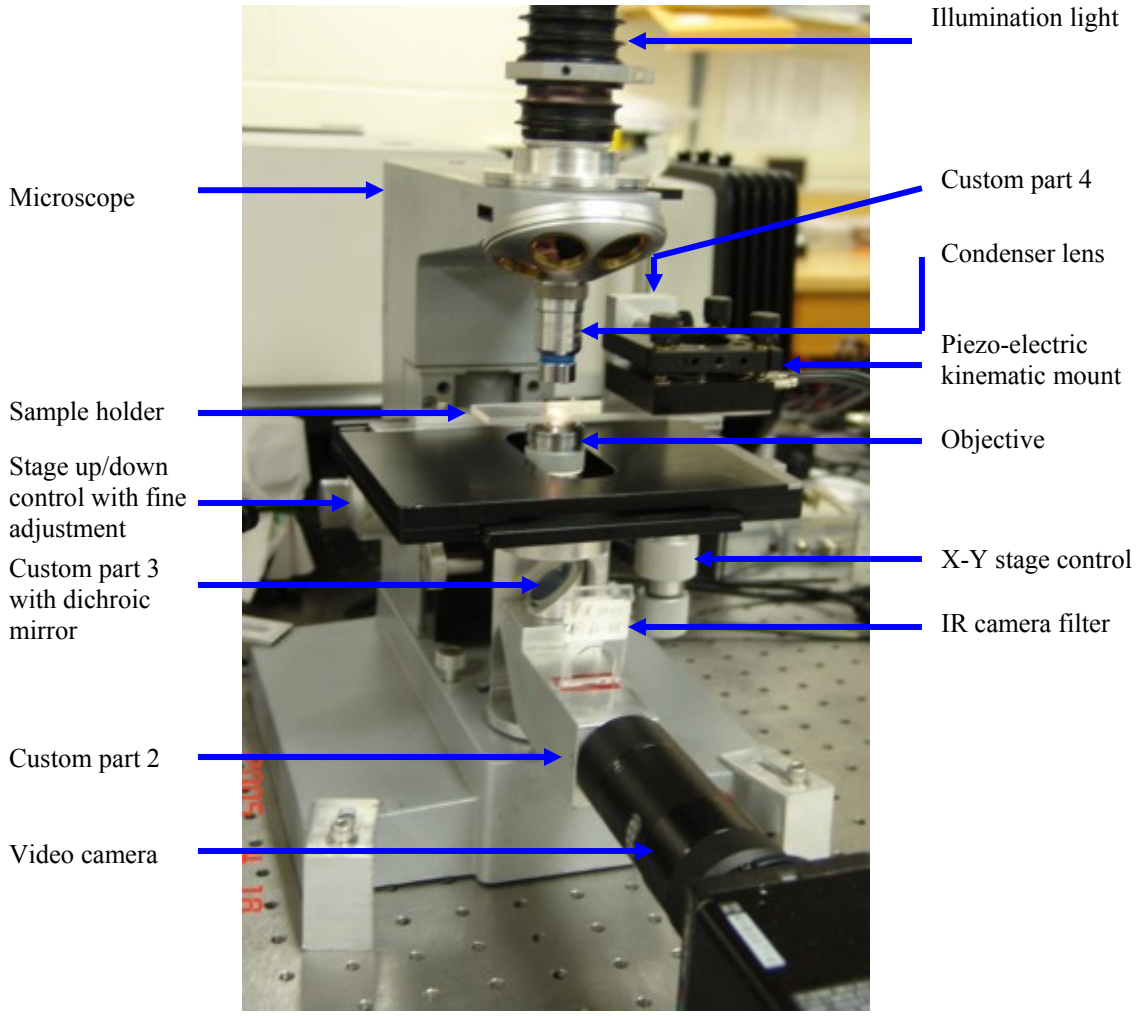


**Figure 17.** Actual picture of modified microscope for the pulsed laser tweezers.

Modifying the microscope was a very important part of building a CW laser tweezers. While designing custom part 2 which was a very vital part of the system, we made sure that the image formed by the objective falls on the front of the video camera. Therefore, dimensions of custom part 2 have to be chosen precisely. X-Y stage control was used to move the stage in X and Y direction. Stage up/down control was used to move the stage in up and down direction. This control also has fine adjustment which

allowed movement of the stage as small as ~ 2μm. A condenser lens was used to focus illumination light onto the sample for better illumination of the sample. The sample holder which contains the sample well was used to hold the sample under consideration. More description about the sample holder and the sample preparation can be found in the section about methods and calibration.

#### 4.2.1.2. Laser and optics

After modifying the microscope the second most important step is to prepare the laser and related optics. Appendix C lists the parts that were used for the CW laser tweezers, including those used for modifying the microscope.

Figure 18 depicts the optics layout used for the CW laser tweezers.

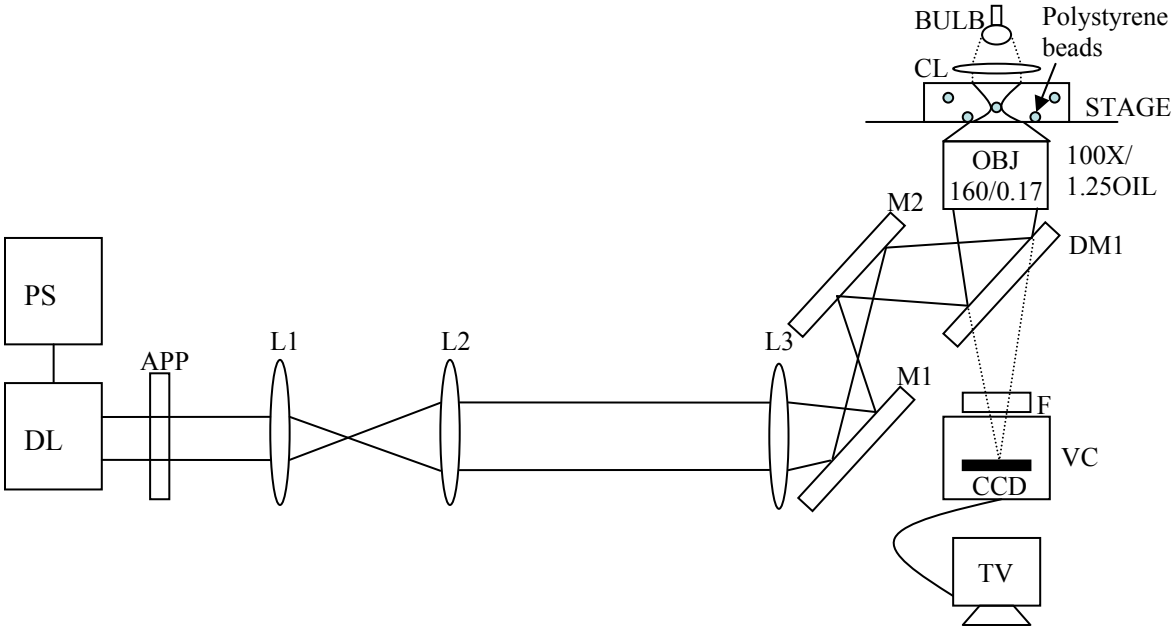


Figure 18. The CW laser tweezers optics layout. DL - Diode laser; APP - Anamorphic prism pair; L1 - Lens 1 (f = 75 mm); L2 - Lens 2 (f = 100 mm); L3 - Lens 3 (f = 150 mm); M1 - Mirror 1; M2 - Mirror 2; DM1 - Dichroic mirror 1; OBJ - Objective; CL - Condenser lens; F - IR laser filter; CCD - Charged coupled device; VC - Video camera; TV - Television; PS - Power supply for laser diode. (Figure not to scale)

A diode laser was mounted on the laser mount made in the lab. This laser mount has adjustable screws. They were adjusted so that laser beam is perfectly parallel to the optical bench on which the whole system is resided. We used collimating lens (Thorlabs Model#A438-B) to make laser beam parallel. A diode laser has to be given controlled power input and this was done by a custom-made diode laser controller designed and built by Dr. Li in the lab. It is very important to supply the diode laser with constant current even in the fluctuating temperature conditions which affect laser power output. The diode laser is operated at about 36 mW output power.

A diode laser emits an elliptical beam. For better trapping efficiency, we need a circular beam shape. To make the beam circular, a pair of anamorphic prisms was used. These prisms are generally used in pairs to provide one dimensional (anamorphic) expansion of the incoming beam. They are particularly useful for correcting the asymmetry in the output of diode lasers. By varying the relative angles of the two prisms, it is possible to change the unidirectional magnification. In this way, the output beam of a diode laser can be circularized very easily. These prisms were mounted in a cell, which is used to hold them in the correct proximity to each other for the magnification. Figure 19 details the use of anamorphic prism. We can get a circular laser beam by changing $\alpha_1$ and $\alpha_2$. Because of this arrangement, we can see the expansion of the beam from D1 and D2. But, this arrangement also results in displacement of the laser beam by small amount $\Delta$, which is an unfavorable outcome. So, after using anamorphic prisms, we have circular, parallel beam, which is also parallel to the optical bench.

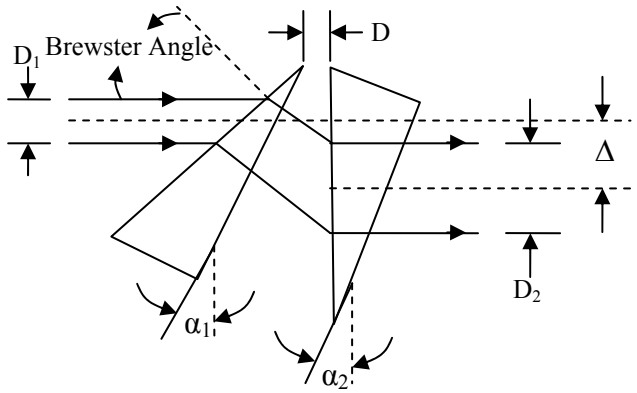


Figure 19. Use of a pair of anamorphic prisms to circularize the laser beam.

After getting the circular laser beam, it needs to be expanded so that it overfills the back aperture (pupil) of the objective. A pair of lenses was used to expand the beam size. 75 mm lens L1 followed by 100 mm lens L2 were used in our setup to expand the beam size. The distance between these two lenses was about 175 mm which resulted in a parallel, circular and expanded laser beam. As shown in Figure 20, the beam size increases from D2 to D3.

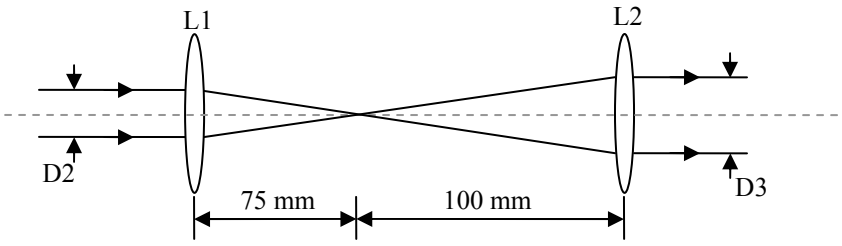


Figure 20. A pair of lenses as a laser beam expander. (Figure not to scale)

A lens L3 with f = 150 mm was used to change the divergence of the laser beam entering the objective. It in turn was used to change the position of the trap focus in the sample plane. Mirror pair of mirror M1 and mirror M2 was used to steer the beam into the objective. They were also used to position the laser trap at the center of the screen. Mirror M3 is not shown in Figure 18, for the simplicity of the diagram. But, it can be seen in Figure 16.

#### 4.2.1.3. System setup

There are many different ways for initially setting up and aligning the trap. We started by aligning the laser beam. By adjusting the collimating lens used in the laser

diode mount, we obtained a parallel laser beam. The best way to determine whether the beam is parallel is by checking the beam size at two distant locations in the path of a beam and make sure its size is same. The diode laser emits light in an elliptical shape. We used a pair of anamorphic prisms to make the laser beam circular. After insertion of this prism pair, the laser beam shifted a little bit horizontally. Therefore, after inserting the anamorphic prisms, we fine adjusted the laser beam using the laser mount adjustment screws. We know that the beam needs to be expanded for better trap efficiency. A pair of lenses with focal lengths, 75 mm and 100 mm were used after the anamorphic prism pair to expand the laser beam. The distance between these two lenses was kept about 175 mm and they were adjusted such that the laser beam would be parallel. After this, mirror M1 and mirror M2 were used to direct the laser beam on the dichroic mirror DM1, and in turn reflects it into the objective. To roughly adjust the laser beam at the center of the objective back aperture, we removed the objective temporarily and used the condenser illumination light to define the optical center of the microscope. We used an IR sensor card for locating the laser light. M1 and M2 were then adjusted such that laser is at the center of the illumination light coming from the condenser lens. After this procedure, the objective was fixed back in its original place. Before fine adjusting the laser beam into the objective, IR camera filter was removed from the custom part 2. Then, M1 and M2 were fine adjusted so that the laser focus is at the center of the TV screen. As the objective used was not infinity corrected, it needs the laser beam to be diverging at the back aperture of the objective. For this purpose, 150 mm tube lens L3 was used. This lens can also be used to change the position of the trap focus in the sample plane. When a

particle is trapped in a sample, it should look crisp clear on the TV screen. The quality and clarity of the picture depends on the position of the trapped particle in the sample plane. When the particle is in the same plane as that of CW laser trap, it appears clear on the TV screen. Otherwise, it looks defocused. A sample of polystyrene beads (2 μm) in water was prepared and a polystyrene bead was trapped. Then, lens L3 was moved very slowly such that the polystyrene bead appeared crisp clear on the TV screen. After the insertion of the lens L3, mirrors M1 and M2 might need to be fine adjusted. This completes the setup of the CW laser tweezers.

### 4.2.2. A pulsed laser tweezers

After building the CW laser tweezers, we modified it as a pulsed laser tweezers. The important part of the setup was to insert the pulsed laser beam into the microscope such that the position of the trapping focus due to the CW laser and the position of the trapping focus due to the pulsed laser are matched in the sample plane. We also need a shutter which allows only a single pulse to pass when directed. This shutter must be controlled to allow passing of pulses for specified amount of time. We also need to control the pulsed laser output power. Our system incorporates all these things along with a few more modifications.

#### 4.2.2.1. A pulsed laser, optics and layout

We started building a pulsed laser tweezers from a CW laser tweezers. Thus, the CW laser tweezers is an integral part of the pulsed laser tweezers. Appendix C gives the list of components used in building the pulsed laser tweezers.

Figure 21 gives the optics layout used for the pulsed laser tweezers. The CW laser tweezers part which has already been explained, is shown in black color, where as, the pulsed laser tweezers part is shown in gray color.

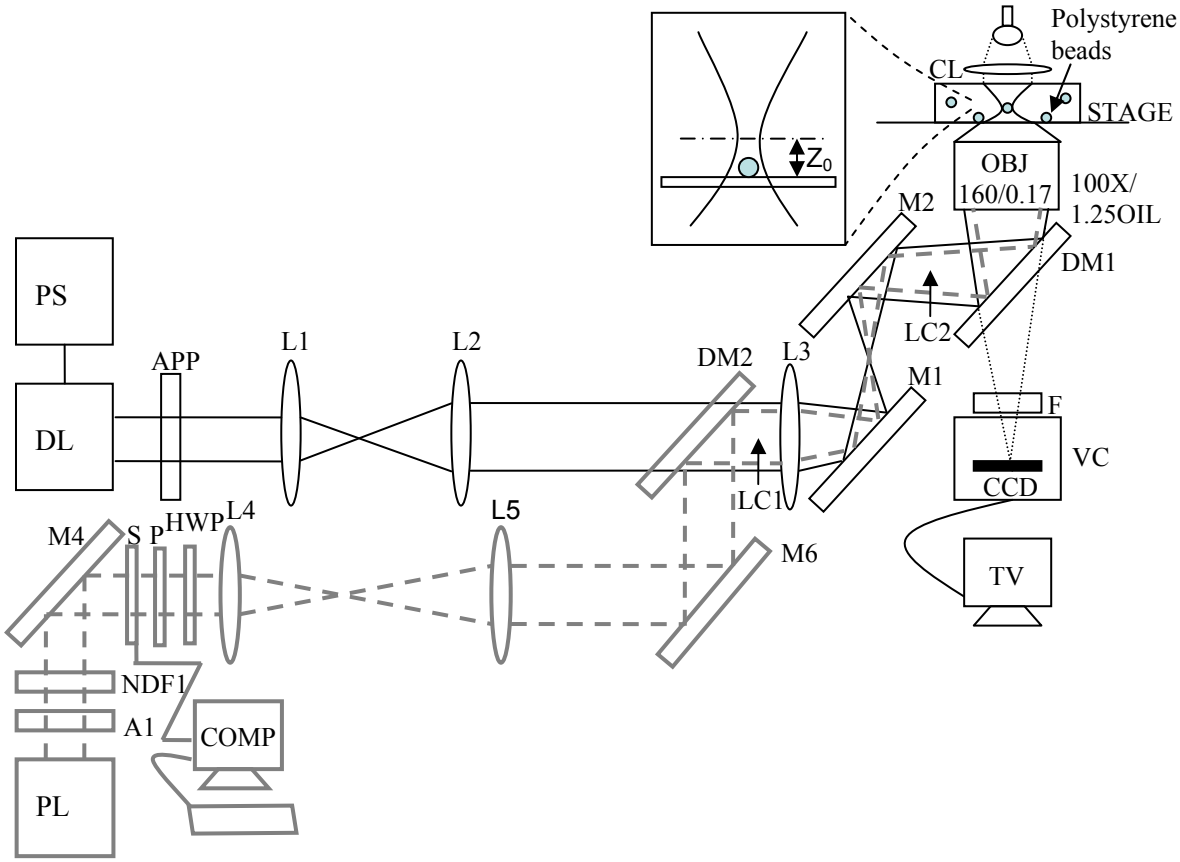


Figure 21. The pulsed laser tweezers optics layout. CW laser beam - Solid line. Pulsed laser beam - dashed line. PL -Pulsed laser; A1 - Aperture; M4 - Mirror 4; M6 - Mirror 6; NDF1 - Neutral density filter 1; P - Polarizer; L4 - Lens 4; L5 - Lens 5; DM2 - Dichroic mirror 2; COMP - Computer; LC1 - Location 1; LC2 - Location 2; PS - Power supply for laser diode. (Figure not to scale)

Before explaining anything about the configuration of the system, it is important to know a few things about the pulsed laser, we used. It was operated without Q-switching at 13 Hz with average pulse duration ($\tau$) of ~45 μs. We limited the beam size using aperture A1. Even after limiting the beam size, average output power of the laser beam was ~150 mW. This much power corresponds to about ~130 W of peak power per pulse. Power of this magnitude is harmful to the microscope objective. Therefore, the neutral density filter NDF1 with 10% transmittance was used to limit the average output power from the pulsed laser. This reduced the average output power to ~15 mW. But, while aligning the system, this much power also can be deleterious for the objective. Therefore, while aligning the laser into the microscope, the minimum laser power should be used. To change the laser power on continuous basis, instead of inserting different values of neutral density filters, a combination of half-wave plate HWP, with polarizer P was used. As shown in Figure 22, if the angle between the electric field vector in a plane or linearly polarized incident beam and the half wave-plate principal plane is $\theta$ (acute), the emergent beam (also plane or linearly polarized) will make an acute angle $\theta$ with the half wave-plate principal plane. Thus the half-wave plate rotates the polarization plane through an angle $2\theta$. Output of the polarizer depends on $\cos(\alpha)$ where $\alpha$ is the angle between the emergent beam (also plane or linearly polarized) and the principle axis of P (polarizer). Therefore, HWP (half wave-plate), was used to change the polarization of the laser beam and in turn to modulate the output power of the pulsed laser.

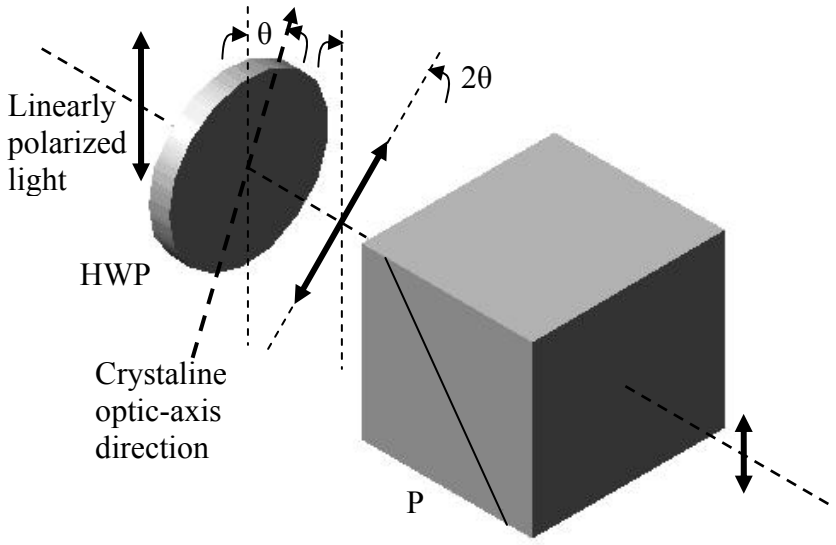


Figure 22. A combination of a half-wave plate and a polarizer to modulate the output power of the pulsed laser.

Mirrors M4 and M5 were used to make the pulsed laser beam parallel to the optical bench and made it almost at the same height from the optical bench as that of the CW laser beam. To combine the pulsed laser beam and the CW laser beam, we used dichroic mirror DM2 in the path of the CW laser beam path. This mirror reflects 90% at 1064 nm at $45^{o}$ and transmits 90% at 785 nm.

It is very important that we do not disturb any part of the CW laser tweezers system we have already setup except doing some fine adjustments. Therefore, aligning the pulsed laser beam into the microscope is a little bit tedious than the earlier version. Use of M4 and M5 gives us a beam parallel to the optical bench almost at the same height from the optical bench as that of the CW laser beam. Initially, we obtained a parallel pulsed laser beam using a pair of 100 mm lenses, L4 and L5. We get a parallel beam, when the distance between these two lenses is ~200 mm. Mirror M6 was used to reflect

this beam on to dichroic mirror DM2. Mirror M6 and dichroic mirror DM2 worked as a beam stirrer for the pulsed laser beam i.e. they do the same work for the pulsed laser beam as mirror M1 and M2 had done for the CW laser beam.

We need the pulsed laser beam to focus at the same position in the sample plane as the CW laser beam. To start with, we tried to bring the pulsed laser beam into the microscope. Firstly, using IR sensor card just after dichroic mirror DM2 (location 1, LC1 in Figure 21) we adjusted the mirror M6 such that beam spot due to the CW laser and the beam spot due to the pulsed laser matched. Then, we observed the laser beams at the position just before the microscope where the laser beams entered the microscope (location 2, LC2 in Figure 21). We tried to coincide the optical paths of the pulsed laser beam and the CW laser beam by adjusting the dichroic mirror DM2. To cross check the alignment, we went back to location 1, and adjusted mirror M6. Then, we again observed the laser beams at location 2 to adjust the dichroic mirror DM2. We continued this process until we confirmed that the optical paths of both the lasers are matched at both of the locations.

Firstly, we blocked the CW laser entering the microscope. As optical paths of the CW laser beam and the pulsed laser beam were roughly matched, we were able to see the pulsed laser blinking on the TV screen (IR camera filter is removed). Then, we fine adjusted the pulsed laser to the center of the screen where the CW laser had already been focused. We require that the position of the pulsed laser focus and the position of the CW laser focus should be same in the sample plane. We used laser light reflected from the coverslip to make this alignment. We allowed the CW laser to enter the microscope. If

the CW laser is focused in the sample, we can see a bigger laser circle on the TV screen, as shown in Figure 23 (a). For alignment purpose, we changed the stage position such that the CW laser was focused on the coverslip. Then we were be able to see a very small spot of laser on the TV screen, as shown in Figure 23 (b).

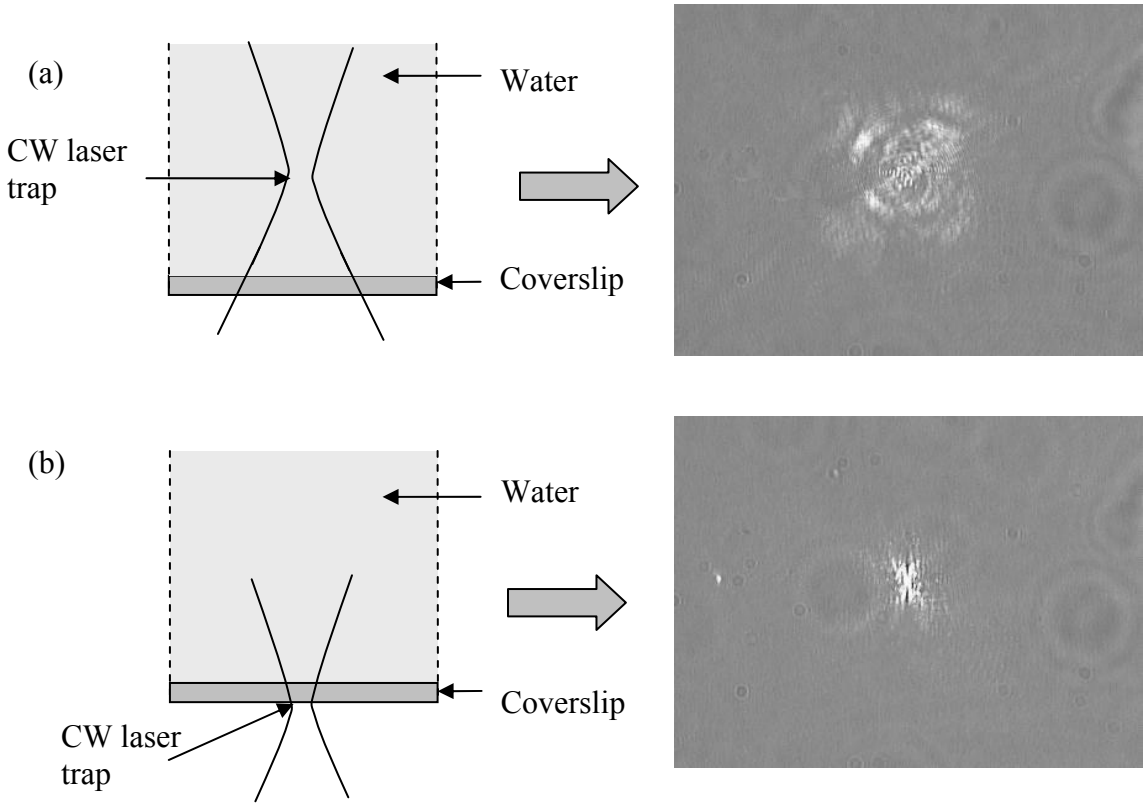


Figure 23. Position of the CW laser focus in the sample plane and the corresponding TV screen shot. (Figures not to scale)

Now, we blocked the CW laser again. If the pulsed laser beam is focused at the same position, we should be able to see a small laser spot blinking on the TV screen. If

not, we will need to modify the distance between lenses L4 and L5. Keeping L4 fixed, we moved L5 such that we could see the smallest spot of beam on the TV screen without changing the position of the microscope stage (i.e. no up/down motion of stage). After this adjustment, we might need to fine adjust mirror M6 and DM2.

We used a shutter to limit the number of pulses. The shutter and the control unit were developed by Dr. Changan Xie and Mr. Jonathan Stutzman in the laboratory. The shutter is supplied with 24 V power supply through the control unit. The shutter can be operated in three modes, manual on when shutter opens, manual off when shutter closes and the computer controlled trigger in which a trigger signal (+ 3 V) is given from the computer to the control unit and in turn to the shutter to control the shutter opening time. The shutter can be opened for the specified amount of time generally as small as ~20 ms. The pulsed laser was operated at 13 Hz. When the shutter was opened for ~70 ms, it allowed a single pulse to pass. A program to control this shutter was written in Visual Basic 6.0. The program can be found in appendix B.

Figure 24 gives the picture of the system. In this picture the red line shows the path of the CW laser beam. The blue line corresponds to the pulsed laser beam path. The green line corresponds to combination of the CW laser beam and the pulsed laser beam.

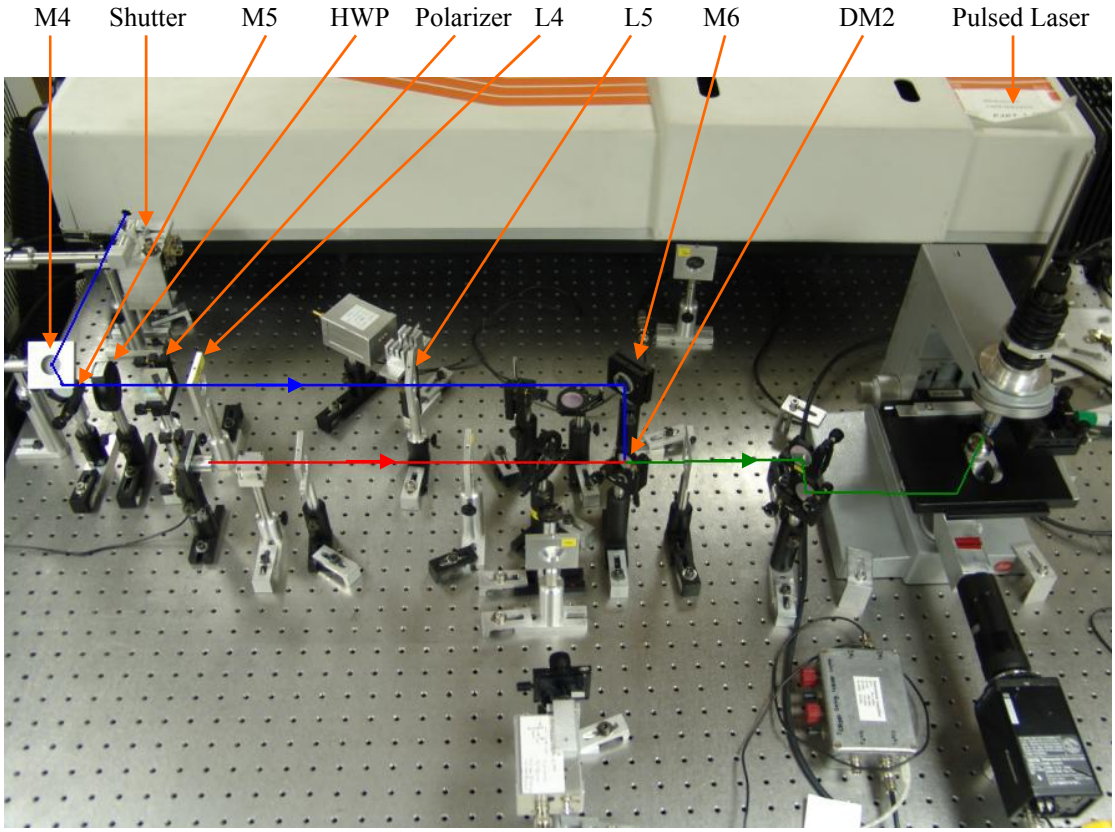


Figure 24. Actual picture of the pulsed laser tweezers.

This completes the setup of the pulsed laser tweezers. To limit the number of pages and complexity, many practical techniques used while building the pulsed laser tweezers are not discussed here. But, overall this chapter gives the basic foundation required for building a pulsed laser tweezers.

## 4.3. Methods and calibration

Before explaining properties and the results obtained using the pulsed laser tweezers, it is important to know how to calibrate the system parameters and the methods and instruments used for measurements. Appendix C lists the components used for measurement and calibration of the pulsed laser tweezers. The most important measurement is measuring the CW laser power and the pulsed laser power.

### 4.3.1. Measurement of the laser power

Earlier in the course of the development, we used a thermoresistor power meter 1 which has accuracy of two decimal places, and later we used a thermoresistor power meter 2 was used with an accuracy of three decimal places. But, practically both read the same value. While measuring the CW laser power, we blocked the pulsed laser and vice versa. We put the power meter at location LC2 shown in Figure 21 i.e. just before the microscope. Measuring the CW laser power is fairly easy which requires us to take the reading from the power meter control unit display directly. The CW laser was operated at 36 mW of output power for all the experiments. Transmittance factor of the microscope that is of dichroic mirror DC1 and objective combined is taken to be about 50 %. This is a good guess and was double checked for the CW laser power by measuring power at location LC2, and after the objective to find transmittance factor. For this measurement a custom made photodetector and the multimeter 1 were used. Therefore, the CW laser power at the sample was 18 mW, given that the CW laser diode output power was 36 mW.

To measure the pulsed laser power on a continuous basis, we inserted a coverslip in the path of the pulsed laser beam just after lens L5. This coverslip reflects a part of laser beam onto the photodetector PD1, as shown in Figure 25. Before falling on the photodetector, it passes through neutral density filter of 1% transmittance which limits the amount of light. This is required to restrict photodetector from going into the saturation mode. The output of photodetector was connected to the digital oscilloscope. The peak could be obsereved on the oscilloscope. We measured the pulsed laser power at location LC2 using thrmoresistor power meter and correlated it with the pulse peak observed on the digital oscilloscope. For our case, we found 1 mW corresponded to ~100 mV of peak on the oscilloscope. This relation depends on how the system is setup and if changed, will need to be calibrated again.

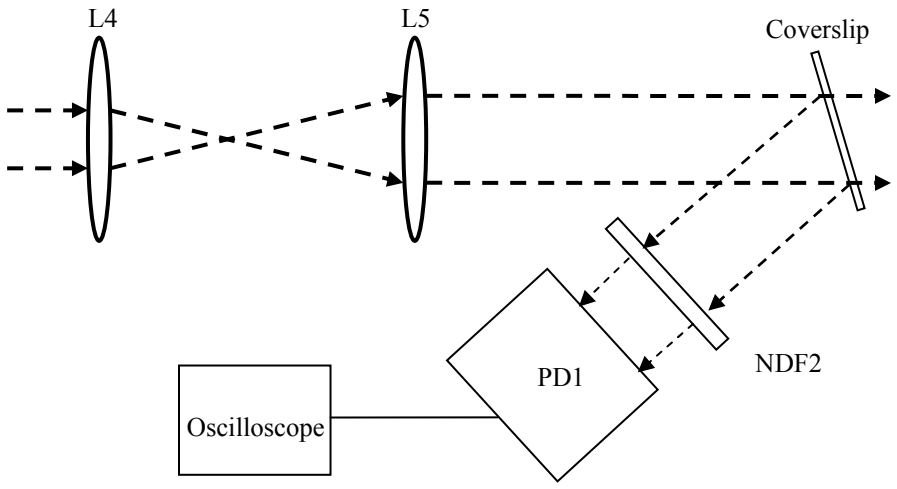


Figure 25. Measurement of the pulsed laser power using photodetector. (Figure not to scale) PD1 - Photodetector 1 (S2386-5K with $R_L = 20k\Omega$); NDF2 - Neutral density filter.

This setup facilitates measuring the pulsed laser power without insertion of any power meter in the path of the laser beam that blocks the laser light totally.

Figure 26 shows the pulse recorded by the digital oscilloscope. We used Origin 5.0 software to analyze the data recorded by the digital oscilloscope. Top two peaks (Figure 26 (a) and (b)) were recorded using photodetector 3 (PIN diode S1223-01) which was faster than photodetector 1, used for calibration. The third graph was recorded using photodetector 1. These graphs show that the pulse duration is about ~45 μs. From the first graph it can be seen that the first peak in the pulse has time period of ~0.20 μs only. For all calculation purposes, we consider pulse duration ($\tau$) to be 45 μs.

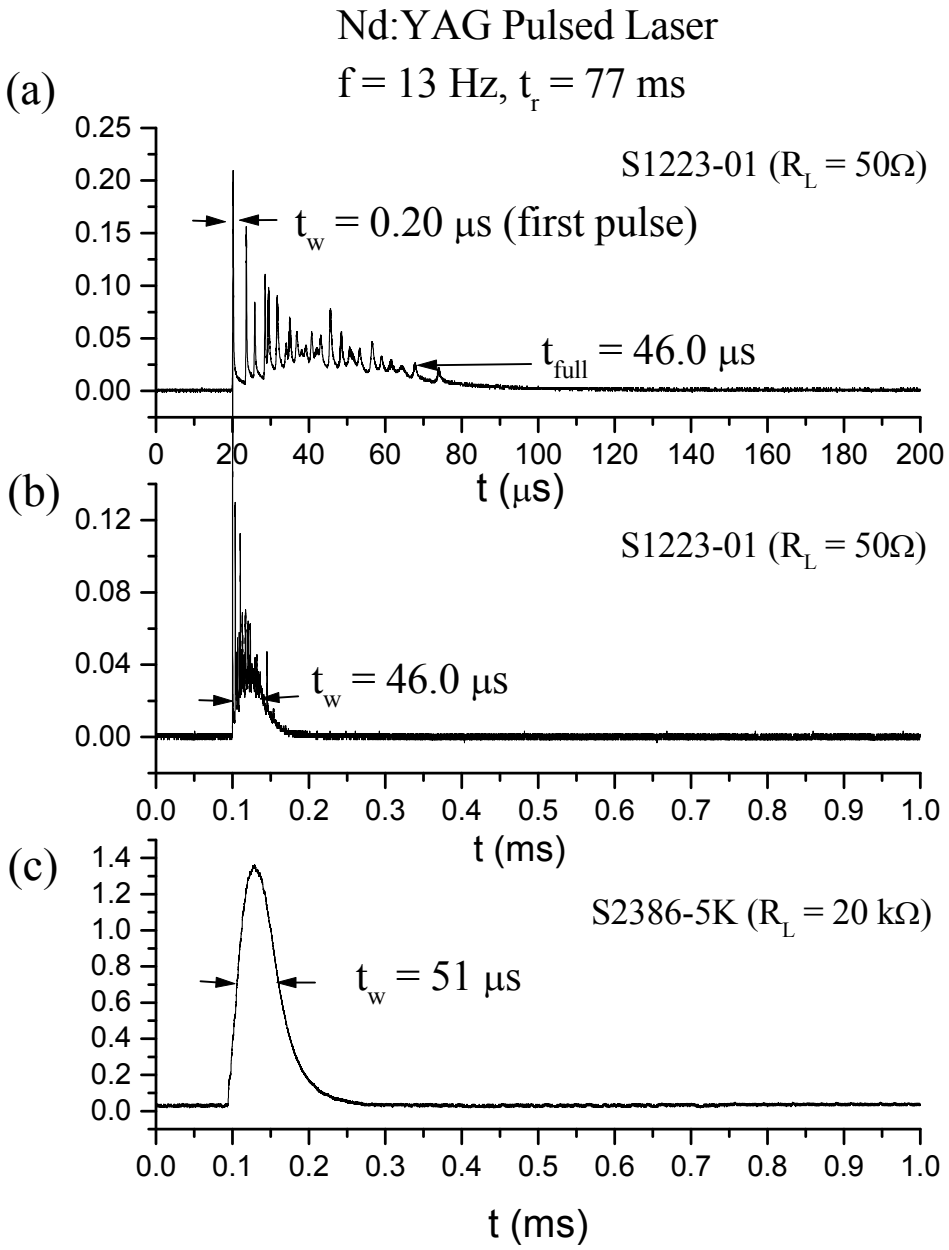


Figure 26. Pulses from the pulsed laser. (a) and (b) The pulse recorded using photodetector 3 (S1223-01), (c) The pulse recorded using photodetector 1 (S2386-5K).

### 4.3.2. Sample preparation

We used 2.0 μm polystyrene beads for most of our experiments. The polystyrene spheres (Model P0020320PN, Bang Laboratories) were diluted in distilled water, and a drop of the fresh sample was transferred to a sample well, in which some beads were found to adhere to the glass coverslip (Model NC9115219, Fisher Scientific) after a few minutes. The custom made sample holder was designed such that it can be fixed in the piezo-electric kinematic mount. The sample preparation technique explained here was used throughout for all the experiments performed, except for a few of them for which a different sample preparation technique is mentioned in the corresponding section of the thesis. The mechanical design used for sample holder is given in appendix A. Figure 27 gives the qualitative view of the sample prepared in the sample holder.

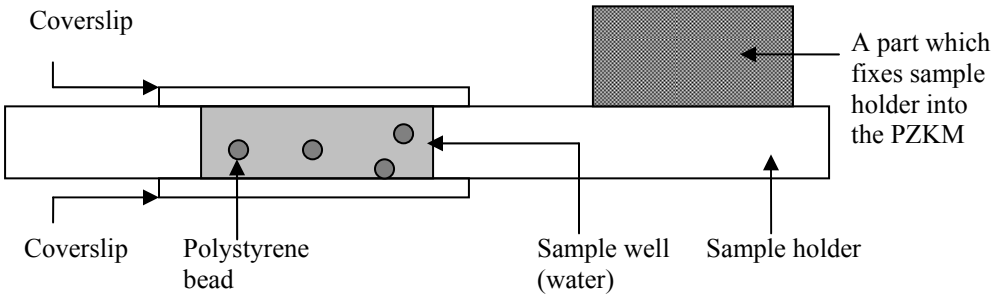


Figure 27. Sample holder. PZKM - Piezo-electric kinematic mount. (Figure not to scale)

### 4.3.3. Piezo-electric kinematic mount:

A piezo-electric kinematic mount is a custom made device which clamps the sample holder in the correct position and can be moved in z direction very precisely using its piezo-electric characteristic. The piezo-electric kinematic mount (Thorlabs KC1-T-

PZ) was modified in addition with custom the part 4. The custom part 4 was fixed to the stage and can be moved in X-Y direction for coarse adjustment using the stage X-Y control shown in Figure 16. The stage also can be moved in Z direction using up/down control. This control also has a fine control which can move the stage in small steps. To find out certain parameters of the pulsed laser tweezers, we need to move the stage by specified distance in Z direction with the precision of micrometers. The mechanical controls of the microscope are not precise and therefore we designed a PZKM (Piezo-electric kinematic mount). Figure 28 shows the actual picture of piezo electric kinematic mount as provided by Thorlabs. It was supplied with a high voltage power supply (Power supply 3) to control the displacement of the mount. Figure 29 shows the schematic of implementation of the PZKM to move the sample holder in Z direction with very high precision. All three piezo crystals were supplied with the same power supply (same voltage) which resulted in displacement of movable part of the PZKM, proportional to the supplied voltage. Figure 30 is an actual picture of piezo-electric kinematic mount.

Figure 28. Thorlabs piezo-electric kinematic mount (PZKM).

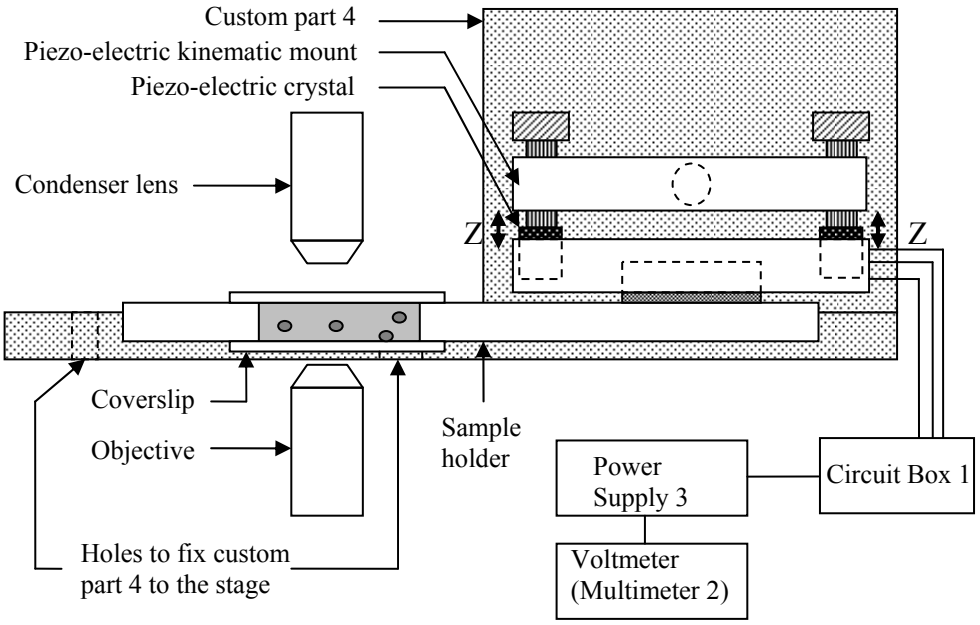


Figure 29. Schematic of implementation of piezo-electric kinematic mount for precise control of displacement of sample holder in Z direction. (Figure not to scale)

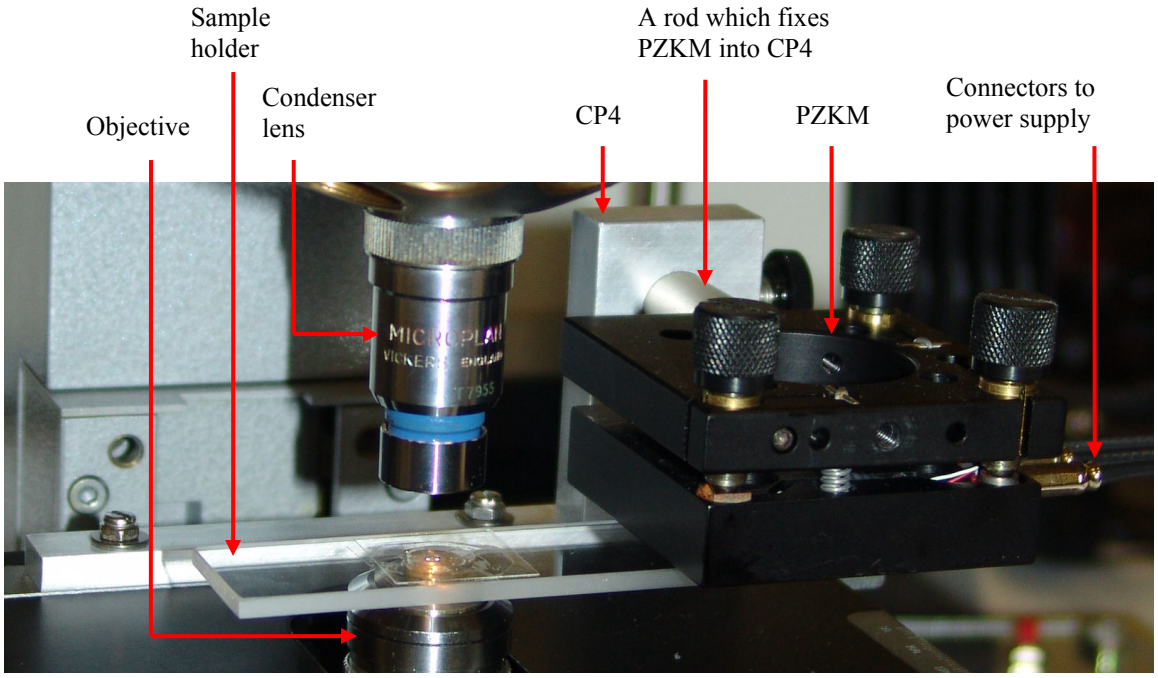


Figure 30. Actual picture of implementation of piezo-electric kinematic mount. CP4: Custom part 4; PZKM: Piezo-electric kinematic mount.

Before using the PZKM (Piezo-electric kinematic mount) in the pulsed laser tweezers, we needed to calibrate it to find the relation between voltage supplied to the PZT (Piezo-electric transducer) and actual displacement of the PZKM. To find out this relation, we did a Michelson interferometer experiment using the PZKM as a mirror mount. Figure 31 gives the schematic of Michelson interferometer. The same diode laser (785 nm) used in the pulsed laser tweezers was used in this experiment. We used an optical isolator (690 nm) to isolate laser from the interferometer. We used the same anamorphic prism pair used in the pulsed laser tweezers to circularize the laser beam. The beam splitter 2 with reflection factor 75 % and transmission factor 25 % was used. Mirror 2 was a fixed mirror and Mirror 1 was fixed into the PZKM. We calibrated the PZKM using two methods, one by using function generator output as a driving voltage for the PZKM, and the other by using a high voltage power supply (Power supply 3) to gradually increase the voltage and record the voltage corresponding to the peaks at the detector. To align two laser beams from mirror 1 and mirror 2 at the same location, screws available on the mirror mounts were used. Detector 3 was used as a detector for this setup. Output of the detector was connected to the digital oscilloscope to record the peaks.

If we consider the original laser beam as an electromagnetic wave, then the wave equation is given as

$$E = E_0 e^{i(kx-\omega t)} \ . \tag{4.1}$$

Then, $$E_1 = \frac{1}{\sqrt{2}} E_0 e^{i(k(x+2.x_1)-\omega t)}, \tag{4.2}$$

and $$E_2 = \frac{1}{\sqrt{2}} E_0 e^{i(k(x+2.x_2)-\omega t)}. \tag{4.3}$$

Consider path difference between $x_1$ and $x_2$ to be $(x_1-x_2) = \Delta x$, where $\Delta l = 2.\Delta x$. $\Delta x$ is the change in the position of mirror 1 due to the displacement of PZKM by PZT. At detector, we detect

$$I = | E_1 + E_2 |^2 , \qquad (4.4)$$

and $$I = I_0(1 + \cos(\frac{4\pi}{\lambda}\Delta x)) , \qquad (4.5)$$

where, $$I_0 = | E_0 |^2 . \qquad (4.6)$$

Therefore, displacement of $\lambda/2$ of mirror 1 gives one peak at detector. That means two consecutive peaks corresponds to displacement of PZKM by 785/2 = 392.5 nm.

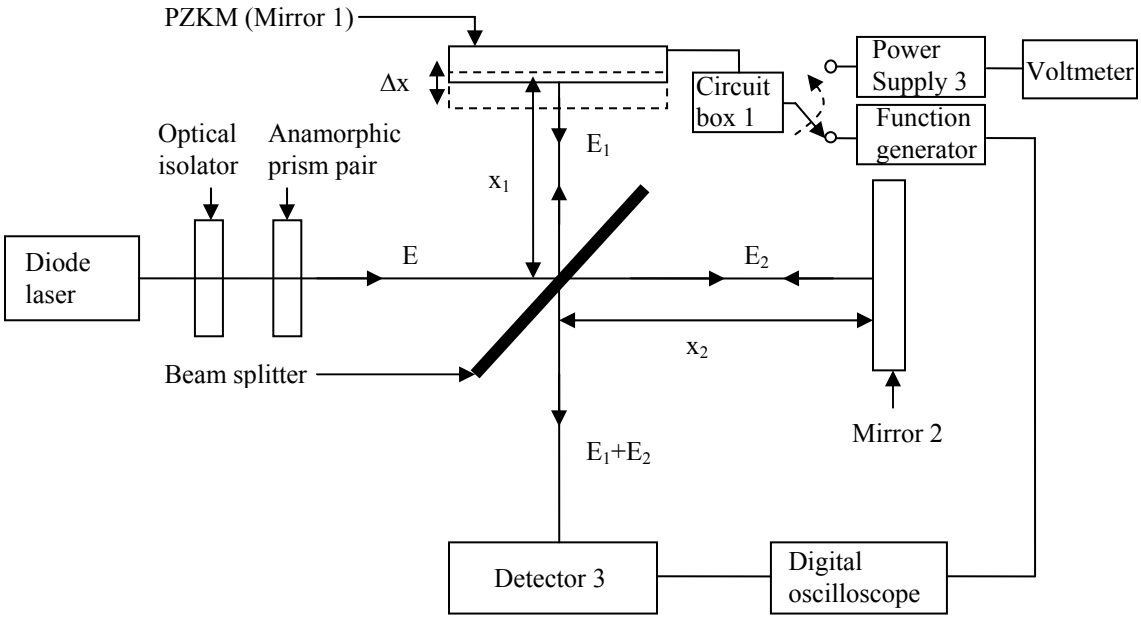


Figure 31. Calibration of PZKM using Michelson interferometer.

In the first part of the experiment, we supplied PZKM by a triangular waveform with amplitude of 15 V. As shown in Figure 32, approximately 7.0 V change in the

voltage corresponds to two consecutive peaks. Both of these waveforms were recorded using a digital oscilloscope. Therefore, ~7.00 V corresponds to 392.5 nm displacement produced by the PZKM. This gave us the relation to be 56.1 nm/V of displacement for +/- 15 V range.

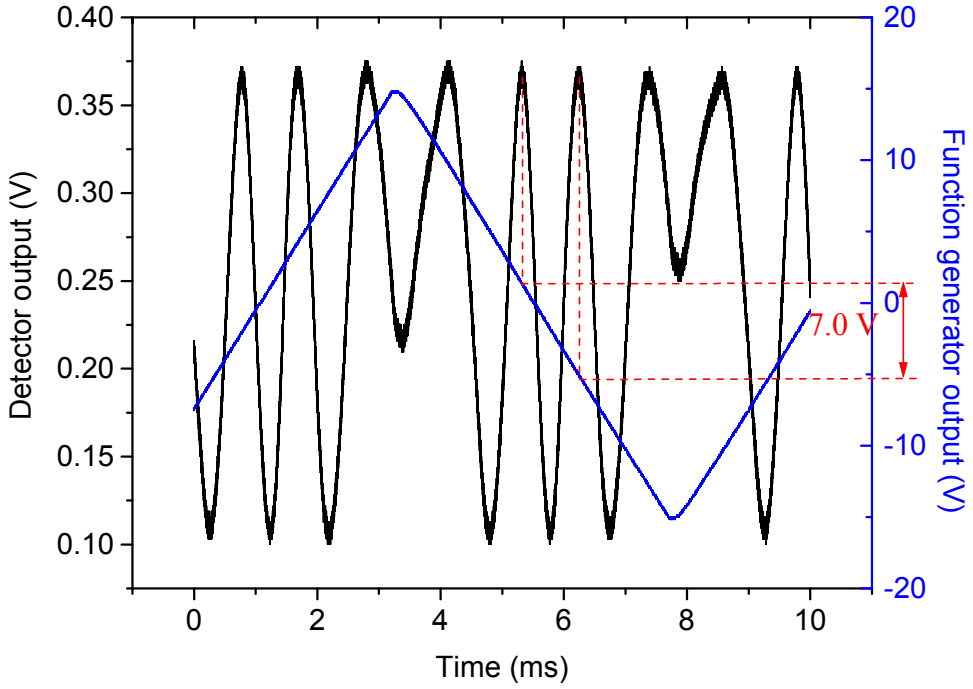


Figure 32. Calibration of PZKM using a function generator. Function generator output (blue) supplied to PZKM and corresponding detector output (black), recorded using a digital oscilloscope.

Since we did not have a function generator which could provide high voltage we double checked the relation just found, using the high voltage power supply (power supply 3). We gradually increased the voltage, and recorded the voltage corresponding to the peaks. Table 2 gives the data recorded using this technique. We repeated the process

three times to get better statistics. Figure 33 gives the data and linear fit to the data. This analysis was carried out using Mathematica 4.1 software.

Table 2. Three trials to determine the relation between displacement of PZKM and the voltage supplied. (Calibration of PZKM)

| Peaks | Trial 1<br>Voltage supplied (V) | Trial 2<br>Voltage supplied (V) | Trial 3<br>Voltage supplied (V) |
|---|---|---|---|
| Peak 1 | 3.9 | 5.4 | 7.3 |
| Peak 2 | 12.9 | 12.9 | 16.2 |
| Peak 3 | 20.4 | 20.6 | 24.9 |
| Peak 4 | 27.4 | 28.4 | 32.1 |
| Peak 5 | 34.0 | 34.5 | 38.2 |
| Peak 6 | 41.0 | 41.9 | 45.2 |
| Peak 7 | 48.0 | 48.9 | 51.2 |
| Peak 8 | 54.2 | 55.2 | 57.5 |
| Peak 9 | 61.2 | 59.7 | 64.2 |
| Peak 10 | 67.6 | 67.2 | 70.1 |
| Peak 11 | 72.8 | 73.2 | 77.1 |
| Peak 12 | 80.8 | 80.2 | 84.7 |
| Peak 13 | 86.2 | 86.3 | 91.8 |
| Peak 14 | 92.5 | 94.0 | 98.2 |
| Peak 15 | 98.3 | 100.9 | 104.5 |
| Peak 16 | 105.9 | 107.4 | 113.1 |
| Peak 17 | 111.6 | 114 | 121.0 |
| Peak 18 | 119.6 | 122.0 | 127.9 |

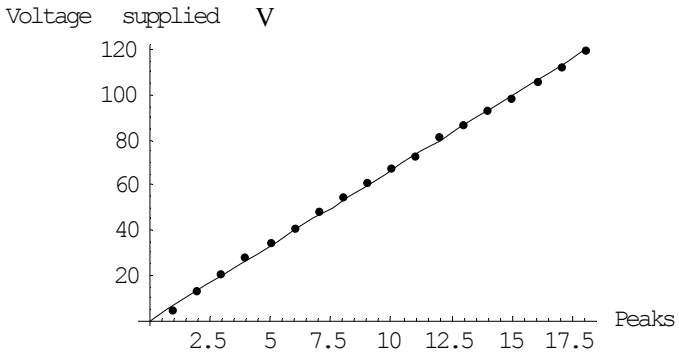


Fit function is:
Y = 6.65 X

Figure 33. (a) Trial 1 data for calibration of PZKM and line fit to data.

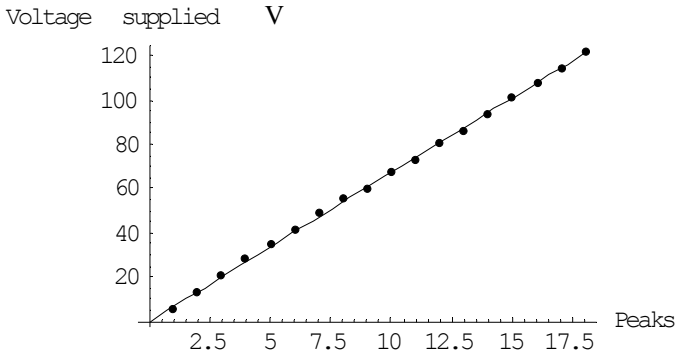


Fit function is:
Y = 6.73 X

Figure 33. (b) Trial 2 data for calibration of PZKM and line fit to data.

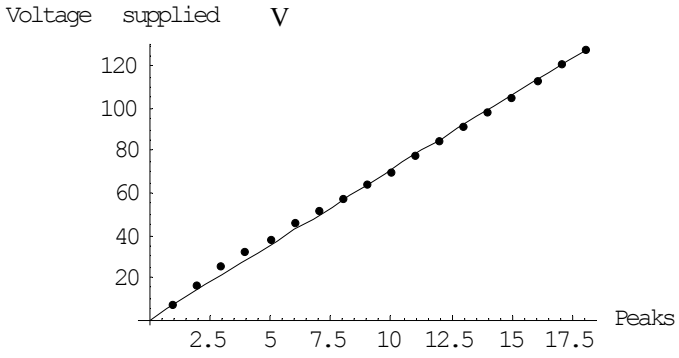


Fit function is:
Y = 7.10 X

Figure 33. (c) Trial 3 data for calibration of PZKM and line fit to data.

From above data fits, we derived the relation between the supplied voltage and the displacement of PZKM to be 57.5 nm/V for 0 to 120 V range. We used this relation to determine the displacement of PZKM. It is in accordance with our earlier result found using function generator. We had a high voltage power supply which is capable of supplying up to ~130 V. Therefore we were able to get displacement of ~7.5 μm maximum directly, using PZKM.

### 4.3.4. Detecting the backscattered light intensity

It is immensely helpful to detect the backscattered light intensity. It can be used to determine the position of the particle before and after trapping, M. E. J. Friese *et al.* determined the force constant of a single beam gradient trap by the measurement of the backscattered light.[101] We used a similar method to the one used by them. C. J. H. Brenan *et al.* used this technique for measurement of the axial force constant of a single-beam gradient photon force trap.[102]

Figure 34 shows the optical layout used to detect the backscattered light intensity. In our scheme, we used a 50/50 beam splitter (BS1) in the path of the CW laser beam to reflect backscattered light onto the photodetector. Lens (L6, f = 150 mm) was used to focus backscattered light on to the photodetector (PD1). While aligning this part of the system, we started without pinhole. Then we inserted pinhole (PH1, d = 400 μm) such that the signal strength at the detector was reduced to half of what it was before inserting the pinhole. This technique increases the sensitivity. The output of the photodetector was connected to the digital oscilloscope through an instrument amplifier. An instrument

amplifier was used with gain 100× to amplify the signal from the photodetector. The power supply of +/-15V required for the instrument amplifier was taken from the CW laser power supply. Filter 1 was used to block the pulsed laser light at 1.06 μm to fall onto the detector. But, even after using this filter some of this light falls on the photodetector due to its relatively high intensity.

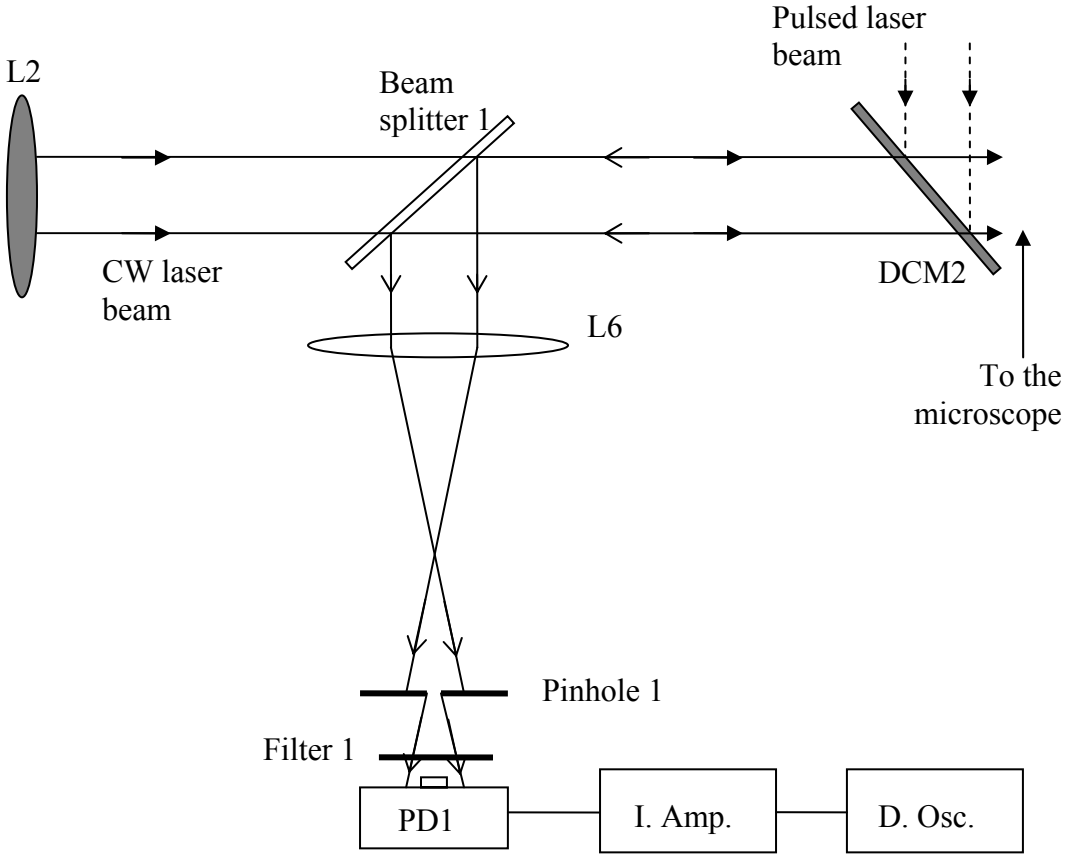


Figure 34. Optics layout used to detect backscattered light. Original parts of the pulsed laser tweezers are shown in gray. PD1 - Photodetector 1; DM2 - Dichroic mirror 2; I. Amp.: Instrument amplifier; L2 - Lens 2 (f = 100 mm); D. Osc. - Digital oscilloscope; L6 - Lens 6 (f = 150 mm). (Figure not to scale)

### 4.3.5. The pulsed laser tweezers with detection schemes

After implementing detection schemes for measuring the pulsed laser power and the backscattered light intensity, we can use this system efficiently to find pulsed laser tweezers parameters. But, before doing that, it is important to know the final setup used for all the measurements. All other measurements except the backscattered light detection for determination of the particle position were carried out without the scheme described in section 6.3.4. The backscattered light intensity detection scheme was implemented at the last. This means that the beam splitter BS1 was absent for all these measurements. In that case, the CW laser power at sample plane was 18 mW. After insertion of the beam splitter BS1, it decreases. Figure 35 gives the final optics layout for the pulsed laser tweezers with detection schemes. Also, when photodetector 1 was used for the backscattered light detection, photodetector 2 or photodetector 3 were used to trigger the digital oscilloscope using the pulse from the pulsed laser. Figure 35 also shows the CW laser trap and the distance $Z_0$ required between the trap focus and the stuck bead for efficient levitation of the stuck particle (polystyrene bead).

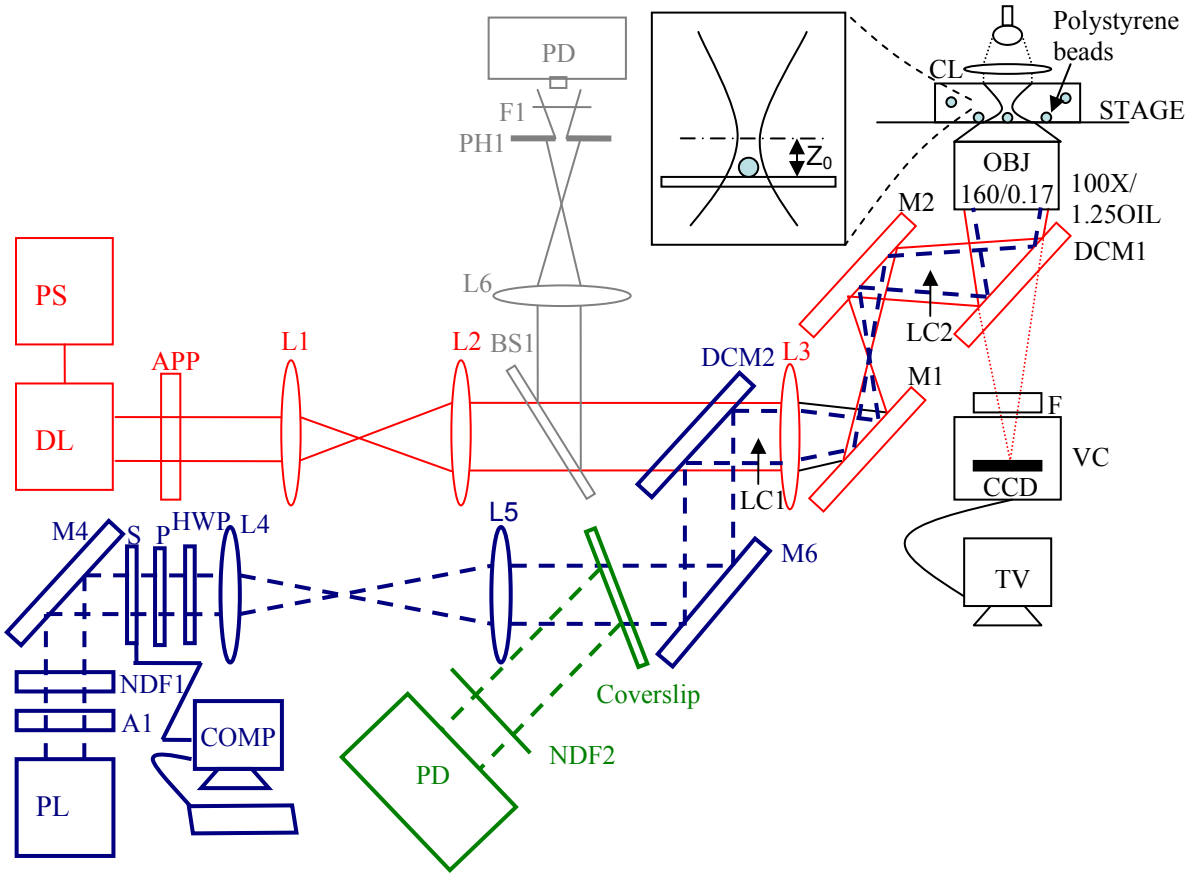


Figure 35. Optics layout of the pulsed laser tweezers with detection schemes for measuring pulsed laser power (green) and for measuring the backscattered light intensity (gray). PD - Photodetector; BS1 - Beam splitter 1; L6 - Lens 6; PH1 - Pinhole 1; F1 - Filter 1; NDF2 - Neutral density filter 2. (Figure not to scale).

# 5. APPLICATION OF THE PULSED LASER TWEEZERS

So far, we discussed the development of the pulsed laser tweezers with detection schemes to detect the pulsed laser power and the backscattered light intensity. The pulsed laser and the CW laser were focused at the same location in the sample plane. Whenever possible, only a single pulse was allowed to pass by controlling the shutter. It is important to know the way the pulsed laser tweezers was used to levitate microparticles. We levitated 2.0 μm polystyrene beads stuck to the coverslip. We also found out the levitation efficiency of the pulsed laser tweezers and its dependence on the initial axial displacement $Z_0$ and the pulse energy. To check the usefulness of the technique, we used the pulsed laser tweezers to levitate stuck yeast cells and bacillus cereus bacteria.

## 5.1. Levitation and manipulation of a stuck polystyrene bead

We used distilled water to prepare the sample. Polystyrene beads were mixed in distilled water. Then, the sample was transferred to the sample well of the sample holder. The sample well was covered with the coverslips from both sides. A small amount of immersion oil was put on the outer part of the coverslip, which is going to be near the objective. The sample holder was then fixed in the PZKM. We waited about 20 minutes until some of the polystyrene beads were stuck to the coverslip. We then tried to trap a stuck polystyrene bead using the CW laser trap. Because of insufficient power of the CW laser, we failed to trap the bead. After, making sure that the CW laser would not be able to trap the stuck bead, we moved the stage such that the CW laser was focused on the

coverslip and we were able to see a very small laser spot on the TV screen. Figure 36 (a) shows two polystyrene beads stuck to the coverslip (initial axial distance $Z_0 = 0$). The bead marked with an arrow is under consideration for trapping. For better visibility of the pictures, we used IR laser camera filter to block the laser light entering the camera. When the CW laser was focused on the coverslip, we were able to see the crisp clear image of the beads as shown in Figure 36 (a). For better levitation efficiency, we needed some finite initial axial distance $Z_0$ between the bead and the trapping focus. The reason for doing so is explained in the later part of the thesis. We supplied voltage to PZKM to lower the position of the sample. We gave about ~130 V to move the sample down by ~8 μm. Now, the CW laser focus and in turn the pulsed laser focus were ~8 μm above the polystyrene bead under consideration. Figure 37 shows the schematic of the polystyrene bead to be levitated and the initial axial displacement $Z_0$ of the polystyrene bead. The initial axial displacement $Z_0$ is the distance between the polystyrene bead and the position of the CW laser focus above the bead. Figure 36 (a)-(d) shows the levitation of the stuck polystyrene bead using the pulsed laser tweezers. Figure 36 (b) shows the beads in the position, just before the levitation pulse was applied. Because the beads were no more in the objective's focal plane, we see them defocused and bigger compared to Figure 36 (a). Then, using a computer program, we opened the shutter such that only a single pulse is fired. During the pulse time period, a very high gradient force pulling the stuck polysturene bead away from the coverslip comes into existence. It levitated the bead from the coverslip and then the bead got trapped in the CW laser trap very easily. In Figure 36 (c), the trapped bead was in the objective's focal plane, and therefore, looks clear

compared to the bead still stuck to the coverslip which looks defocused and unclear. Figure 36 (d) shows that even after moving the stage in +X direction, the trapped bead remained in the CW laser trap.

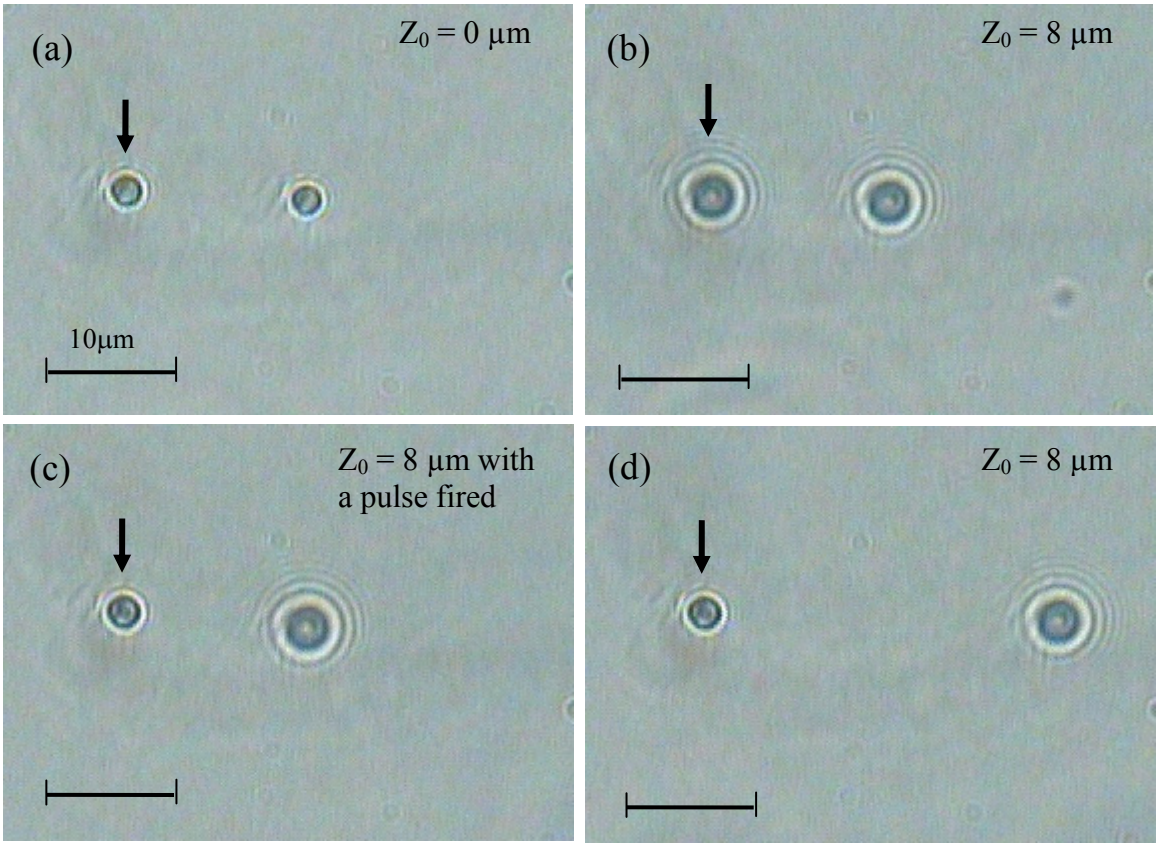


Figure 36. Levitation and manipulation of a stuck polystyrene bead using the pulsed laser tweezers. (a) Two beads stuck on the coverslip. (b) The beads were defocused with $Z_0 \sim$ 8μm before the application of the pulse. (c) The marked bead was levitated after the application of the pulse and was trapped into the CW trap. (d) The levitated bead is manipulated while stage was moved in +X direction.

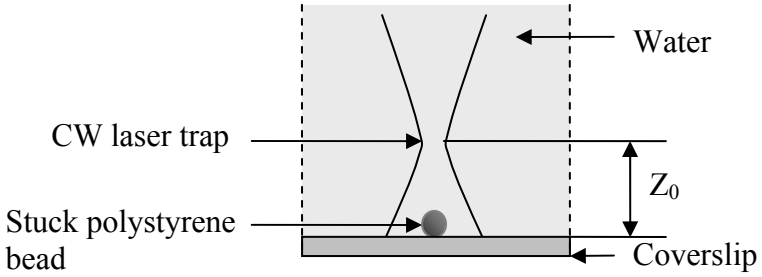


Figure 37. Schematic showing the positions of the laser trap and the polystyrene bead before the levitation pulse is applied. Initial axial displacement $Z_0$ is required for the efficient levitation of the stuck polystyrene bead. (Figure not to scale).

## 5.2. Detecting the levitation of a stuck polystyrene bead using backscattered light intensity

To detect the axial position of the stuck polystyrene bead, we employed backscattered light intensity detection. The scheme developed for this method has already been explained in the section 4.3.4 of the thesis. When the polystyrene bead was stuck to the coverslip and was in the position shown in Figure 37, we detected very small amount of backscattered light. After firing a pulse, the particle got levitated and got trapped in the CW laser focus. Because of that, we detected higher intensity of backscattered light. We also were able to detect the transition of the suck polystyrene bead from the stuck state to the trapped state as shown in Figure 38. A small peak due to the pulse laser appeared with the transition signal (~45 μs). But after the bead was transferred to the stuck position, we got higher backscattered light intensity as long as it was in the trap. Figure 39 shows a typical plot of the backscattered light intensity as the function of time, recorded with the digital oscilloscope. Two distant intensity levels were observed; the lower is for the case when the particle is stuck on the coverslip, and the higher is for the particle in the trap

after the pulse was applied. The transition time was typically less than 15 ms. Even when the polystyrene bead is in the trap, small fluctuations can be seen in the backscattered light intensity. They are blamed to the thermal agitation of the polystyrene bead.

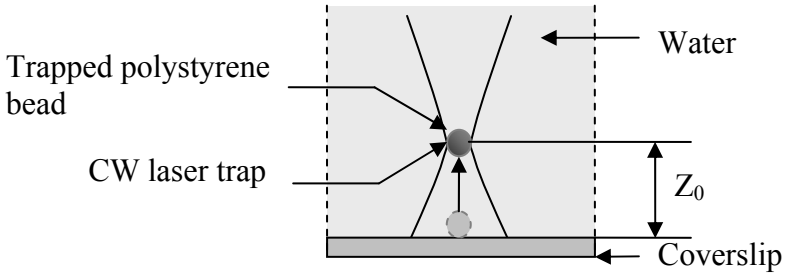


Figure 38. Schematic showing the position of the bead after the levitation. The stuck polystyrene bead gets levitated after a single shot of the pulsed laser, and gets trapped in the CW laser trap. (Figure not to scale).

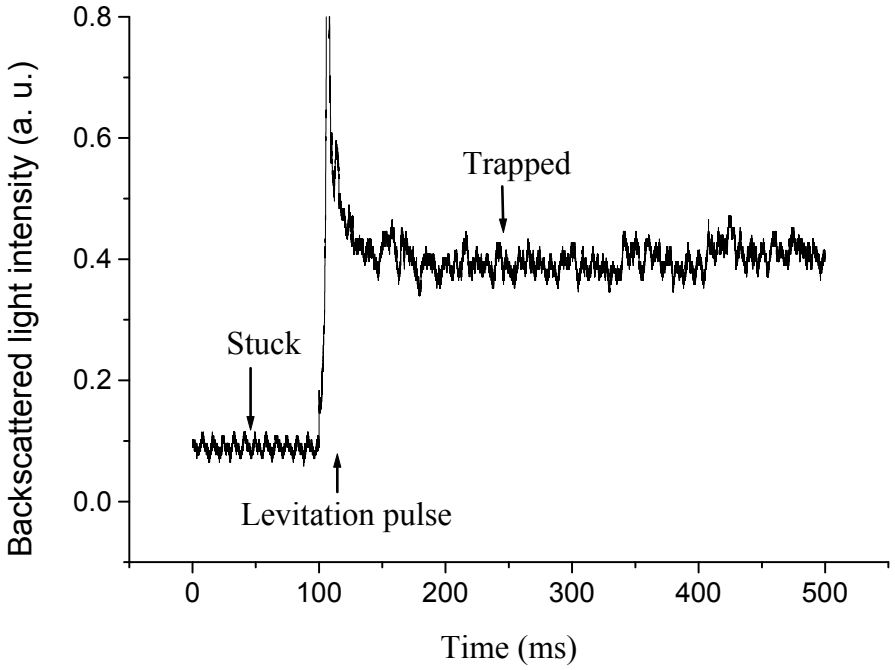


Figure 39. Backscattered light intensity recorded at the detector as a stuck polystyrene bead was levitated with an infrared pulse and jumped into the CW trap.

## 5.3. Levitation efficiency

We define the levitation efficiency as the number of particles successfully levitated to the total number of particles that we tried for levitation. We found that the levitation efficiency greatly depends on two parameters of the pulsed laser tweezers. They are the pulsed laser power and the initial axial displacement of the particle. We also tried to find the dependence of the levitation efficiency on the % NaCl concentration of the sample.

### 5.3.1. Dependence on the pulse energy

To find the dependence of the levitation efficiency on the single pulse energy, we prepared a sample in the same way, discussed earlier in the section about preparing a sample. That is, 2.0 μm polystyrene beads were suspended in the distilled water. The initial axial displacement $Z_0 \sim 8$ μm was used for all the measurements done to find the dependence of the levitation efficiency on the individual pulse energy. The average output power of the pulsed laser was modulated from 2 mW to 14 mW, using the combination of the half wave-plate and the polarizer. We used the calibrated phtotodetector output connected a digital oscilloscope to measure the average pulse output power. We randomly selected 50 stuck particles for levitation, and fired only one pulse for each particle. If the particle was levitated and trapped in the CW laser trap, it was recorded as a success, and if not, as a failure. The number of success to the total particles tried, gave us the levitation efficiency. This process was repeated for different single pulse energies corresponding to the average output power of the pulsed laser from

1 mW to 14 mW. Figure 40 gives the plot of the single pulse levitation efficiency versus the energy of the pulse at the sample plane. The line curve is the Boltzman fit of the experimental data. One can see from this graph that increase in the pulse energy gave us higher levitation efficiency. The pulse energy is directly related to the gradient force generated by the pulse. Therefore, the increase in the pulse energy facilitates the levitation of the stuck particles which have relative higher binding force between them and the coverslip. We were able to achieve the efficiency as high as 88 % at ~450 μJ, using this technique.

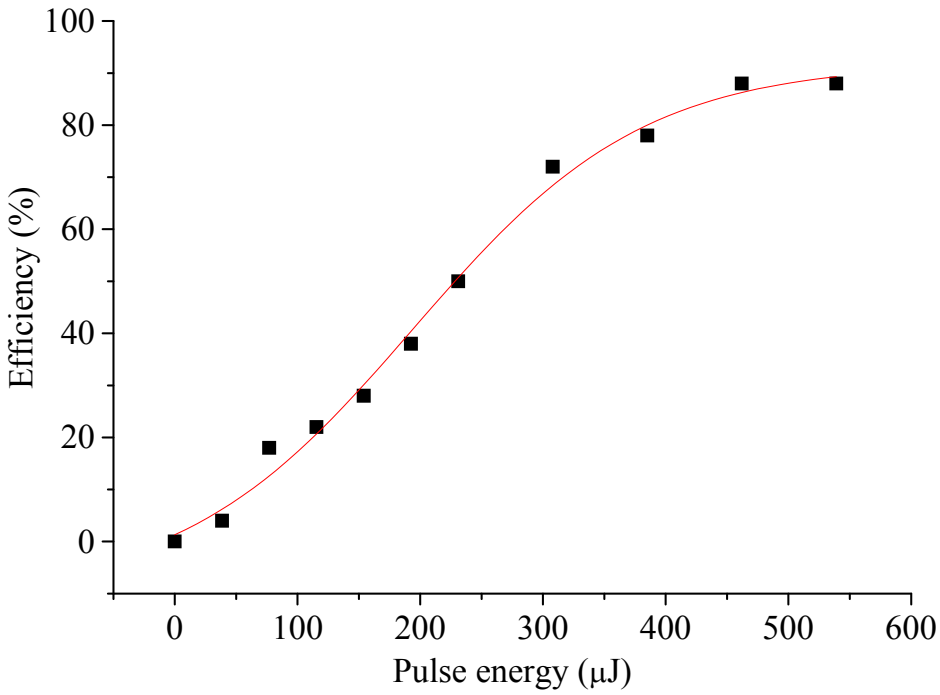


Figure 40. Single pulse levitation efficiency versus pulse energy in μJ at $Z_0 = 8$ μm.

### 5.3.2. Dependence on the initial axial displacement

We also found that the single pulse levitation efficiency greatly depends on the initial axial displacement $Z_0$. We prepared a sample using 2.0 μm polystyrene beads in the distilled water. The sample holder was fixed in the PZKM and using power supply 3, we changed the initial axial displacement of the particles under consideration. The relation found earlier and explained in the methods and calibration section of the thesis gives us relation between the voltage supplied and the PZKM displacement to be 57.5 nm/V. We used this relation to precisely set the initial axial displacement of the particle before the pulse was fired. Figure 41 depicts the method used to set the correct initial axial displacement. We focused the CW laser on the coverslip such that a very small spot of laser was seen on the TV screen. Then, using the PZKM, we lowered the position of the sample holder such that we got the required initial axial displacement $Z_0$. In this case, the CW laser was focused deep in the sample and distance $Z_0$ above the particle under consideration. Figure 42 shows the dependence of the levitation efficiency on the displacement $Z_0$ with the pulse energy kept at 385 μJ. For each displacement $Z_0$, we tried to levitate 20 stuck particles. The optimum efficiency was observed at $Z_0$~8μm for the 2.0-μm beads and it decreased drastically on the slight change in $Z_0$. The percentage efficiency graph plotted depends on the statistical fluctuations and therefore, if repeated, it might not form the exact shape. But, it gives the qualitative picture of how the initial axial displacement plays a vital role in the levitation process.

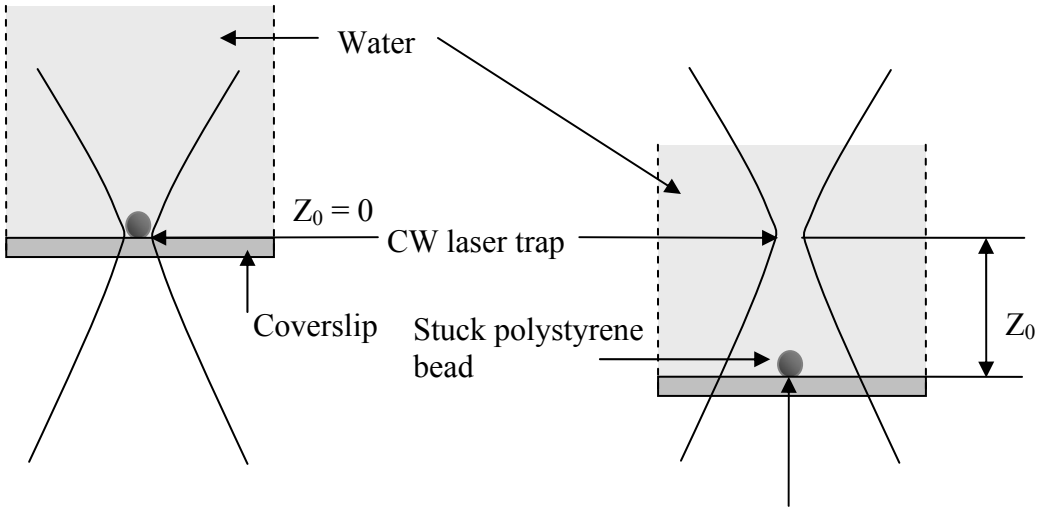


Figure 41. Setting the correct initial axial displacement.

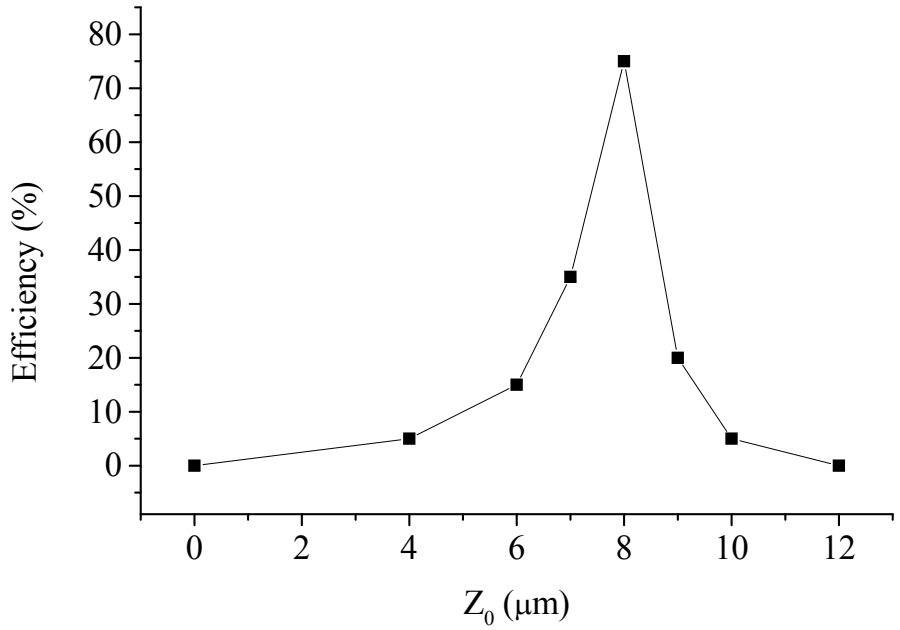


Figure 42. Single pulse levitation efficiency versus the initial axial displacemet ($Z_0$) in μm between the particle position and the laser focus (with a constant pulse energy of 385 μJ).

### 5.3.3. Dependence on % NaCl in the sample

After preparing a sample, we found that some of the polystyrene beads suspended in water got stuck to the coverslip. The binding force between the stuck bead and the glass surface was found to be dependent on the NaCl concentration of the sample. To find this dependence, we suspended 2.0 μm polystyrene beads in the aqueous solution having different NaCl concentrations. These samples are made in small plastic tubes. These tubes were left for a day on shelf. On the next day, we used them to prepare the samples for use. The plastic tubes were shaken well before a drop of the solution was transferred from them to the sample well. We allowed the polystyrene beads to settle and stick to the coverslip. After about an hour, we started taking readings by trying to levitate the stuck particles in the sample. The stuck particles for levitation were randomly selected. Figure 43 shows the dependence of the levitation efficiency on the percentage NaCl present in the sample, with the pulse energy kept at 385 μJ and initial axial displacement $Z_0$ kept at 6 μm. For each percentage concentration, we tried to levitate 20 stuck particles. We found the highest levitation efficiency for 0.1% NaCl and it decreased with increase in the percentage NaCl. For 0.3%, 0.5%, 0.7% and 1.0% NaCl sample the levitation efficiency remained almost constant. The dependence of the levitation efficiency on the % NaCl concentration in the sample can be explained using positive ion double layer formation. As explained earlier, we used polystyrene beads with diameter of d = 2.0 μm. When such beads are dispersed in water, the ionic groups bonded to their surfaces dissociate and give rise to a screened electrostatic interaction.[103] The polystyrene particles

in water have a titrable charge (~0.1 e/nm$^2$) on their surfaces.[104] This effective charge is given by,

$$Z^* = C(a / \lambda_B), \qquad (5.1)$$

where, $$\lambda_B = z^2 e^2 / \varepsilon k_B T, \qquad (5.2)$$

for a 1:1 electrolyte in water at 25$^o$C and $C$ is constant around 10, and $a$ is the radius of the polystyrene beads.[105] NaCl is a 1:1 electrolyte in water i.e. ionic strength is equal to molality. For 2.0 μm polystyrene bead, $Z^*$ = 9.8 × 10$^3$ e. This effective charge is negative. Around a negatively charged polystyrene bead, a positive ion double layer is formed. The formation of double layer depends on the concentration of the NaCl in the sample. Formation of this double layer enhances the interaction force between the stuck particle and the glass surface (coverslip). Glass plates have negative charge (~ 0.5e/nm$^2$).[104] It can be seen from the Figure 43 that increase in the concentration of NaCl increases the interaction force (decrease in levitation efficiency) initially, but there is almost no effect on the interaction force (no change in the levitation efficiency) for the higher concentration of NaCl. This can be explained by saturation of positive ions required to form double layer. Due to that, there is no more increase in the effective charge of the polystyrene beads keeping the interaction force almost constant. (Note: All this explanation is qualitative in nature. More work is required for detailed analysis of this graph.)

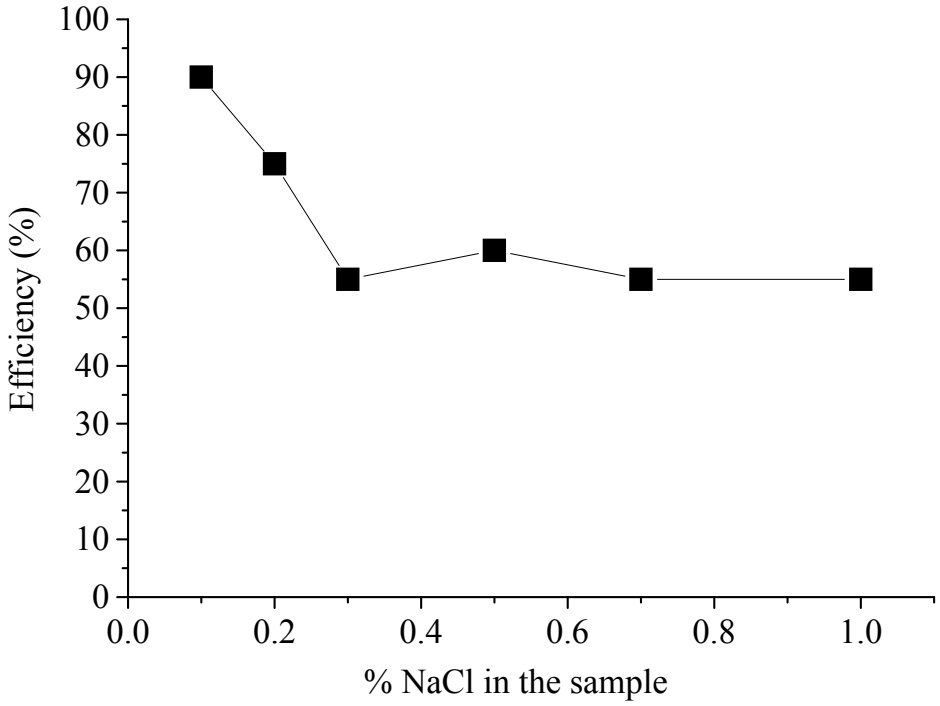


Figure 43. Levitation efficiency versus percentage NaCl in the sample (with the constant pulse energy of 385 μJ and the constant initial axial displacement $Z_0$).

### 5.3.4. Dependence on the initial axial displacement and % NaCl in the sample

We also tried to find the dependence of the single pulse levitation efficiency on the initial axial displacement and the percentage NaCl concentration in the sample. The sample preparation method used for this experiment was similar to the one explained in the section 5.3.3. Figure 44 is a plot of the single pulse levitation efficiency versus the initial axial displacement. There are two curves in the figure, the top one corresponds to the % NaCl concentration of 0.1% and the bottom one corresponds to the % NaCl concentration of 0.3% with constant pulse energy of 385 μJ. For 0.3% NaCl, we found

the maximum efficiency at 8 µm, but for 0.1% NaCl, we found it at 6 µm. This may be due to the statistical fluctuations.

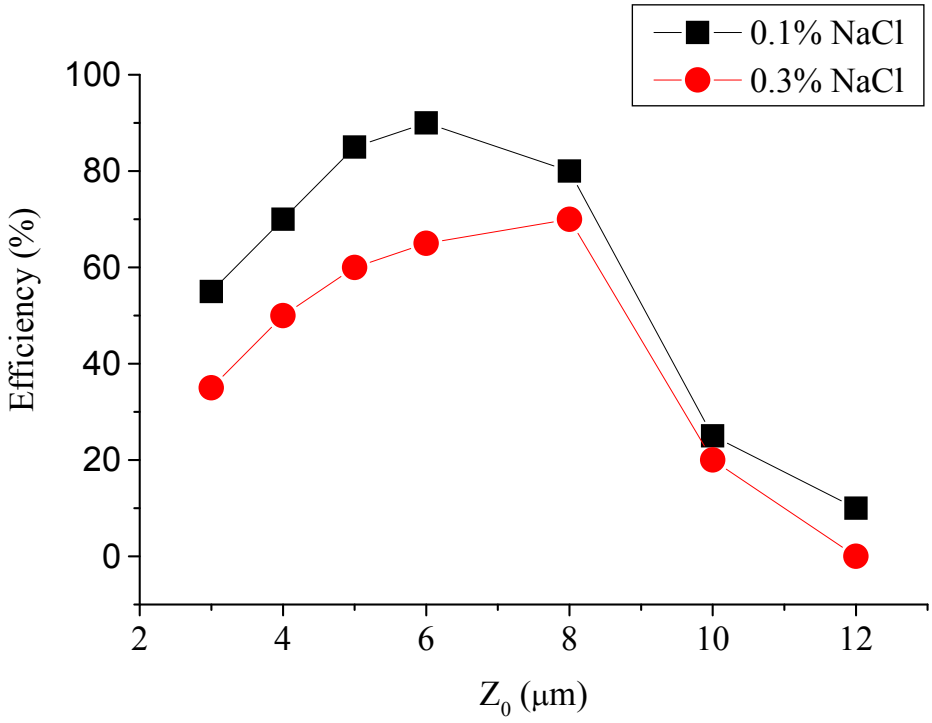


Figure 44. Levitation efficiency versus the initial axial displacement $Z_0$ (with the constant pulse energy of 385 µJ) for 0.1% NaCl sample and 0.3% NaCl sample.

## 5.4. Levitation of a stuck yeast cell and a stuck *Bacillus cereus* bacterium

After the success in levitating the polystyrene beads, we examined the applicability of this technique for the levitation of microorganisms. To start with we suspended the yeast cells in 0.1% NaCl solution. After a few minutes, we observed that some of the yeast cells were stuck to the coverslip. We confirmed their binding to the

coverslip by attempting to trap them using the CW laser trap. The yeast cells which could not be trapped using the CW laser were chosen for levitation. Figure 45 (a) shows three of such yeast cells stuck to the coverslip. The yeast cell marked with an arrow was under consideration and was tried for levitation. Figure 45 (b) shows the yeast cells blurred because the sample was lowered using PZKM such that the initial axial displacement $Z_0$ was ~8 μm. We opened the shutter either by using manual on, or by using the computer program, until the yeast cell under consideration was levitated. The number of pulses required for levitation varied and found to be greatly dependent on the binding force between the coverslip and the individual yeast cell. We found that generally a single pulse is not sufficient to levitate yeast cells as the binding force between yeast cells and the coverslip is comparatively greater than what was observed in the case of polystyrene beads. Figure 45 (c) shows the yeast cell under consideration was levitated and trapped in the CW laser trap. For better visibility, IR camera filter was used which blocked the laser light from entering the camera. Figure 45 (d) shows the manipulation of the trapped yeast cell. Even after moving the stage in +Y direction, the trapped yeast cell remained in the trap and hence its position is unchanged from Figure 45 (c) to Figure 45 (d).

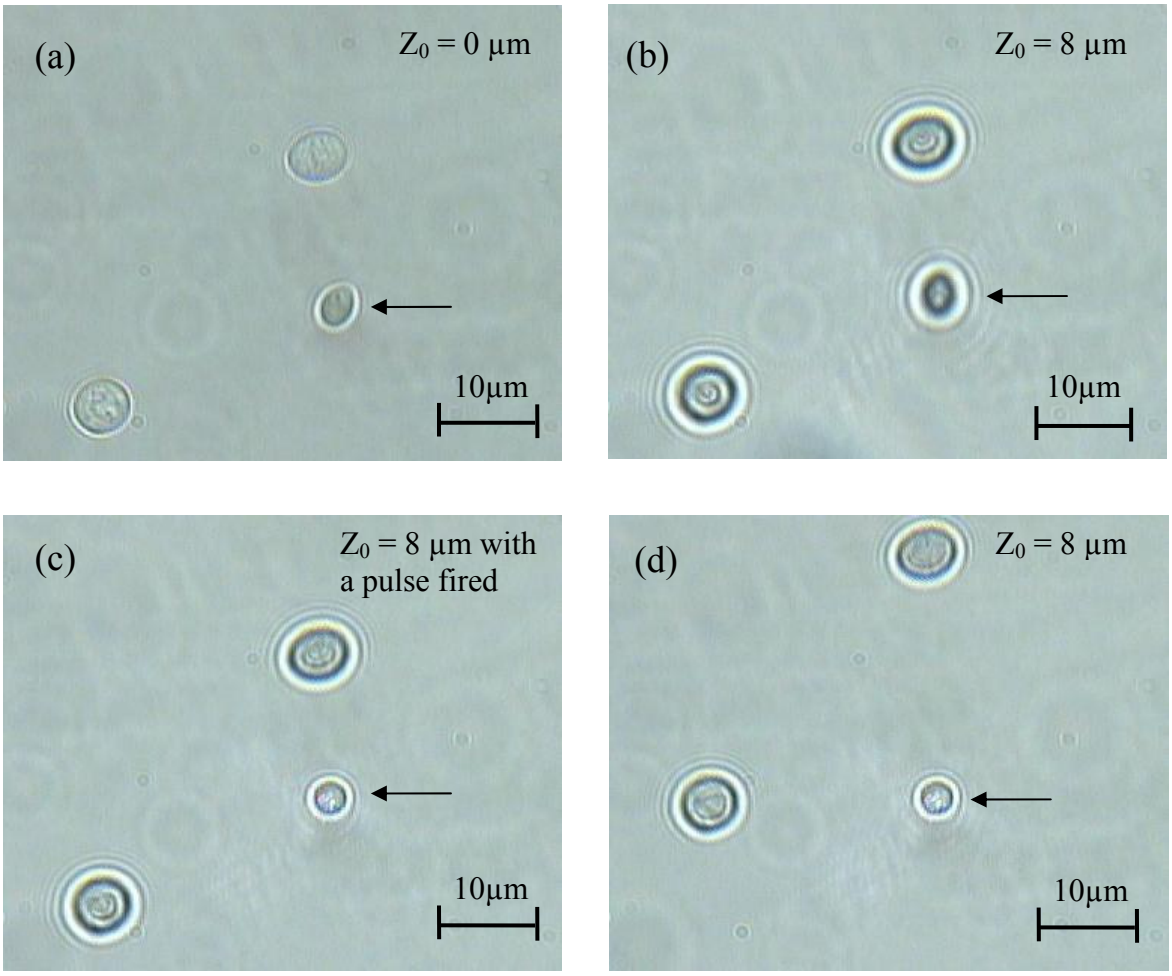


Figure 45. Levitation and manipulation of a yeast cell stuck on the coverslip. (a) Yeast cells stuck to the coverslip. (b) Yeast cells were defocused before the application of the pulse. (c) The marked yeast cell was levitated with infrared pulses and was trapped into the CW trap after levitation. (d) The levitated and trapped yeast cell was manipulated while stage was moved in +Y direction.

The levitation of a stuck bacillus cereus bacterium was carried out in a similar way as it was done for the yeast cell. Figure 46. (a)-(d) depict the levitation of the stuck *Bacillus cereus* bacterial cells suspended in a LB medium (with 0.01% NaCl). In this experiment, we first focused the microscope to see the clear image of the stuck bacteria, as shown in Figure 46 (a), and positioned the target cell (marked with an arrow) into the

laser spot while the trapping beam was on. Then, the image of the target bacterium was defocused with $Z_0$~8μm, as shown in Figure 46 (b). And then, the infrared laser pulses were fired and the target stuck bacterium was levitated and moved to the CW trap (showing clear images), as shown in Figure 46 (c). The successful levitation of the stuck cells was confirmed by the clear cell image, as well by the manipulation in either X or Y direction with the CW trapping beam. Figure 46 (d) shows the bacterium remained in trap even after moving the stage in -Y direction. The binding interaction of the biological cells with the surface is usually stronger than that of the polystyrene beads and we found that in many cases a few individual pulses are required to levitate a stuck bacterium.

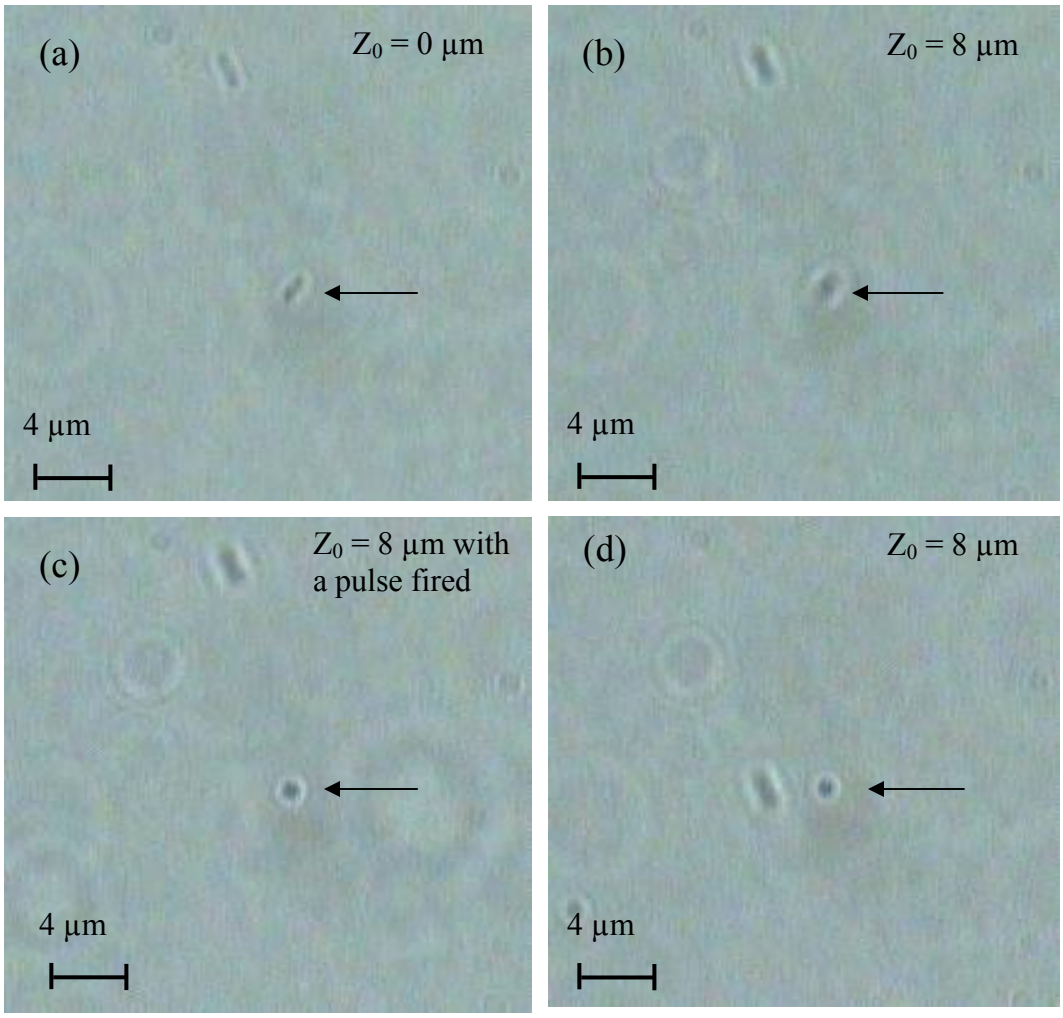


Figure 46. Levitation and manipulation of a *Bacillus cereus* bacterium stuck on the coverslip. (a) Two Bacillus cereus bacteria stuck on the coverslip. (b) The stuck bacterial cells were defocused. (c) The marked bacterium was levitated and jumped into the CW trap. (d) The levitated and trapped *Bacillus cereus* bacterium was manipulated while stage was moved in -Y direction.

# 6. THEORETICAL MODELING

In the pulsed laser tweezers, the pulsed laser was used to generate a large gradient force within a short duration that overcomes the adhesive interaction between the stuck particles and the surface; and then the low power CW laser was used to capture the levitated particle. Recently, Deng, Wei, Wang and Li have published a paper on numerical modeling of optical levitation and trapping of the "stuck" particles with a pulsed optical tweezers.[106] They described the gradient force generated by the pulsed optical tweezers and modeled the binding interaction between the stuck beads and glass surface by the dominative van der Waals force with a randomly distributed binding strength. The equation of motion for the bead was used to describe the trajectory of the bead's position as the stuck bead is detached from the surface and moves to the trap center. The single pulse levitation efficiency for polystyrene beads as the function of the pulse energy, the initial axial displacement the pulse duration was calculated by solving the equation of motion for the polystyrene bead.[106]

The optical force due to the CW laser is described by[106]

$$F_{cw} = -k_z \frac{z}{\left(1+\left(z/z_s\right)^2\right)^2} \exp\left(-\left(\frac{z}{z_s}\right)^4\right), \qquad (6.1)$$

where $k_z$ is the spring constant and $z$ is the position deviation of the bead center from the beam focus. The restoring force acting on the bead is described as $-k_z z$ for $z \ll z_s$. The distance parameter $z_s$ is defined as $z_s=\pi\omega_0^2/\lambda_0$ where $\omega_0$ is the radius of the beam waist at the point $z=0$.

The optical force due to the pulsed laser is described by[106]

$$F_{\text{pulse}} = -\frac{2.\text{E}}{\tau\sqrt{\pi}} \frac{\text{z}}{\left(1+\left(\text{z}/\text{z}_\text{s}\right)^2\right)^2} \exp\left(-\left(\frac{t}{\tau}\right)^2\right) \exp\left(-\left(\frac{z}{z_s}\right)^4\right), \quad (6.2)$$

where $E$ is a parameter in proportion to the single pulse energy $U$, $\tau$ is the pulse duration.

As a pulse is fired to the stuck bead, the bead will be detached under the action of the pulse gradient force and then moves to the trap center under the action of the cw gradient force.[106] The equation of motion describing this levitation process of the bead can be represented as[106]

$$\text{m}\ddot{\text{z}} = \text{F}_{\text{cw}} + \text{F}_{\text{pulse}} + \text{F}_\text{S} + \text{F}_\text{V}\ , \quad (6.3)$$

where m is the mass of the bead, $\text{F}_\text{S}$ the viscose force, $\text{F}_\text{V}$ the van der Waals force. The adhesive interaction between the stuck bead and the surface is modeled by the van der Waals force because it dominates at short distance comparing to the electrostatic force.

The van der Waals force, $\text{F}_\text{V}$, can be approximately expressed as[106]

$$F_V = -\frac{Aa}{6h^2} f(p), \quad (6.4)$$

where $f(p) = (1+3.54\,p)/(1+1.77\,p)$ for p<1 and $f(p) = 0.98/p - 0.434/p^2 + 0.067/p^3$ for p>1 with $p = 2\pi h/\lambda_L$, $\lambda_L$ is the London retardation wavelength, usually of the order of 100nm, $A$ is the Hamaker constant, typically in the order of $10^{-19}$~$10^{-21}$J.[106]

The viscose force, $\text{F}_\text{S}$, exerted on the bead due to the viscosity of the suspending medium is given by[106]

$$\text{F}_\text{S} = -6\pi\,\text{a}\eta\lambda\,\dot{\text{z}} = \text{-D}\dot{\text{z}} \quad (6.5)$$

where D is the damping coefficient ( $D = 6\pi a\eta\lambda$ ), $\eta$ the viscosity of the surrounding medium, and $\lambda$ a correction term that depends on the proximity of the bead to a planar boundary surface such as the coverslip. For the motion near a planar boundary, this position-dependent term is represented by[106]

$$\lambda = \frac{1}{1 - \frac{9}{8}\left(\frac{a}{h+a}\right) + \frac{1}{2}\left(\frac{a}{h+a}\right)^3} \quad . \tag{6.6}$$

The equation of motion equation (6.3) can be solved numerically for the bead's position at different time after a laser pulse is introduced to a target stuck bead.[106]

We found that even with the same pulsed gradient force (so as the same pulse energy, duration, and axial displacement), some beads can be successfully levitated, but some beads in the same liquid sample cannot be levitated. It can be attributed to the effect of the variation in binding condition between the individual stuck bead and the surface. This leads to the levitation efficiency at a given pulse energy, the pulse duration, or the axial displacement $Z_0$.[106] The change in the adhesive interaction between the stuck beads and the glass surface among individual beads is modeled by considering the Hamaker constant $A$ as a randomly distributed parameter, satisfying a normal distribution, with a probability density function of[106]

$$p\{A\} = \frac{1}{\sqrt{2\pi}\,\sigma} e^{-(A-\zeta)^2 / 2\sigma^2} \quad , \tag{6.7}$$

where $\zeta$ and $\sigma^2$ are the mean value and the variance of $A$, respectively. The cumulative distribution function of the normal distribution is[106]

$$P\{A\} = \frac{1}{\sqrt{2\pi}\ \sigma} \int_{-\infty}^{A} e^{-(t-\zeta)^2} \Big/ 2\sigma^2 \ dt = \Phi\left( \frac{A - \zeta}{\sigma} \right), \qquad (6.8)$$

where $\Phi(u) = \int_{-\infty}^{u} \frac{1}{\sqrt{2\pi}} e^{-t^2/2} \ dt$.

For the detailed analysis of the theoretical modeling, the paper (Ref. 106) published by Deng *et al.* has to be referred.

Figure 47 (a)[106] is the theoretical levitation efficiency versus the $E$ (that is proportional to single pulse energy) for a fixed $Z_0 = 6\mu\text{m}$ and pulse duration $\tau = 45\mu\text{s}$. Figure 47 (b) is the experimental results discussed in the section 5.3.1 of the thesis and re-plotted here for comparison.

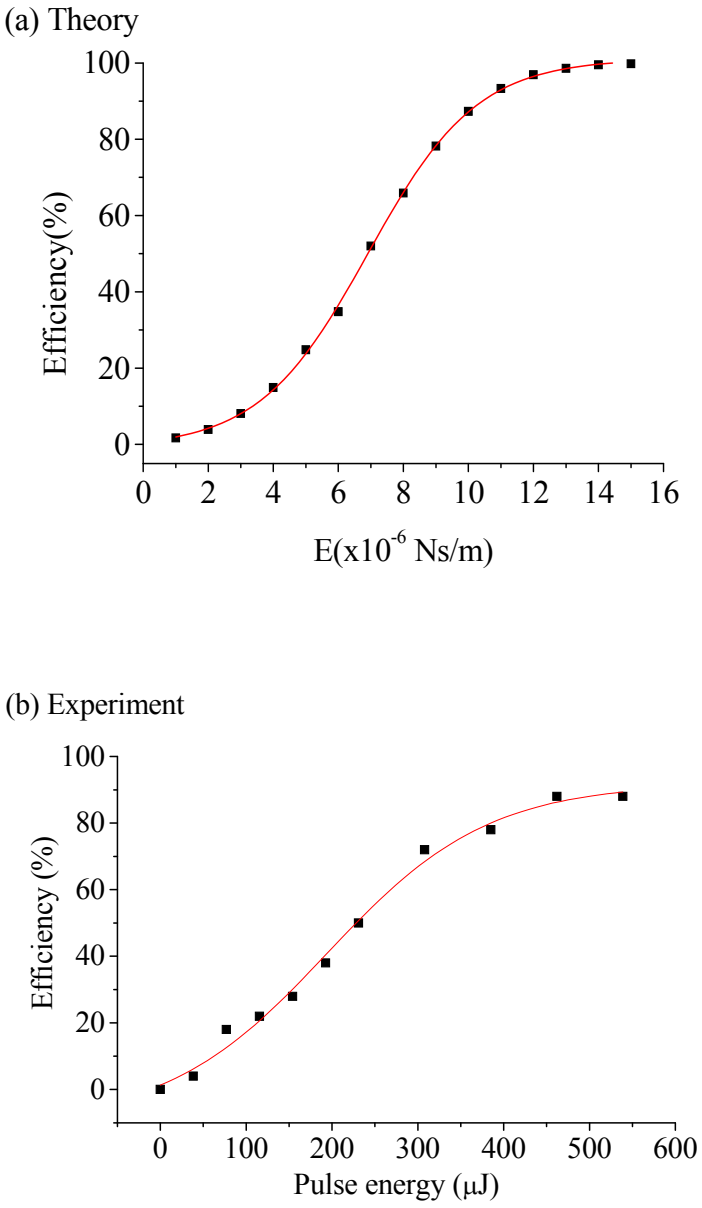


Figure 47. Comparison between the theoretical and the experimental results. (a) The levitation efficiency versus the E with a fixed $Z_0$ = 6 μm and τ = 45μs using theoretical model.[103] (b) The levitation efficiency versus the pulse energy with a fixed $Z_0$ = 8 μm and τ = 45μs found experimentally.

Deng *et al.* theoretically calculated the single pulse levitation efficiency as a function of the initial axial displacement.[106] The theoretical results found by them are in agreement with the experimental results.

There is supposed to be one more approach to model the levitation of the stuck microparticles or more precisely the binding force between the stuck particle and the glass surface. It is known as nanobubbles.[104] This model describes the force found between hydrophobic (water repellent) surfaces being orders of magnitude stronger than the van der Waals attraction. This force is supposed to have a measurable range of 10–100 nm compared to van der Walls attraction which has range of 1 nm or so.[104] This force, although somewhat variable, was measured in a number of laboratories. A wide ranging debate about its origins finally confirmed that the attractive force was due to the bridging of submicroscopic bubbles (nanobubbles) that existed on the hydrophobic surfaces.[107] This mechanism was based upon the observation of steps in the force at long range, signifying a bridging event, and the form and magnitude of the attraction was consistent with thermodynamic calculations of the force due to a bridging bubble.[104] More work is required to actually model levitation of stuck microparticles by the pulsed laser tweezers using nanobubbles model.

# 7. CONCLUSION - OUTLOOK

The main objective of the thesis was to develop a pulsed laser tweezers that can be used to levitate and manipulate stuck microparticles. The results presented in previous chapters demonstrated that this goal has been achieved. By employing the gradient force of a highly focused CW laser beam, optical tweezers can conveniently hold the particles suspended in water without any physical contact. But, the stuck particles can not be trapped using the tweezers that employs only CW laser. The pulsed laser tweezers has all the benefits of a CW laser tweezers with additional benefit of a pulsed laser for levitation.

We used the pulsed laser tweezers to levitate 2.0 μm polystyrene beads stuck to the coverslip. We found that the single pulse levitation efficiency for 2.0 μm polystyrene beads can be as high as 88 % using this technique. We also found that the single pulse levitation efficiency depends on the single pulse energy, the initial axial displacement and NaCl concentration of the sample. Results in chapter five give the actual dependence trend as found by us. We also applied our technique to levitate the stuck yeast cells and the stuck *Bacillus cereus* bacteria.

The paper published by Deng *et al.* gives the theoretical modeling for the levitation process realized by the pulsed laser tweezers.[106] The experimental results match qualitatively with the theoretical analysis.

A pulsed laser tweezers can also be used to directly measure the gradient force developed by the pulsed laser tweezers. We have used it to track the levitation motion. That can be used to find the dependence of the levitation motion on various system

parameters. Because of time limitations and incomplete results, the work done by us in this regard is not included as part of this thesis. A pulsed laser tweezers can also be combined with the laser scissors and the LPC technique to make a comprehensive system which can handle all sorts of biological manipulations required by the scientists. It would be fascinating to actually realize such comprehensive micromanipulation system. We have tried to develop such a system, but more work is required for the actual system to come into existence.

Thus, a pulsed laser tweezers gives us an ability to manipulate a broad range of particles from inanimate polystyrene beads to yeast cells and bacteria. It also gives us the ability to levitate and trap any of such particles that were impossible to manipulate using the CW laser tweezers, to date. Due to the ability of a pulsed laser tweezers to handle the wide range of particles, it may also find wide range of applications in cell biology and molecular biology.

# REFERENCES


1. A. Ashkin (1970), "Acceleration and trapping of particles by radiation pressure", Physical Reviews Letters, **24**:156-159.

2. A. Ashkin (1971), "Optical levitation by radiation pressure", Applied Physics Letters", **19**:283-285.

3. A. Ashkin, J. M. Dziedzic, J. E. Bjorkholm, and S. Chu (1986), "Observation of a single-beam gradient force optical trap for dielectric particles", Optics Letters, **11**:288-300.

4. A. Ashkin (2000), "History of optical trapping and manipulation of small-neutral particles, atoms and molecules", IEEE Journal on Selected Optics in Quantum Electronics, **6**(6):841-856.

5. K. C. Neuman, and S. M. Block (2004), "Optical trapping", Review of Scientific Instruments, **75**(9):2787-2809.

6. A. Ashkin (1978), "Trapping of atoms by resonance radiation pressure", Physical Review Letters, **40**:729-732.

7. A. Ashkin, and J. M. Dziedzic (1975), "Optical levitation of liquid drops by radiation pressure", Science, **187**:1073-1075.

8. A. Ashkin, and J. M. Dziedzic (1975), "Optical levitation in high vacuum", Applied Physics Letters, **28**:333-335.

9. G. Roosen, and C. Imbert (1979), "Optical levitation by means of two horizontal laser beams: a theoretical and experimental study", Physics Letters, **59A**:6:8.

10. S. Chu (1992), "Laser trapping of neutral particles", Scientific American, **266**(2):49-54.

11. A. Ashkin, and J. M. Dziedzic (1987), "Optical trapping and manipulation of viruses and bacteria", Science, **235**:1517-1520.

12. A. Ashkin, J. M. Dziedzic, and Y. Yamane (1987), "Optical trapping and manipulation of single cells using infrared laser beams", Nature, **330**:769-771.

13. A. Ashkin, and J. M. Dziedzic (1989), "Internal cell manipulation using infrared laser traps", Proceeding of the National Academy of Sciences of the United States of America, **86**(20): 7914-7918.

14. A. Ashkin, K. Schutze, J. M. Dziedzic, U. Euterneuer, M. Schliwa (1990), "Force generation of organelle transport measured *in vivo* by an infrared laser trap", Nature, **348**:346-347.

15. K. Svoboda, and S. M. Block (1994), "Biological applications of optical forces", Annual Review of Biophysics and Biomolecular Structure, **23**: 247-285.

16. W. D. Wang, H. Yin, R. Landick, and J. Gelles, S. M. Block (1997), "Stretching DNA with optical tweezers", Biophysical Journal, **72**:1335-1346.

17. S. M. Block, H. C. Blair, and H. C. Berg (1989), "Compliance of bacterial flagella measured with optical tweezers", Nature, **338**:514-517.

18. J. T. Finer, R. M. Simmons, and J. A. Spudich (1994), "Single myosin molecule mechanics: piconewton forces and nanometre steps", Nature, **368**:113-118.

19. H. Liang, W. H. Wright, C. L. Rieder, E. D. Salmon, G. Profeta, J. Andrews, Y. Liu, G. J. Sonek, and M. W. Berns (1994), "Directed movement of chromosome arms and fragments in mitotic newt lung cells using optical scissors and optical tweezers", Experimental Cell Research, **213**: 308-312.

20. Y. Liu, G. J. Sonek, M. W. Berns, K. Konig, and B. J. Tromberg (1995), "2-photon fluorescence excitation in continuous-wave infrared optical tweezers", Optics Letters, **20**(21): 2246-2248.

21. K. Visscher, G. J. Brakenhoff, and K. J. Krol (1993), "Micromanipulation by multiple optical traps generated by a single fast scanning trap integrated with the bilateral confocal scanning laser microscope", Cytometry, **14**(2): 105-114.

22. L. P. Ghislain, and W. W. Webb (1993), "Scanning-force microscope based on an optical trap", Optics Letters, **18**:1678-1680.

23. M. W. Berns, W. H. Wright, and R. W. Sterbing (1991), "Laser microbeam as a tool in cell biology", International Review of Cytology, **129**:1-44.

24. M. W. Berns, W. H. Wright, B. J. Tromberg, G. A. Profeta, J. J. Andrews, and R. J. Walter (1989), "Use of a laser-induced optical force trap to study chromosome movement on the mitotic spindle", Proceeding of the National Academy of Sciences of the United States of America, **86**(12): 4539-4543.

25. H. Liang, W. H. Wright, W. He, and M. W. Berns (1991), "Micromanipulation of mitotic chromosomes in $PTK_2$ cells using laser-induced optical forces ("Optical Tweezers")", Experimental Cell Research, **197**: 21-35.

26. A. Vorobjev, H. Liang, W. H. Wright, and M. W. Berns (1993), "Optical trapping for chromosome manipulation: a wave-length dependence of induced chromosome bridge", Biophysical Journal, **64**:533-538.

27. H. Liang, W. H. Wright, S Cheng, W He, and M. W. Berns (1993), "Micromanipulation of Chromosome in $PTK_2$ cell using laser microsurgery (optical scalpel) in combination with laser-induced optical force (optical tweezers)", Experimental Cell Research, **204**: 110-120.

28. J. Grimbergen, K. Visscher, and D. M. Gomes de (1993), "Isolation of single yeast cells by optical trapping", Yeast, **9**: 723-732.

29. H. Liang, W. H. Wright, C. L. Rieder, E. D. Salmon, G. Profeta, J. Andrews, Y. Liu, G. J. Sonek, and M. W. Berns (1994), "Directed movement of chromosome arms and fragments in mitotic newt lung cells using optical scissors and optical tweezers", Experimental Cell Research, **213**: 308-312.

30. H. Liang, K. T Vu, T. C. Trang, D. Shin, Y. E. Lee, D. C. Nguyen, B. Tromberg, and M. W. Berns (1997), "Giant cell formation in cells exposed to 740 nm and 760 nm optical tweezers", Lasers in Surgery and Medicine, **21**:159-165.

31. J. Zalatanova, and S. H. Leuba (2002), "Stretching and imaging single DNA molecule and chromatin", Journal of Muscle Research and Cell Motility, **23**:377-395.

32. L. H. Pope, M. L. Bennink, and J. Greve (2002), "Optical tweezers stretching of chromatin", Journal of Muscle Research and Cell Motility, **23**:397-407.

33. J. E. Molloy, J. E. Burns, J. Kendrick-Jones, R. T. Tregear, and D. C. S. White (1995), "Movement and force produced by a single myosin head", Nature, **378**:209-211.

34. J. E. Molloy, D. Dholakia, and M. J. Padgett (2003), "Preface: optical tweezers in a new light", Journal of Modern Optics, **50**:1501-1507.

35. R. M. Berry, and H. C. Berg (1997), "Absence of a barrier to backwards rotation of the bacterial flagellar motor demonstrated with optical tweezers", Proceedings of the National Academy of Sciences, **94**:14433-14437.

36. W. S. Ryu, R. M. Berry, and H. C. Berg (2000), "Torque-generating units of the flagellar motor of *Escherichia coli* have a high duty ratio", Nature, **403**:444-451.

37. S. Chu (1991), "Laser manipulation of atoms and particles", Science, **253**:861-866.

38. S. B. Smith, Y. Cui, and C. Bustamante (1996), "Overstretching B-DNA: The elastic response of individual double-stranded and single-stranded DNA molecules", Science, **271**:795-799.

39. A. D. Mehta, M. Rief, J. A. Spudich, D. A. Smith, and R. M. Simmons (1999), "Single-molecule biomechanics with optical methods", Science, **283**:1689-1695.

40. J. P. Gordon (1973), "Radiation forces and momenta in dielectric media", Physical Review A, **8**:14-21.

41. D. G. Grier (2003), "A revolution in optical manipulation", Nature, 424:810-816.

42. Roy, M. Elisha, and N. Philip (1998), "Dynamic excitation in membranes induced by optical tweezers", Biophysical Journal, **75**:294-320.

43. L. Shun, and G. D. Apostolos (1999), "Laser-generated stress waves and their effects on the cell membrane", IEEE Journal of Selected Topics in Quantum Electronics, **5** (4): 997-1003.

44. H. Sylvie, L. Guilllaume, R. Alain, and G. Francois (1999), "A new determination of the shear modulus of the human erythrocyte membrane using optical tweezers", Biophysical Journal, **76**:1145-1151.

45. M. M. Brandão. A. fontes, M. L. Barjas-Castro, L. C. Barbosa, F. F. Costa, C. L. Cesar, and S. T. O. Saad (2003), "Optical tweezers for measuring red blood cell elasticity: application to the study of drug response in sickle cell disease", European Journal of Haematology, **70**:207-211.

46. R. W. Steubing, S. Cheng, W. H. Wright, Y. Numajiri, and M. W. Berns (1991), "Laser induced cell fusion in combination with optical tweezers: the laser cell fusion trap", Cytometry, **12**:505-510.

47. M. Zahn, J. Renken, and S. Seeger (1999), "Fluorimetric multiparameter cell assay at the single cell level fabricated by optical tweezers", FEBS *Letters*, **443**:337-340.

48. D. Raucher, and M. P. Sheetz (1999), "Membrane expansion increases endocytosis rate during mitosis", Journal of Cell Biology, **144**:497-506.

49. D. Raucher, and M. P. Sheetz (2000), "Cell spreading and lamellipodial extension rate during mitosis", Journal of Cell Biology, **148**:127-136.

50. Y. Sako, A. Nagafuchi, S. Tsukita, M. Takeichi, and A. Kusumi (1998), "Cytoplasmic regulation of the movement of E-cadherin on the free cell surface as studied by optical tweezers and single particle tracking: Corralling and tethering by the membrane skeleton" Journal of Cell Biology, **140**:1227-1240.

51. M. Tomishigie, Y. Sako, and A. Kusumi (1998), "Regulation mechanism of the lateral diffusion of band 3 in erythrocyte membranes by the membrane skeleton"**,** Journal of Cell Biology, **142**:989-1000.

52. M. Eriksson, G. Leitz, E. Fallman, O. Axner, J. C. Ryan, M. C. Nakamura, and C. L. Sentman (1999), "Inhibitory receptors alter natural killer cell interactions with target cells yet allow simultaneous killing of susceptible targets", Journal of Experimental Medicine, **190**:1005-1012.

53. C.A. Xie, M. A. Dinno, and Y.Q. Li (2002), "Near-infrared Raman spectroscopy of single optically trapped biological cells", Optics Letters, **27**:249-251.

54. C.A. Xie, and Y.Q. Li (2002), "Raman spectra and optical trapping of highly refractive and nontransparent particles", Applied Physics Letters, **81**:951-953.

55. C.A. Xie, and Y.Q. Li (2003), "Confocal micro-Raman spectroscopy of single biological cells using optical trapping and shifted excitation difference techniques", Journal of Applied Physics, **93:**2982-2986.

56. J. K. H. Horber (2002), Atomic force microscopy in Cell Biology, p. **1-31**, San Diego: Academic.

57. P. T. Korda, M. B. Taylor, and D. G. Grier (2002), "Kinetically Locked-In Colloidal Transport in an Array of Optical Tweezers", Physical Review Letters, **89**:128301-128302.

58. L. A. Hough, and H. D. Ou-Yang (2002), "Correlated motions of two hydrodynamically coupled particles confined in separate quadratic potential wells", Physical Review E, **65**:021906-021912.

59. B. Lin, J. Yu, and S. A. Rice (2000), "Direct measurements of constrained Brownian motion of an isolated sphere between two walls", Physical Review E, **62**:3909–3919.

60. J. C. Crocker, and D. G. Grier (1996), "When Like Charges Attract: The Effects of Geometrical Confinement on Long-Range Colloidal Interactions", Physical Review Letters, **77**:1897-1900.

61. J. C. Crocker, and D. G. Grier (1994), "Microscopic measurement of the pair interaction potential of charge-stabilized colloid", Physical Review Letters, **73**:352-355.

62. S. Thalhammer, G. Lahr, A. Clement-Sengewald, W. M. Heckl, R. Burgemeister, and K. Schutze (2003), "Laser microtools in cell biology and molecular medicine", Laser Physics, **13**:1-11.

63. M. Besis, F. Gires, G. Myre, and G. Nomarski (1962), "Irradiation des organites cellulaire a l'aide d'um laser rubis", Comptes Rendus de l'Academie des Sciences, **225**:1010-1012.

64. N. M. Saks, R. Zudo, and M. J. Kopac (1965), "Microsurgery of living cells by ruby laser irradiation", Annals of the New York Academy of Sciences, **122**:695-712.

65. M. W. Berns, R. S. Olson, and D. E. Rounds (1970), "In vitro production of chromosomal lesions using an argon laser microbeam", Nature, **221**:74-75.

66. M. W. Berns, J. Aist, J. Edwards, K. Strahs, J. Girton, P. Mcneil, J. B. Rattner, M. Kitzes, M. Hammer-Wilson, L. H. Liaw, A. Siemens, M. Koonce, S. Peterson, S. Brenner, J. Burt, R. Walter, D. van Dyk, J. Coulombe, T. Cahill, and G. S. Berns (1981), "Laser microsurgery in cell and developmental biology", Science, **213**:505-513.

67. M.W. Berns, Y. Tadir, H. Liang, and B. Tromberg (1998), "Laser scissors and tweezers", Methods in Cell Biology, vol.55, ed. M.P. Sheetz, p.**71-98**, San Diego: Academic.

68. K. Schuze, and A. Clement-Sengewald (1994), "Catch and move--cut or fuse", Nature, **368**:667:669.

69. M. W. Berns, D. E. Rounds, and R. S. Olson (1969), "Effects of laser micro-irradiation on chromosomes", Experimental Cell Research, **56**:292-298.

70. M. W. Berns, J. Aist, J. Edwards, K. Strahs, J. Girton, P. McNeill, J. B. Rattner, M. Kitzes, M. Hammer-Wilson, L.-H. Liaw, A. Siemens, M. Koonce, S. Peterson, S. Brenner, J. Burt, R. Walter, P. J. Bryant, D. Van Dyk, J. Coulombe, T. Cahill, G. S. Berns (1981), "Laser Microsurgery in Cell and Developmental Biology", Science, **213**:505-513.

71. K. Schütze, I. Becker, K. Becker, S. Thalhammer, R. Stark, W. M. Heckl, M. Böhm, and H. Pösl (1997), "Cut out or poke in—the key to the world of single genes: laser micromanipulation as a valuable tool on the look-out for the origin of disease", Genetic Analysis: Biomedical Engineering, **14**:1-8.

72. K. Schüitze & G. Lahr (1998), "Identification of expressed genes by laser-mediated manipulation of single cells", Nature Biotechnology, **16**:737-742.

73. R. Hobza, M. Lengerova, H. Cerenohorska, J. Rubes, and B. Vyskot (2004), "FAST-FISH with laser beam microdissected DOP-PCR probe distinguishes the sex chromosomes of *Silene latifolia*", Chromosome Research, **12**:245-250.

74. A. Ashkin (1998), "Forces of a single-beam gradient laser trap on a dielectric sphere in the ray optics regime", Methods in Cell Biology, vol.55, ed. M.P. Sheetz, p.**1-27**, San Diego: Academic.

75. G. Roosen and C. Imbert (1976), "Optical levitation by means of 2 horizontal laser beams- theoretical and experimental study**"** Optics Communication, **26**(3): 432-436.

76. E. Fallman, and O. Axner (2003), "Influence of a Glass-Water Interface on-axis trapping of micrometer-sized objects by optical tweezers", Applied Optics, **42**:3915-3926.

77. J. P. Barton, D. R. Alexander, and S. A. Schaub (1989), "Theoretical determination of net radiation force and torque for a spherical particle illuminated by a focused laser beam", Journal of Applied Physics, **66**:4594-4602.

78. Rohrbach, E. H. K. Stelzer (2002), "Trapping forces, force constants, and potential depths for dielectric spheres in the presence of spherical aberrations", Applied Optics, 41(13): 2494-2507.

79. P. C. Chaumet, M. Nieto-Vesperinas (2000), "Time-averaged total force on a dipolar sphere in an electromagnetic field", Optics Letters, **25**(15):1065-1067.

80. P. C. Chaumet, and M. Nieto-Vesperinas (2000), "Coupled dipole method determination of the electromagnetic force on a particle over a flat dielectric substrate", Physical Review B, **61**:14119-14127.

81. Y. Harada, and T. Asakura (1996), "Radiation forces on a dielectric sphere in the Rayleigh scattering regime", Optics Communication, **124**:529-541.

82. J. P. Barton, D. R. Alexander, S. A. Schaub (1989), "Theoretical determination of net radiation force and torque for a spherical particle illuminated by a focused laser beam", Journal of Applied Physics, **66**:4594-4602.

83. J. P. Barton, D. R. Alexander (1989), "Fifth-order corrected electromagnetic field components for a fundamental Gaussian beam", Journal of Applied Physics, **66**:2800-2802.

84. K. F. Ren, G. Gréha, and G. Gouesbet (1994), "Radiation pressure forces exerted on a particle arbitrarily located in a Gaussian beam by using the generalized Lorenz-Mie theory, and associated resonance effects", Optics Communication, **108**:343-354.

85. A. Rohrbach, H. Kress, and E. H. K. Stelzer (2003), "Three-dimensional tracking of small spheres in focused laser beams: influence of the detection angular aperture", Optics Letters, **28**:411-413.

86. A. Rohrbach, H. Kress, and E. H. K. Stelzer (2002), "Three-dimensional position detection of optically trapped dielectric particles", Journal of Applied Physics, **91**(8): 5474-5488.

87. O. Muller, M. Schliwa, and H. Felgner (1995), "Calibration of light forces in optical tweezers", Applied Optics, **34**(6):977-982.

88. N. Malagino, G. Pesce, A. Sasso, and E. Arimondo (2002), "Measurement of trapping efficiency and stiffness in optical tweezers", Optics Communications, **214**:15-24.

89. J. E. Molloy, and M. J. Padgett (2002), "Lights, action: optical tweezers", Contemporary Physics, **43**(4):241-258.

90. A. Ishijima, T. Doi, K. Sakurada, T. Yanagida (1991), "Sub-piconewton force fluctuations of actomyosin invitro**"** Nature, **352**: 301-306.

91. M.W. Berns, Y. Tadir, H. Liang, and B. Tromberg (1998), "Basic laser tweezers", Methods in Cell Biology, vol.55, ed. M.P. Sheetz, p.**29-41**, San Diego: Academic.

92. M. Abramowitz (2003), Microscope Basics and Beyond, vol.1, p.**1-42**, Melville: Olympus America Inc.

93. K. C. Neuman, E. H. Chadd, G. F. Liou, K. Bergman, and S. M. Block (1999), "Characterization of Photodamage to *Escherichia coli* in Optical Traps", Biophysical Journal, **77**: 2856–2863.

94. A. Ashkin, and J. M. Dziedzic (1989), "Optical trapping and manipulation of single living cells using infra-red laser beams", Berichte der Bunsen-Gesellschaft - Physical Chemistry, **93**:254 –260.

95. Y. Liu, G. J. Sonek, M. W. Berns, and B. J. Tromberg (1996), "Physiological monitoring of optically trapped cells: assessing the effects of confinement by 1064-nm laser tweezers using microfluorometry", Biophysical Journal, **71**:2158 – 2167.

96. M. W. Berns (1976), "A possible two-photon effect in vitro using a focused laser beam", Biophysical Journal, **16**:973–977.

97. K. Konig, Y. Tadir, P. Patrizio, M. W. Berns, and B. J. Tromberg (1996), "Effects of ultraviolet exposure and near infrared laser tweezers on human spermatozoa", Human Reproduction, **11**:2162–2164.

98. P. P. Calmettes, and M. W. Berns (1983), "Laser induced multiphoton processes in living cells", Proceeding of the National Academy of Sciences of the United States of America, **80**:7197–7199.

99. S. P. Gross (2003), "Application of optical traps *in Vivo*", Methods in Enzymology, **361**:162-174.

100. Hitachi (1995), "Operating Principles", Opto Data Book, pp. 41-58, Hitachi America Ltd.

101. M. E. J. Friese, H. Rubinsztein-Dunlop, N. R. Heckenberg, and E. W. Dearden (1996), "Determination of the force constant of a single-beam gradient trap by measurement of backscattered light", Applied Optics, **35**:71127116.

102. J. H. Brenan, R. David, M. R. Graham, and I. W. Hunter (1999), "Progress towards photon force-based sensors: A system identification approach based on laser intensity modulation for measurement of the axial force constant of a single-beam gradient photon force trap", Proceedings of SPIE, **3834**:30-39.

103. T. G.M. Van De Ven (1989), Colloidal Hydrodynamics, p.**78**, London: Academic.

104. G. M. Keppler and S. Fradem (1994), "Attractive potential between confined colloids at low ionic strength", Physical Review Letters, **73**:356-359.

105. J. C. Crocker and D. G. Grier (1994), "Microscopic measurement of the pair interaction potential of charge-stabilized colloid," Physical Review Letters, **73**:352-355.

106. J. L. Deng, Q. Wei, and Y. Z. Wang, and Y. Q. Li (2005), "Numerical modeling of optical levitation and trapping of the "stuck" particles with a pulsed optical tweezers", Optics Express, **13**:3673-3680.

107. P. Attard, M. P. Moody, and J. W. G. Tyrrell (2002), "Nanobubbles: the big picture", Physica A, **314**:696-705.

# APPENDIX A. MECHANICAL DRAWINGS

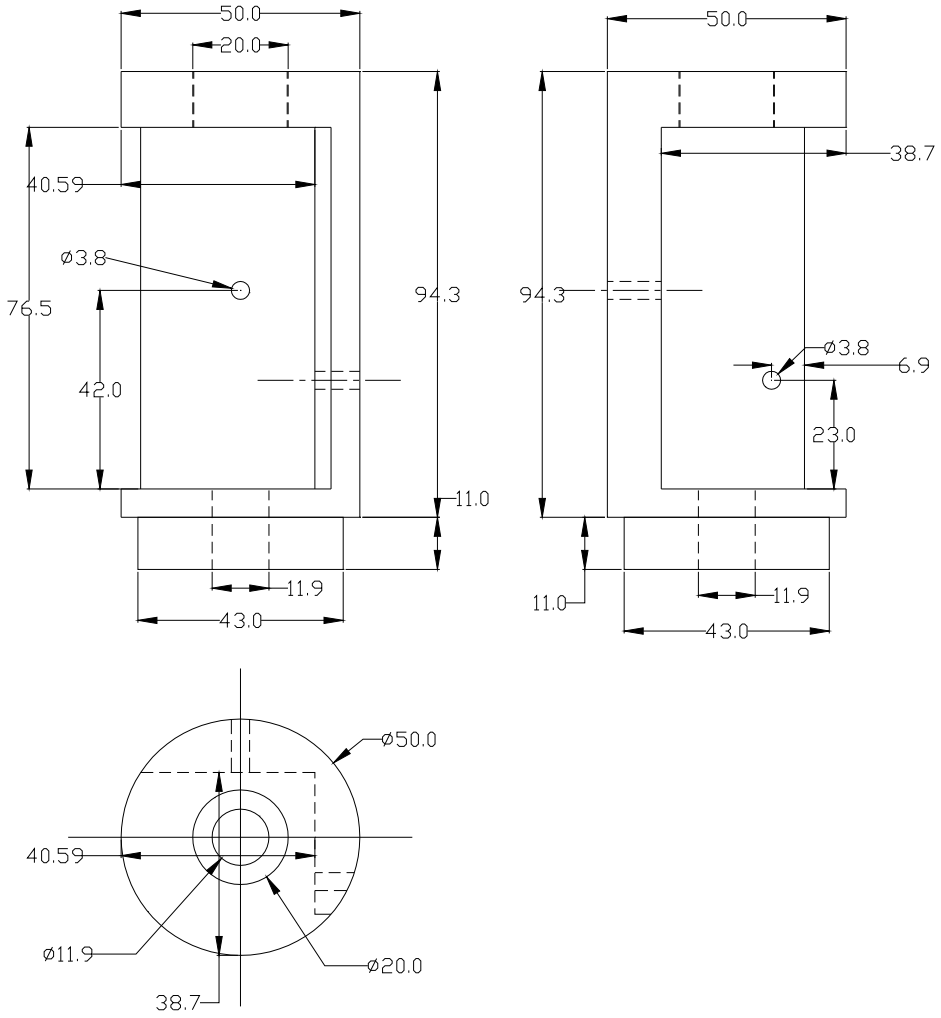


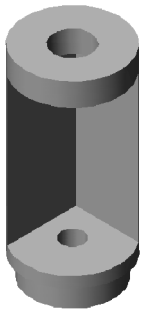

Mechanical drawing 1. Custom part 1.

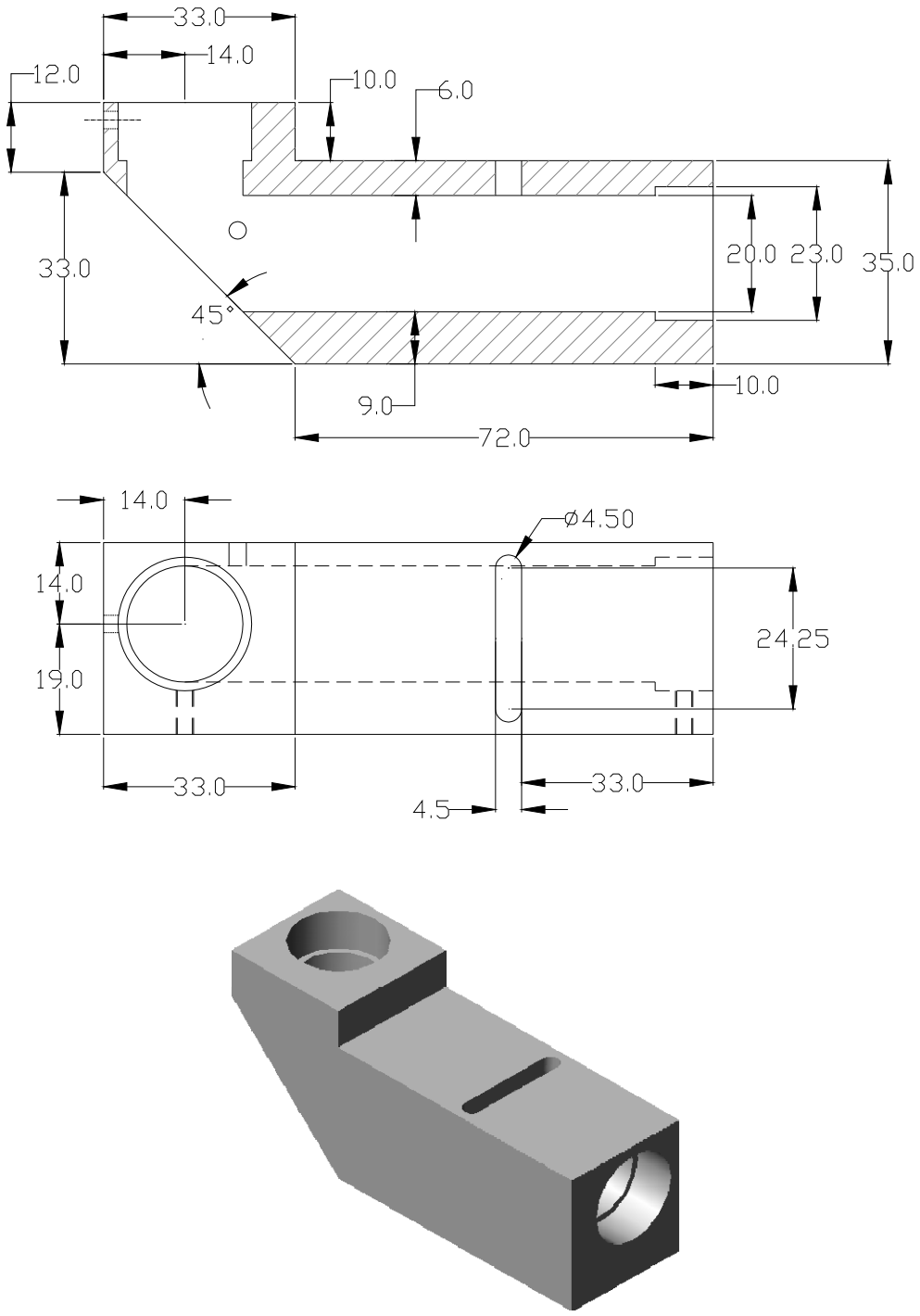


Mechanical Drawing 2. Custom part 2.

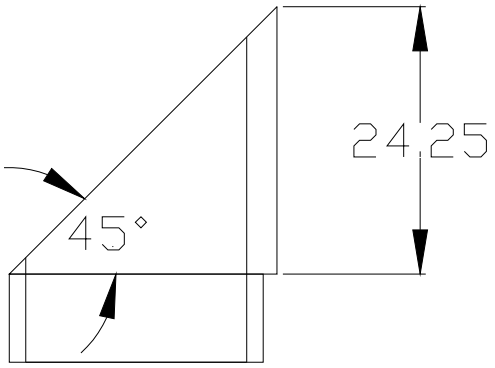


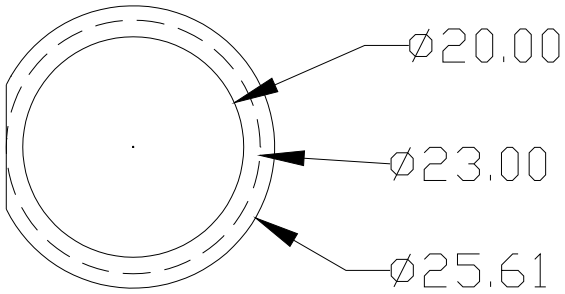


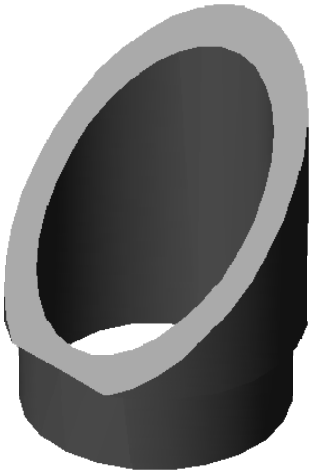

Mechanical drawing 3. Custom part 3.

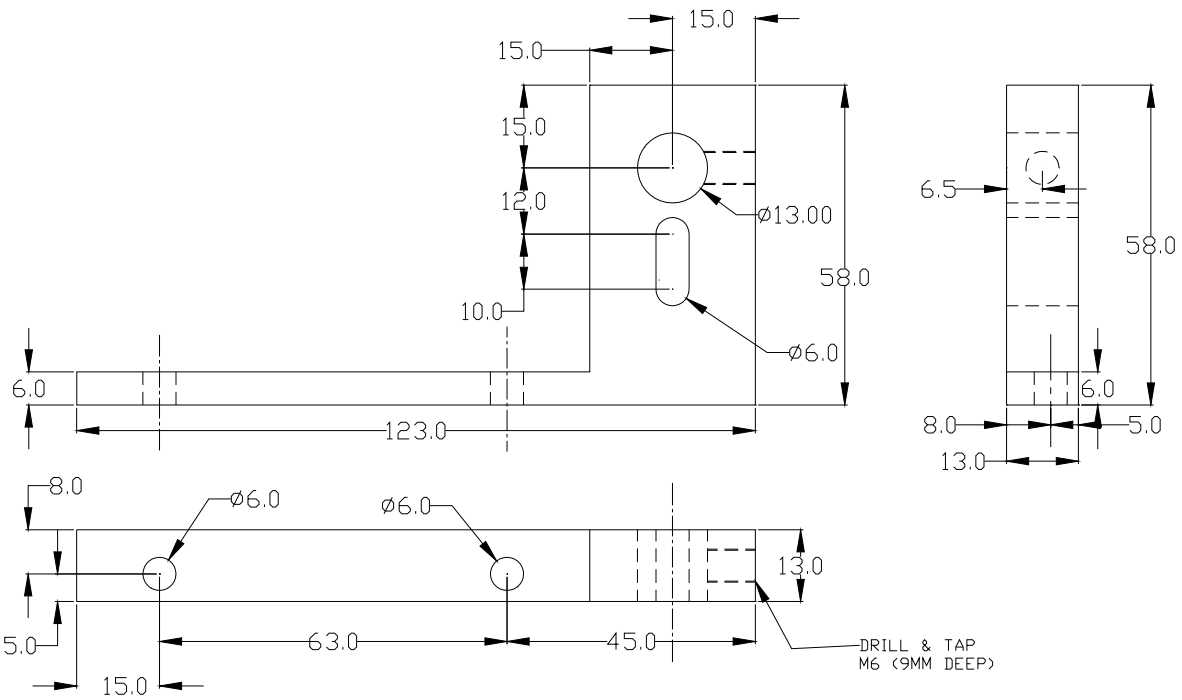


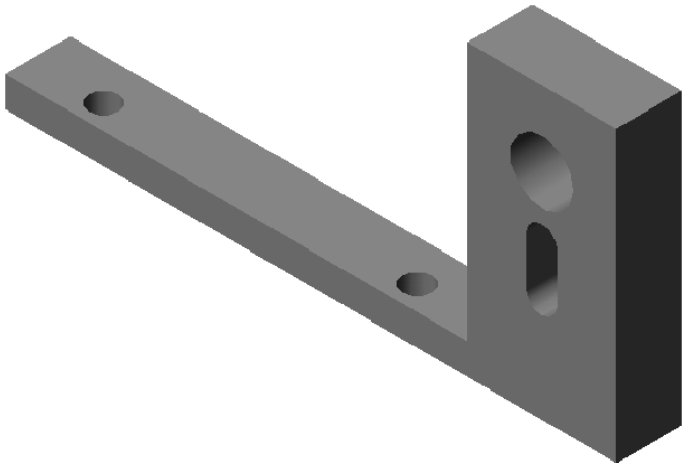

Mechanical drawing 4. Custom part 4.

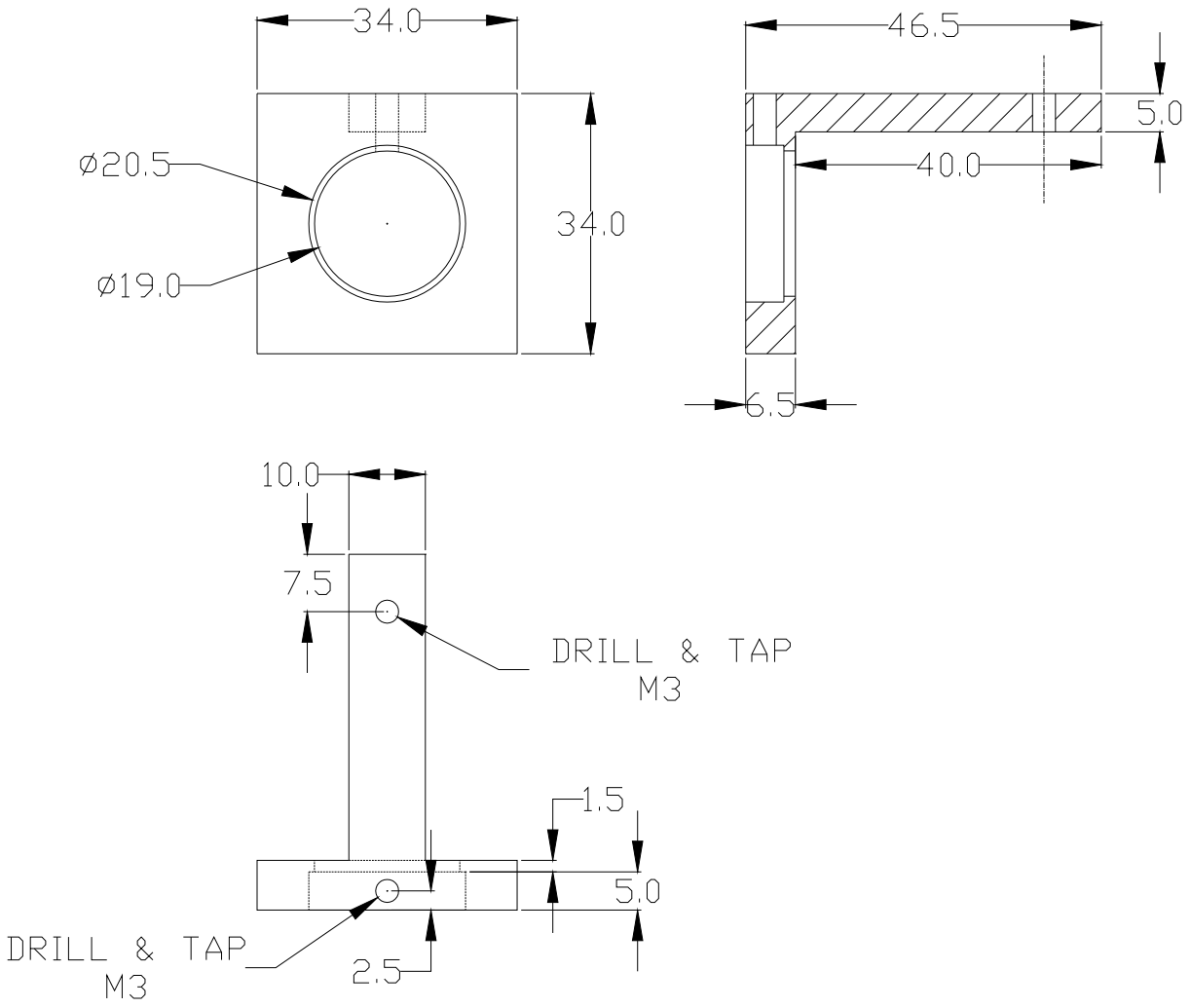


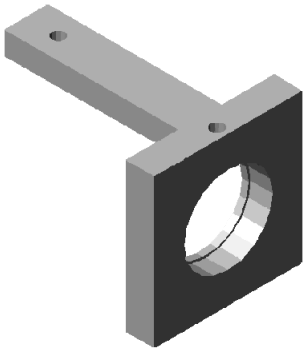

Mechanical drawing 5. Custom part 5.

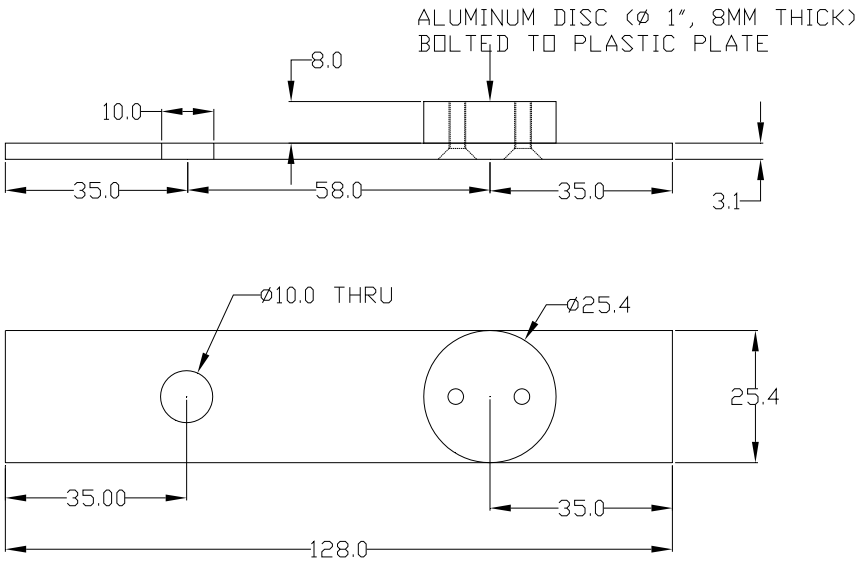


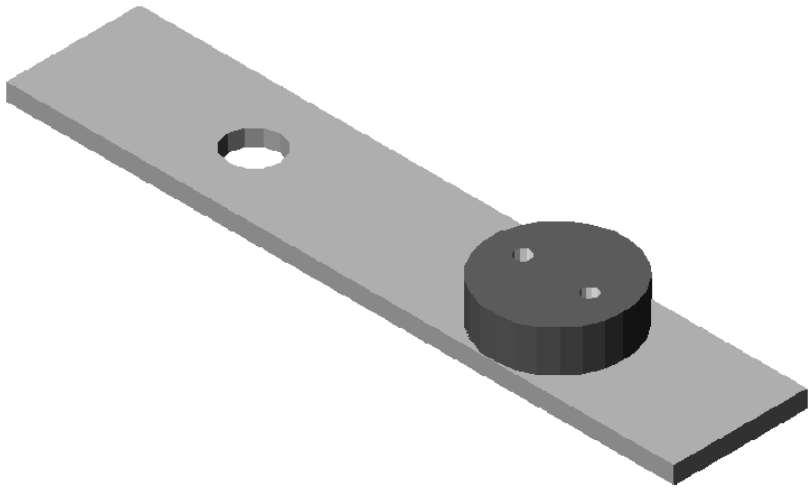

Mechanical drawing 6. Sample holder.

# APPENDIX B. VISUAL BASIC PROGRAM

## GUI (Graphical User Interface)

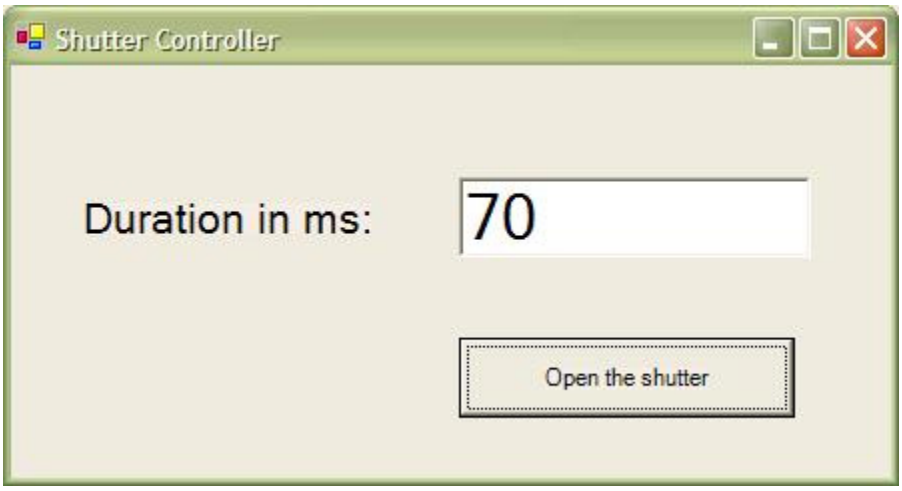


## Program Code

```
Private Sub Form_Unload(Cancel As Integer)
    CWAOPoint1.ChannelString = 0   '//Activate channel 0
    CWAOPoint1.SingleWrite 0       '//Set output voltage = 0 V
End Sub

Private Sub pulse_Click()
    Timer1.Interval = period.Text      '//Set timer interval = time period given by the user
    Timer1.Enabled = True              '//Enable timer
```

```
    CWAOPoint1.ChannelString = 0   '//Activate channel 0
    CWAOPoint1.SingleWrite 3       '//Set output voltage = 3 V
End Sub

Private Sub Timer1_Timer()
    CWAOPoint1.ChannelString = 0   '//Activate channel 0
    CWAOPoint1.SingleWrite 0       '//Set output voltage = 0 V
    Timer1.Enabled = False         '//Disable timer
End Sub
```

# APPENDIX C. LIST OF MAJOR COMPONENTS USED

| Component | Specifications |
|---|---|
| Anamorphic prism pair | Edmund Scientific Model# NT 47-244 |
| Beam splitter 1 | Edmund Scientific Model# 43736,<br>R = 50, T = 50 |
| Beam splitter 2 | R = 75, T = 25 |
| Circuit box 1 | 1 way to 3 way for connecting inputs of piezo-electric kinematic mount to power supply 3 |
| Collimating lens for diode laser | Thorlabs Model# A438-B<br>f = 4.5 mm, NA = 0.55<br>AR coated 600 - 1050 nm |
| Computer | Dell Optiplex 110<br>Windows 2000 |
| Condenser lens | Microplan Vickers (England) T 7955<br>20×/0.5 |
| Control unit for shutter | Custom made |
| Coverslip | Fisher Scientific, Model# NC9115219<br>22×22×0.1 mm |
| Custom part 1 | Appendix A |
| Custom part 2 | Appendix A |
| Custom part 3 | Appendix A |
| Custom part 4 | Holds piezo-electric kinematic mount, Appendix A |
| Custom part 5 | Holds filter 1, Appendix A |
| Dichroic mirror 1 | Hot Mirror, Edmund Scientific |
| Dichroic mirror 2 | 1.06 μm HR mirror @ $45^{o}$ |
| Digital oscilloscope | Lecroy 9310C<br>Dual 400 MHz Oscilloscope |
| Filter 1 | HR @ 1.06 μm |
| Half-wave plate | Thor Labs |
| Illumination bulb | GE 1493, 6.5V, 2.75A |
| Infrared diode laser: | Sanyo DL-7140-201S<br>Wavelength : 785 nm (Typ.)<br>Low threshold current : $I_{th}$ = 30 mA (Typ.)<br>High operating temperature : 60°C at 70mW (CW) |

| Component Name | Specifications |
|---|---|
| Instrument amplifier | Gain: 1× (Bandwidth 1 MHz)<br>10× (Bandwidth 400kHz), 100× (Bandwidth 150kHz), 1000× (Bandwidth 25kHz) |
| Lens 1 | f = 75 mm, d = 1 inch |
| Lens 2 | f = 100 mm, d = 1 inch |
| Lens 3 | f = 150 mm, d = 1 inch |
| Lens 4 | f = 100 mm, d = 1 inch |
| Lens 5 | f = 100 mm, d = 1 inch |
| Lens 6 | f = 150 mm, d = 1 inch |
| Mirror 1 | Thorlabs Model# BB1-E03 |
| Mirror 2 | Thorlabs Model# BB1-E03 |
| Mirror 3 | Aluminum Mirror |
| Mirror 4 | Thorlabs Model# BB1-E03 |
| Mirror 5 | Thorlabs Model# BB1-E03 |
| Mirror 6 | Thorlabs Model# BB1-E03 |
| Multimeter 1 | Beckman Industrial Corporation<br>Model# DM27XT |
| Multimeter 2 | John Fluke Manufacturing Company,<br>Model# 8050 Digital Multimeter |
| Neutral density filter 1 | T= 10 %, OD 1.0 |
| Neutral density filter 2 | T = 1 %, OD 2.0 |
| Objective | Leitz Wetzlar (Germany) Model# 519804<br>160/0.17, 100×/1.25(Oil) |
| Optical isolator | Optical isolator 690 nm |
| Photodetecor 1 | Custom made circuit using Si-photodiode S2386-5K<br>$t_r$ = 3.6 μs, $R_L$ = 20 kΩ |
| Photodetector 2 | Custom made circuit using PIN photodiode S4752(3) |
| Photodetector 3 | Custom made circuit using PIN photodiode S1223-01<br>$R_L$ = 50 Ω |
| Piezo-electric kinematic mount | Holds sample holder modified from piezo-electric kinematic mount.<br>Thorlabs Model# KC1-T-PZ |
| Pinhole 1 | d = 400 μm |
| Polarizer | Casix Model# PGM5210 (0033) |

| Component | Specifications |
|---|---|
| Polystyrene spheres | Bang Laboratories, Model# P0020320PN, d = 2.03 μm |
| Power supply 1 for illumination bulb | American optical company Model# 11144 |
| Power supply 2 for shutter | Hewlett Packard Model# 6253A (24 V) |
| Power supply 3 | Heathkit regulated H.V. power supply Model# IP-17 |
| Power supply for laser diode | Custom made by Dr. Li |
| Pulsed laser | Continuum: YG580 Series: SF version Actively Q-switched Nd:YAG laser |
| Sample Holder | Custom made, Appendix A |
| Shutter | Custom made |
| Television | Panasonic TV/VCR combo Model# 11144 |
| Thermoresister power meter 1 | Ophir optronics ltd., Model# 30-(150)A-P-He |
| Thermoresister power meter 2 | Coherent, Model# PM10 |
| Video camera | Panasonic industrial color CCD camera Model# GP - KR222 |

# APPENDIX D. PUBLICATION LIST

## Journal publications

Amol Ashok Ambardekar and Yong-qing Li (2005), "Optical levitation and manipulation of stuck particles with pulsed optical tweezers", Optics Letters, **30(14)**, in print.

## Conference proceedings and presentations

"Pulsed optical tweezers for levitation and manipulation of stuck biological particles", *Conference on Lasers and Electro-Optics*, **CFN3**, Baltimore, Maryland, May 22-27, 2005.